

THE STRUCTURE OF NON-EQUILIBRIUM
ANGULAR MOMENTUM POLARIZATIONS IN POLYATOMIC GASES

**THE STRUCTURE OF NON-EQUILIBRIUM
ANGULAR MOMENTUM POLARIZATIONS IN POLYATOMIC GASES**

PROEFSCHRIFT

**TER VERKRIJGING VAN DE GRAAD VAN DOCTOR
IN DE WISKUNDE EN NATUURWETENSCHAPPEN
AAN DE RIJKSUNIVERSITEIT TE LEIDEN, OP GEZAG
VAN DE RECTOR MAGNIFICUS DR. A.A.H. KASSENAAAR,
HOOGLEERAAR IN DE FACULTEIT DER GENEESKUNDE,
VOLGENS BESLUIT VAN HET COLLEGE VAN DEKANEN
TE VERDEDIGEN OP DONDERDAG 10 DECEMBER 1981
TE KLOKKE 16.15 UUR**

DOOR

ERIC MAZUR

GEBOREN TE AMSTERDAM IN 1954

**1981
DRUKKERIJ J.H. PASMANS B.V., 's-GRAVENHAGE**

Promotor: PROF. DR. J.J.M. BEENAKKER

Dit proefschrift is tot stand gekomen mede onder leiding van dr. L.J.F. Hermans

Het onderzoek is uitgevoerd mede onder verantwoordelijkheid van
wijlen prof. dr. H.F.P. Knaap

Het in dit proefschrift beschreven onderzoek werd uitgevoerd als onderdeel van het programma van de werkgemeenschap voor Molecuulfysica van de Stichting voor Fundamenteel Onderzoek der Materie (FOM) en is mogelijk gemaakt door financiële steun van de Nederlandse Organisatie voor Zuiver-Wetenschappelijk Onderzoek (ZWO).

CONTENTS

PREFACE		9
CHAPTER I	KINETIC THEORY OF NON-UNIFORM GASES IN THE PRESENCE OF EXTERNAL FIELDS	11
	1. Introduction	11
	2. The basic equations	12
	3. The non-equilibrium state	14
	4. Formal expressions for phenomenological coefficients in the field free case	15
	5. Example: heat conduction in a simple gas	17
	6. External fields	18
	7. The splitting of the collision operator	21
	8. General properties of phenomenological coefficients	24
	9. The field dependence of phenomenological coefficients	26
	10. Mixtures	28
	11. Field dependence in a polyatomic gas - noble gas mixture	32
	12. The heat flux, the diffusion velocity and the viscous pressure tensor	33
CHAPTER II	EXPERIMENTS ON THE VISCOSITY OF POLAR GASES IN MAGNETIC AND ELECTRIC FIELDS	37
	1. Introduction	37
	2. Theory	39
	3. Description of the experimental set-up	42
	4. Corrections	44
	5. Experimental results	47
	6. Discussion	56
CHAPTER III	EXPERIMENTS ON THE INFLUENCE OF A MAGNETIC FIELD ON DIFFUSION IN N_2 -NOBLE GAS MIXTURES	59
	1. Introduction	59
	2. Theory	60
	3. Description of the experimental set-up	63
	4. Experimental checks and corrections	65
	5. Results	66
	6. Discussion	71
APPENDIX	Derivation of a general relation between field effects	76

CHAPTER IV	A COMPARISON OF DATA ON THE VISCOMAGNETIC EFFECT, FLOW BIREFRINGENCE AND DEPOLARIZED RAYLEIGH LINE BROADENING	78
	1. Introduction	78
	2. The viscomagnetic effect	80
	3. Flow birefringence	81
	4. Comparison of the viscomagnetic effect and flow birefringence	85
	5. Depolarized Rayleigh line broadening	86
	6. Comparison with the viscomagnetic effect and the flow birefringence	91
	7. Model calculations	93
APPENDIX	A. Symmetric top molecules	95
APPENDIX	B. Mixtures	95
CONCLUDING REMARKS		99
REFERENCES		101
NOMENCLATURE		105
SAMENVATTING		109
CURRICULUM VITAE		111

The chapters of this thesis will be submitted for publication to Physica

PREFACE

In the kinetic theory of non-equilibrium phenomena in dilute polyatomic gases there is a characteristic difference between the treatment of non-spherical and spherical particles. This difference stems from the fact that in a polyatomic gas, i.e. a gas of non-spherical particles, in the non-equilibrium state not only the distribution of molecular velocities becomes anisotropic, but that also the distribution of the orientations of the molecules is affected by macroscopic thermodynamic forces. These deviations from an isotropic distribution of angular momenta, or *polarizations*, are generally complicated in nature and may depend on both velocity and angular momentum. Their presence was first realized by Pidduck in 1922. In their book on non-uniform gases Chapman and Cowling were aware of the anisotropies in both the velocity and the rotational angular momentum, but in subsequent calculations they neglected the effects of the angular momentum dependent terms. Later in 1961, Kagan and Afanas'ev showed that for a simplified classical model such terms give rise to sizable contributions to the transport properties.

Experimental information on polarizations are obtained in various ways. First of all, field effects on transport phenomena, which as Kagan and Maksimov showed are a direct consequence of the existence of such polarizations, yield a wealth of data. Secondly, information is obtained by measuring the non-equilibrium birefringence caused by the anisotropy in the orientational distribution of the molecules. Additional information on certain aspects, e.g. relaxation times of polarizations, can be obtained from a study of phenomena which are determined by (equilibrium) fluctuations, such as the depolarized Rayleigh line broadening and nuclear magnetic resonance.

Polarizations can be thought of as consisting of two parts: a tensorial factor (of rank one or higher) depending on the orientation of the molecule and

the direction in which the molecule is moving, and a scalar factor depending on the magnitudes of both the molecular velocity and the rotational angular momentum.

From studies of the dependence of field effects on the orientation of the field with respect to the gradient, the tensorial factors of polarizations produced by various macroscopic thermodynamic forces have been determined unambiguously. On the scalar structure, however, no information can be obtained from these experiments separately.

An analogous situation exists with respect to the importance of higher order Sonine polynomials in the molecular velocity when one considers transport phenomena of noble gases. Measurement of one transport property by itself does not allow any conclusions to be drawn in this regard. One can, however, resort in this case to the verification of specific relations existing between different transport properties, such as the relation involving the Eucken factor. In a similar way internal consistency checks and a comparison of field effects with optical measurements might lead to more detailed information about the structure of polarizations in polyatomic gases. So far such comparisons have not or only partially been carried out.

In this thesis two experiments are described which enable some decisive consistency checks to be performed. In chapter II experiments on the influence of external electric and magnetic fields on the viscosity of some polar gases are described. Next, in chapter III, experiments on the influence of a magnetic field on diffusion in N_2 -noble gases are presented. These experiments - apart from yielding new numerical results - show very clearly that the structure of polarizations is much more complicated than was usually assumed so far, and that it is not possible to get detailed quantitative information on the scalar factor from experiments on field effects alone. For this reason a detailed analysis and comparison between the results of field effects and the results of optical measurements has been carried out. As we will see in chapter IV this comparison indeed clarifies the structure of polarizations.

In order to present the results in a uniform and unambiguous way the kinetic theory of rotating molecules, which for this purpose has been modified and extended, is formulated at the beginning of this thesis in chapter I*).

*) The author acknowledges the inspiring help offered by Professor I. Kuščer in working out the theoretical chapter during a stay at the "Oddelek za fiziko" of the University of Ljubljana, Yugoslavia.

CHAPTER I

KINETIC THEORY OF NON-UNIFORM GASES IN THE PRESENCE OF EXTERNAL FIELDS

1. Introduction

In 1930 Senftleben discovered that the thermal conductivity of oxygen changes in a magnetic field¹⁾. The first analysis of this effect on the basis of a mean free path theory was given by Gorter^{2,3)} in 1938 and worked out in more detail by Zernike and Van Lier⁴⁾ in 1939. In 1961 Kagan and Afanas'ev stated that, in a polyatomic gas, the presence of gradients gives rise to anisotropies not only in the velocity distribution, but also in the internal angular momentum distribution⁵⁾. Subsequently Kagan and Maksimov showed that the latter anisotropy is the basic cause of field effects⁶⁾.

After the demonstration by Beenakker in 1962⁷⁾ that field effects are a general property of polyatomic gases and not only of paramagnetic molecules such as oxygen, these effects have been studied quite intensively both experimentally and theoretically. For a theoretical description the original form of the Boltzmann equation is no longer applicable since this equation does not take into account the internal degrees of freedom of the molecule. An adequate generalization was derived independently by Waldmann⁸⁾ and Snider⁹⁾. To solve this Waldmann-Snider equation, techniques generally based upon the solution procedures for the classical Boltzmann equation have been developed. A generalization of the Chapman and Enskog procedure was given by McCourt and Snider^{10,11)} and Snider^{12,13)} and formulated in a compact way in terms of inverse operators¹⁴⁻¹⁶⁾, while Waldmann presented a generalization of the moment method^{17,18)}.

The large amount of experimental information about field effects in dilute polyatomic gases accumulated in the last two decades has greatly contributed to the further development of the theory. It is the purpose of this chapter to

summarize the theory for transport phenomena in dilute polyatomic gases in the presence of external fields, taking into account the latest experimental results. The foundations of the theory will be given only schematically, for the details the reader is referred to the works cited above.

For the sake of clarity, we shall first present in sections 2 through 5 the general scheme for the derivation of phenomenological coefficients for a simple gas in the absence of external fields, and introduce in the subsequent sections the modifications needed in the presence of such fields. In sections 10 and 11 a generalization of the scheme will be given for mixtures.

The description will be restricted to dilute gases of diamagnetic symmetric top molecules (including linear molecules). Moreover only rotational states will be taken into account, since for most gases considered here vibrationally excited states do not play a significant role at room temperature.

2. The basic equations

To describe a gas of molecules with internal states one needs a quantum mechanical representation. The state of a molecule is then described by a single particle density matrix depending on time, on the position of the molecule and on the internal (vibrational, rotational and magnetic) quantum numbers. In practical cases however, the translational motion of the molecule can very well be described classically. We therefore introduce a quantity f , which is simultaneously a distribution function in molecular phase space and a statistical operator, or density matrix, in internal state space. This operator f will simply be called distribution.

We shall assume that f is diagonal in the angular momentum quantum numbers, i.e. J for linear molecules and J and K for symmetric top molecules (J and K correspond to the total angular momentum and to its projection on the symmetry axis of the molecule, respectively). Therefore, f can be expressed in terms of the dimensionless operator \underline{J} ($\hbar \underline{J}$ is the molecular angular momentum). Physically this is justified if, as is usually the case, the spacing between energy levels is large compared to \hbar -times the collision frequency of the molecules. Under such condition, during the time between collisions off-diagonal elements are destroyed by phase randomization¹⁹).

The evolution of f in time t is described by the Waldmann-Snider equation. Schematically this equation reads

$$\frac{\partial f}{\partial t} + \underline{c} \cdot \frac{\partial f}{\partial \underline{r}} + \underline{a} \cdot \frac{\partial f}{\partial \underline{c}} + \frac{i}{\hbar} [H_{int}, f] = \left(\frac{\partial f}{\partial t} \right)_{coll} , \quad (1)$$

with \underline{r} , \underline{c} and \underline{a} the position, velocity and acceleration of the molecule; H_{int} is the internal-state Hamiltonian and $[H_{int}, f]$ the commutator of H_{int} and f . The main difference with the classical Boltzmann equation, however, lies in the explicit form of the collision term, which represents the rate of change of f due to binary collisions. It is to be understood that this term is restricted to the part diagonal in J and K .

If only rotational states are considered, the local equilibrium solution of the Waldmann-Snider equation can be written as

$$f^o = n \frac{1}{Z_{rot}} \left(\frac{m}{2\pi kT} \right)^{\frac{3}{2}} \exp \left\{ -W^2 - \frac{H_{rot}}{kT} \right\} , \quad (2)$$

with the reduced molecular velocity

$$\underline{W} = \sqrt{\frac{m}{2kT}} (\underline{c} - \underline{v}) \quad (3)$$

and the rotational partition function

$$Z_{rot} = \text{Tr} \exp \left\{ -\frac{H_{rot}}{kT} \right\} . \quad (4)$$

In these equations n , \underline{v} and T are the local values of particle density, mean flow velocity and temperature respectively, m is the molecular mass and k the Boltzmann constant. The symbol "Tr" denotes the trace with respect to the internal quantum numbers. The dependence of f^o on the angular momentum \underline{J} is contained in the Hamiltonian. For symmetric top molecules e.g., one has

$$H_{rot} = \frac{\hbar^2}{2I_{\perp}} [\underline{J}^2 + \left(\frac{I_{\perp}}{I_{\parallel}} - 1 \right) J_{\parallel}^2] , \quad (5)$$

where J_{\parallel} is the component of \underline{J} along the symmetry axis of the molecule (for linear molecules $J_{\parallel} = 0$) and I_{\parallel} and I_{\perp} are the moments of inertia of the molecules with respect to an axis parallel and perpendicular to the symmetry axis.

3. The non-equilibrium state

In order to find a solution for f in the non-equilibrium state, a procedure analogous to the Enskog successive approximation method²⁰⁾ is followed. Only the first-order approximation will be considered. We therefore write the distribution f in the form

$$f = f^0 (1 + \phi) . \quad (6)$$

The function ϕ , which describes the deviation of the actual distribution from local equilibrium, is considered to be small.

The solution for f may be used to determine the mean macroscopic values of any observable quantity A (a self-adjoint density matrix) according to

$$\langle A \rangle = \frac{1}{n} \text{Tr} \int A f d\underline{c} . \quad (7)$$

If the equilibrium average $\langle A \rangle_0$ vanishes we can rewrite $\langle A \rangle$ as follows

$$\langle A \rangle = \frac{1}{n} \text{Tr} \int A f^0 \phi d\underline{c} . \quad (8)$$

This leads us to introduce a Hilbert space of operators such as A and ϕ , with the scalar product as in eq. (8),

$$\langle A | \phi \rangle = \frac{1}{n} \text{Tr} \int A^\dagger f^0 \phi d\underline{c} . \quad (9)$$

The dagger has been added in case A is not self-adjoint. In such a case, if $\langle A \rangle_0$ vanishes

$$\langle A \rangle \equiv \langle A^\dagger \rangle^* \equiv \langle A | \phi \rangle^* . \quad (10)$$

By substituting the known zeroth-order (equilibrium) distribution f^0 into the left hand side of the Waldmann-Snyder equation (1) and retaining only linear terms with respect to ϕ in the rest of the equation, we obtain the following equation for ϕ

$$-\psi = n \mathcal{R} \phi . \quad (11)$$

Here, the term ψ contains derivatives of f^0 and \mathcal{R} is the linearized Waldmann-

Snider collision (super)operator¹³). The explicit form of \mathcal{R} is not important for the present discussion, the only properties required being its isotropy, its linearity and its dissipative nature. The operator is positive semi-definite¹³), but in general \mathcal{R} is not self-adjoint. One should moreover keep in mind that the collision operator has a 5-fold zero eigenvalue associated with the hydrodynamic eigenfunctions (the collisional invariants) 1, \underline{W} , and $E = W^2 + E_{int} / kT$. The formal solution of eq. (11) reads^{14,15,19})

$$\phi = -\frac{1}{n} \mathcal{R}^{-1} \psi . \quad (12)$$

The inverse operator \mathcal{R}^{-1} appearing in eq. (12) is defined on the subspace orthogonal to the collisional invariants (the "non-hydrodynamic subspace"). We shall use eq. (12) in the next section where we derive formal expressions for the phenomenological coefficients.

4. Formal expressions for phenomenological coefficients in the field free case

The general macroscopic conservation laws for mass, momentum and energy contain irreversible fluxes \underline{j}^α such as the diffusion flux, the heat flux and the viscous pressure tensor, which vanish in equilibrium. In non-equilibrium these fluxes obey linear phenomenological laws in the so-called linear regime. For vectorial forces and fluxes e.g., one has

$$\underline{j}^\alpha = - \sum_{\beta} \underline{L}^{\alpha\beta} \cdot \underline{X}^\beta , \quad (13)$$

where \underline{X}^β is the thermodynamic force conjugate (in the sense of Onsager, see e.g., ref. 21) to \underline{j}^β and $\underline{L}^{\alpha\beta}$ a phenomenological tensor which couples the flux \underline{j}^α to the force \underline{X}^β . Since the gas in equilibrium is isotropic, forces and fluxes of different tensorial character do not couple.

The macroscopic irreversible fluxes are averages of microscopic quantities and may be written as

$$\underline{j}^\alpha = \text{Tr} \int f [(\underline{c} - \underline{v}) Q_\alpha] d\underline{c} , \quad (14)$$

where Q_α is a molecular quantity such as mass, momentum or energy. We now introduce microscopic fluxes $\underline{\Psi}^\alpha = k^{-1}(\underline{c} - \underline{v})Q_\alpha$ and rewrite eq. (14) according to

eq. (9) as

$$\underline{J}^\alpha = nk < \underline{\Psi}^\alpha | \phi >^* . \quad (15)$$

On the other hand the inhomogeneous term ψ may be written as a sum of products of conjugate thermodynamic forces and microscopic fluxes^{10,22)}

$$\psi = \sum_{\beta} \underline{\Psi}^\beta \cdot \underline{X}^\beta . \quad (16)$$

By substituting the formal solution of the deviation (12) into eq. (15) we now obtain

$$\underline{J}^\alpha = -k \sum_{\beta} < \underline{\Psi}^\alpha | \mathcal{R}^{-1} \underline{\Psi}^\beta >^* \cdot \underline{X}^\beta . \quad (17)$$

Comparing this result to eq. (13) we find that the phenomenological coefficient can formally be written as

$$\underline{L}^{\alpha\beta} = k < \underline{\Psi}^\alpha | \mathcal{R}^{-1} \underline{\Psi}^\beta >^* , \quad (18)$$

which, for $\alpha = \beta$ reduces to

$$\underline{L}^{\alpha\alpha} = k < \underline{\Psi}^\alpha | \mathcal{R}^{-1} \underline{\Psi}^\alpha >^* . \quad (19)$$

Expression (18) has been derived for vectorial transport phenomena, i.e., \underline{J} , \underline{X} and $\underline{\Psi}$ are vectors. For those cases where \underline{J} and \underline{X} (and consequently $\underline{\Psi}$) are tensors of rank n we have to replace the second order tensors \underline{L} in these expressions by tensors of rank $2n$.

According to the Curie symmetry principle, spatial symmetries of the system influence the coupling of (components of) fluxes and forces. In particular, for isotropic systems, the tensors $\underline{L}^{\alpha\beta}$ and $\underline{L}^{\alpha\alpha}$ are isotropic. Consequently, in the linear laws (13) these tensors can be replaced by scalar coefficients $L^{\alpha\beta}$ and $L^{\alpha\alpha}$. Though for simple gases only diagonal phenomenological coefficients $L^{\alpha\alpha}$ occur in practice, we will continue to keep the scheme more general, for the sake of subsequent extension to mixtures.

5. Example: heat conduction in a simple gas

As an illustration of the preceding paragraph we will now discuss the vectorial phenomenon of heat conduction. For polyatomic gases both translational and internal degrees of freedom contribute to the transport of energy. The heat flux \underline{j}^Q is defined as

$$\underline{j}^Q = \text{Tr} \int f(\underline{c} - \underline{v}) \left[\frac{1}{2} m (\underline{c} - \underline{v})^2 + E_{\text{int}} \right] d\underline{c} . \quad (20)$$

This flux is related to the thermodynamic force

$$\underline{X}^Q = \frac{\nabla T}{T^2} \quad (21)$$

by the linear law

$$\underline{j}^Q = -\underline{L}^{QQ} \cdot \underline{X}^Q . \quad (22)$$

This is Fourier's law and is customarily written in the form

$$\underline{q} = -\underline{\lambda} \cdot \nabla T , \quad (23)$$

where $\underline{\lambda} = \underline{L}^{QQ}/T^2$ is the thermal conductivity tensor and $\underline{q} \equiv \underline{j}^Q$.

We now introduce a microscopic flux

$$\underline{\psi}^Q = T \sqrt{\frac{2kT}{m}} \left(W^2 - \frac{5}{2} + \mathcal{E} - \langle \mathcal{E} \rangle \right) \underline{W} , \quad (24)$$

with the dimensionless rotational energy per molecule

$$\mathcal{E} = \frac{E_{\text{rot}}}{kT} . \quad (25)$$

The heat flux (20) can now be rewritten as a scalar product of the vector $\underline{\psi}^Q$ with the deviation ϕ :

$$\underline{j}^Q = nk \langle \underline{\psi}^Q | \phi \rangle^* . \quad (26)$$

On the other hand, for a heat conducting gas, the inhomogeneous term reads

$$\underline{\psi} = \underline{\psi}^Q \cdot \frac{\nabla T}{T^2} \quad (27)$$

and consequently, if we substitute the formal solution (12) of the Waldmann-Snider equation,

$$\underline{\underline{L}}^{qq} = k \langle \underline{\Psi}^q | \mathcal{R}^{-1} \underline{\Psi}^q \rangle^* . \quad (28)$$

The thermal conductivity tensor of eq. (23) then becomes

$$\underline{\underline{\lambda}} = kT^{-2} \langle \underline{\Psi}^q | \mathcal{R}^{-1} \underline{\Psi}^q \rangle^* . \quad (29)$$

By symmetry this tensor is isotropic and therefore equal to a scalar thermal conductivity coefficient λ times the unit tensor.

6. External fields

In the presence of external fields the internal-state Hamiltonian can be written as

$$H_{\text{int}} = H_{\text{rot}} + H_{\text{field}} , \quad (30)$$

where we have again neglected vibrationally excited states. As we want the distribution to remain diagonal in the quantum numbers J and K , we only need to consider the diagonal part of H_{int} in the commutator $[H_{\text{int}}, f]$ appearing in eq. (1). The reason for this restriction is the same as for the collision term (cf. section 2). For diamagnetic symmetric top molecules in magnetic and electric fields we have²³⁾

$$H_{\text{Zeeman},d} = -\mu_N \left(\underline{\underline{g}} : \frac{\underline{\underline{J}}\underline{\underline{J}}}{J^2} \right) \underline{\underline{J}} \cdot \underline{\underline{B}} \quad (31)$$

and²⁴⁾

$$H_{\text{Stark},d} = -\mu_e \frac{J_{\parallel}}{J^2} \underline{\underline{J}} \cdot \underline{\underline{E}} , \quad (32)$$

respectively. Here, μ_N and μ_e are the nuclear magneton and the electric dipole moment of the molecule, respectively, and $\underline{\underline{g}}$ the rotational Landé tensor

$$g = \begin{pmatrix} g_{\perp} & 0 & 0 \\ 0 & g_{\perp} & 0 \\ 0 & 0 & g_{\parallel} \end{pmatrix}, \quad (33)$$

where the symmetry axis of the molecule has been taken in the third direction (for spherical top molecules $g_{\parallel} = g_{\perp}$). The symbol — denotes the symmetric traceless part of a tensor.

Consequently, eq. (1) will contain an additional term of the form $i\hbar^{-1}\mathcal{L}\phi$, where \mathcal{L} is the (field dependent part of the) Liouville operator, defined according to

$$\hbar \mathcal{L} \phi = -\omega [\mathcal{J}_z, \phi]. \quad (34)$$

Here and henceforth the field is taken in the z -direction. The Larmor frequency ω (which has the opposite sign of the precession frequency of the molecules) reads

$$\omega = \frac{g_{\perp} \mu_N}{\hbar} \left[1 + \frac{g_{\parallel} - g_{\perp}}{g_{\perp}} \frac{K^2}{J(J+1)} \right] B \quad (35)$$

and

$$\omega = \frac{\mu_e}{\hbar} \frac{K}{J(J+1)} E \quad (36)$$

in magnetic and electric fields, respectively.

Equation (11) now becomes

$$-\psi = \hbar (\mathcal{R} + i\mathcal{L}) \phi \quad (37)$$

and expression (18) for the phenomenological coefficient $\underline{L}^{\alpha\beta}$ has to be modified accordingly,

$$\underline{L}^{\alpha\beta} = k \langle \underline{\psi}^{\alpha} | (\mathcal{R} + i\mathcal{L})^{-1} \underline{\psi}^{\beta} \rangle^* \quad (38)$$

For the evaluation of phenomenological coefficients, such as given by eq. (38) it is convenient to introduce a basis κ of orthonormalized tensors to span the Hilbert space. Their general form is given by

$$\Phi_{\underline{\mu}\underline{\nu}}^{pq\mathcal{S}} = \left(\frac{2^p}{p!}\right)^{\frac{1}{2}} [\underline{W}]^p [\underline{J}]^q P_{\mathcal{S}}, \quad (39)$$

where $[\underline{W}]^p$ is an irreducible tensor²⁵⁻²⁷⁾ of rank p in \underline{W} and $[\underline{J}]^q$ a normalized irreducible tensor of rank q formed from the operator \underline{J} according to

$$[\underline{J}]^q = (2q+1)^{\frac{1}{2}} \frac{[\underline{J}]^q}{\{[\underline{J}]^q \bullet [\underline{J}]^q\}^{\frac{1}{2}}}. \quad (40)$$

The dot in the denominator denotes a q -fold contraction of indices. The zero eigenvalue of \underline{J} can be excluded since molecules with $J = 0$ do not play any role in field effects. This means that the inverse operator \underline{J}^{-1} is positive definite and consequently the square root in eq. (40) can be taken. The remaining normalized scalar factor $P_{\mathcal{S}}$ may depend upon W^2 , J^2 and J_{\parallel} .

In spherical components the normalization condition reads

$$\langle \Phi_{\underline{\mu}\underline{\nu}}^{pq\mathcal{S}} | \Phi_{\underline{\mu}'\underline{\nu}'}^{p'q'\mathcal{S}'} \rangle = \delta_{pp'} \delta_{qq'} \delta_{\mathcal{S}\mathcal{S}'} \delta_{\underline{\mu}\underline{\mu}'} \delta_{\underline{\nu}\underline{\nu}'}, \quad (41)$$

with

$$\Phi_{\underline{\mu}\underline{\nu}}^{pq\mathcal{S}} = \left(\frac{2^p}{p!}\right)^{\frac{1}{2}} [\underline{W}]_{\underline{\mu}}^p [\underline{J}]_{\underline{\nu}}^q P_{\mathcal{S}}. \quad (42)$$

The relation between spherical and Cartesian components of a vector \underline{r} are²⁸⁾

$$r_0 = r_z; \quad r_{\pm 1} = \mp \frac{1}{2} \sqrt{2} (r_x \pm i r_y) \quad (43)$$

and similarly for tensors.

The matrix elements of the inverse operator $(\mathcal{R} + i\mathcal{L})^{-1}$ in eq. (38) will be approximated in terms of matrix elements of \mathcal{R} by aid of the set of orthonormal tensors. Because of the isotropy of \mathcal{R} , these matrix elements can be decomposed according to the Wigner-Eckart theorem. Following the coupling scheme of Chen, Moraal and Snider²⁹⁾, we have

$$\begin{aligned} \langle \Phi_{\underline{\mu}\underline{\nu}}^{pq\mathcal{S}} | \mathcal{R} \Phi_{\underline{\mu}'\underline{\nu}'}^{p'q'\mathcal{S}'} \rangle &= \sum_{L,M} i^{p-p'+q-q'} (-1)^{L+p+q+\mu+\nu'} \sqrt{\Omega(p p' L) \Omega(q q' L)} \\ &\times \begin{pmatrix} p & p' & L \\ -\mu & \mu' & -M \end{pmatrix} \begin{pmatrix} q & q' & L \\ -\nu & \nu' & M \end{pmatrix} S_L \begin{pmatrix} p & q & \mathcal{S} \\ p' & q' & \mathcal{S}' \end{pmatrix}. \end{aligned} \quad (44)$$

The isotropic tensorial factor is represented in terms of $3j$ -symbols²⁸⁾ and the factor

$$\Omega(\ell_1 \ell_2 \ell_3) = \frac{(\ell+1)! (\ell-2\ell_1)! (\ell-2\ell_2)! (\ell-2\ell_3)!}{(2\ell_1)! (2\ell_2)! (2\ell_3)!} \frac{3 - (-1)^\ell}{2}, \quad (45)$$

with $\ell = \ell_1 + \ell_2 + \ell_3$. The reduced matrix element S_L is a scalar and is expressed in terms of an effective cross section $\mathfrak{S}_L(pq, s, p'q', s')$, which describes the collisional coupling of the pqs and the $p'q's'$ tensor, as follows

$$S_L(pq, s, p'q', s') = \langle v \rangle \mathfrak{S}_L(pq, s, p'q', s'). \quad (46)$$

As far as the notation of the \mathfrak{S} 's is concerned the subscript L is omitted if only one value is possible. Furthermore, if $pqs = p'q's'$ one row of indices will be suppressed and similarly the last column if $p_s = p_{s'} = 1$. The nomenclature is as follows: a cross section with $pqs \neq p'q's'$ is called a production cross section when either q or q' equals zero and a transfer cross section when neither q nor q' is zero. If $pqs = p'q's'$ and $q \neq 0$ it is called a decay cross section. The factor $\langle v \rangle$ is the average relative speed

$$\langle v \rangle = \sqrt{\frac{16 kT}{\pi m}}. \quad (47)$$

Next, we have

$$L \Phi_{\mu\nu}^{pq, s} = -\frac{1}{n} \omega \nu \Phi_{\mu\nu}^{pq, s} \quad (48)$$

and thus the matrix elements of the Liouville operator are

$$\langle \Phi_{\mu\nu}^{pq, s} | L \Phi_{\mu'\nu'}^{p'q', s'} \rangle = -\delta_{pp'} \delta_{qq'} \delta_{ss'} \delta_{\mu\mu'} \delta_{\nu\nu'} \frac{1}{n} \nu \langle P_s^2 \omega \rangle. \quad (49)$$

For linear molecules ω does not depend on \underline{J} and consequently $\langle P_s^2 \omega \rangle = \omega$.

7. The splitting of the collision operator

The coupling between \underline{H} and \underline{J} is only non-zero for a non-spherical potential. It is still small in the cases of interest here, as one can conclude from the observed magnitude of field effects. Therefore the complete set of tensors $\Phi^{pq, s}$ (39) is split into a part π_0 containing all tensors which are

isotropic in the angular momentum ($q = 0$) and a complementary part κ_1 ($q \neq 0$). In the same way also the collision operator is decomposed^{30,19,22,31)}

$$\mathcal{R} = \mathcal{R}_d + \mathcal{R}_{nd}, \quad (50)$$

where the diagonal part \mathcal{R}_d couples the tensors within each set κ_0 and κ_1 and the non-diagonal part \mathcal{R}_{nd} accounts for the weaker coupling between tensors from κ_0 and those from κ_1 . The operator $(\mathcal{R} + i\mathcal{L})^{-1}$ can now be expanded in terms of \mathcal{R}_{nd} as

$$(\mathcal{R} + i\mathcal{L})^{-1} = (\mathcal{R}_d + i\mathcal{L})^{-1} + (\mathcal{R}_d + i\mathcal{L})^{-1} \mathcal{R}_{nd} (\mathcal{R}_d + i\mathcal{L})^{-1} + (\mathcal{R}_d + i\mathcal{L})^{-1} \mathcal{R}_{nd} (\mathcal{R}_d + i\mathcal{L})^{-1} \mathcal{R}_{nd} (\mathcal{R}_d + i\mathcal{L})^{-1} + \dots \quad (51)$$

Since the microscopic fluxes $\underline{\Psi}^\alpha$ and $\underline{\Psi}^\beta$ are isotropic in \underline{J} , the zeroth-order contribution to $L_{\mu\mu}^{\alpha\beta}$, is

$$L_{\mu\mu}^{\alpha\beta 101} = k \langle \underline{\Psi}_\mu^\alpha | (\mathcal{R}_d + i\mathcal{L})^{-1} \underline{\Psi}_\mu^\beta \rangle^* = \langle \underline{\Psi}_\mu^\alpha | \mathcal{R}_d^{-1} \underline{\Psi}_\mu^\beta \rangle, \quad (52)$$

which, to a good approximation, represents the field free isotropic value of the spherical $\mu\mu'$ component of $\underline{L}^{\alpha\beta}$. We now introduce normalized (cf. eq. (41)) microscopic fluxes

$$\underline{\Phi}^\alpha = \frac{\underline{\Psi}^\alpha}{C^\alpha}, \quad \underline{\Phi}^\beta = \frac{\underline{\Psi}^\beta}{C^\beta}, \quad (53)$$

(both have the same rank \underline{n} in \underline{W} and zero in $[\underline{J}]$, but their scalar factors may be different) and apply the Wigner-Eckart theorem (cf. eq. (44), with $q = q' = 0$)

$$L_{\mu\mu}^{\alpha\beta 101} = k C^\alpha C^\beta \langle \underline{\Phi}_\mu^\alpha | \mathcal{R}_d^{-1} \underline{\Phi}_\mu^\beta \rangle = \delta_{\mu\mu} k C^\alpha C^\beta S^{-1}(\alpha)_\beta. \quad (54)$$

The reduced matrix element $S^{-1}(\alpha)_\beta$ is the $\alpha\beta$ -element of the inverse of the matrix S consisting of matrix elements of \mathcal{R}_d with respect to the complete set $\kappa_0: \{ \underline{\Phi}^\alpha, \underline{\Phi}^\beta, \dots \}$

$$S = \begin{pmatrix} S(\alpha) & S(\alpha)_\beta & \dots \\ S(\beta)_\alpha & S(\beta) & \dots \\ \vdots & \vdots & \ddots \end{pmatrix} = \langle v \rangle \begin{pmatrix} \mathcal{Q}(\alpha) & \mathcal{Q}(\alpha)_\beta & \dots \\ \mathcal{Q}(\beta)_\alpha & \mathcal{Q}(\beta) & \dots \\ \vdots & \vdots & \ddots \end{pmatrix}. \quad (55)$$

In the simplest approximation, i.e. if only one tensor Φ^α from \mathcal{K}_0 would be taken into account, we have, e.g.,

$$S^{-1} = \frac{1}{\langle \nu \rangle \mathcal{G}(\alpha)} . \quad (56)$$

The first-order contribution $L_{\mu\mu'}^{\alpha\beta[1]}$ vanishes, due to the odd number of non-diagonal couplings. The second-order contribution will to a good approximation contain the field dependent part of $L_{\mu\mu'}^{\alpha\beta}$,

$$L_{\mu\mu'}^{\alpha\beta[2]} = k \langle \Psi_\mu^\alpha | \mathcal{R}_d^{-1} \mathcal{R}_{nd} (\mathcal{R}_d + i\mathcal{L})^{-1} \mathcal{R}_{nd} \mathcal{R}_d^{-1} \Psi_{\mu'}^\beta \rangle^* . \quad (57)$$

We are mainly interested in the change of phenomenological coefficients in magnetic or electric fields which is given by

$$\Delta L_{\mu\mu'}^{\alpha\beta} \equiv L_{\mu\mu'}^{\alpha\beta}(B, E) - L_{\mu\mu'}^{\alpha\beta}(0) = L_{\mu\mu'}^{\alpha\beta[2]}(B, E) - L_{\mu\mu'}^{\alpha\beta[2]}(0) . \quad (58)$$

If we write

$$\underline{\chi}^\alpha = \mathcal{R}_{nd} \mathcal{R}_d^{-1} \underline{\Psi}^\alpha , \quad \underline{\chi}^\beta = \mathcal{R}_{nd} \mathcal{R}_d^{-1} \underline{\Psi}^\beta , \quad (59)$$

the expression for this change becomes

$$\Delta L_{\mu\mu'}^{\alpha\beta} = k \langle R \chi_\mu^\alpha | [(\mathcal{R}_d + i\mathcal{L})^{-1} - \mathcal{R}_d^{-1}] \chi_{\mu'}^\beta \rangle^* , \quad (60)$$

where we have used the property of \mathcal{R} that its (superoperator) adjoint is equal to \mathcal{R}^\dagger)

$$\mathcal{R}^\dagger = R \mathcal{R} R , \quad (61)$$

with R the angular momentum reversal operator (a combination of time reversal and space inversion). The saturation value of the effect is then given by

$$\Delta L_{\mu\mu'}^{\alpha\beta}(\infty) = -k \langle R \chi_\mu^\alpha | \mathcal{R}_d^{-1} \chi_{\mu'}^\beta \rangle . \quad (62)$$

This equation will be useful for the discussion of some general properties of phenomenological coefficients in the next section.

8. General properties of phenomenological coefficients

In the absence of external fields the phenomenological coefficients are given by a matrix element of the inverse collision operator (cf. eq. (18)).

The field independent collision operator is isotropic, with the consequence that only microscopic fluxes of the same tensorial rank and parity couple. The phenomenological coefficients are therefore real isotropic tensors¹⁹⁾

$$L_{\mu\mu}^{\alpha\beta} = \delta_{\mu\mu} L^{\alpha\beta} . \quad (63)$$

From the time reversal invariance of molecular interaction one obtains the Onsager relations

$$L^{\alpha\beta} = L^{\beta\alpha} , \quad (64)$$

where we have used the fact that the microscopic fluxes which couple have the same time reversal symmetry. Since \mathcal{R} is a positive semidefinite operator and its inverse is positive definite on the non-hydrodynamical subspace, we have

$$L^{\alpha\alpha} , L^{\beta\beta} > 0 \quad (65)$$

and (from the Schwartz inequality)

$$(L^{\alpha\beta})^2 \leq L^{\alpha\alpha} L^{\beta\beta} . \quad (66)$$

Note that eqs. (65) and (66) are a consequence of the dissipative nature of the collision term. Both properties can also be derived from the fact that entropy production is positive definite²¹⁾.

In the presence of an external field $L_{\mu\mu}^{\alpha\beta}$, is given by (38). Since the operator $(\mathcal{R} + i\mathcal{L})^{-1}$ occurring in this equation is still invariant for rotations around the field direction, the phenomenological tensors in the presence of an external (magnetic or electric) field are diagonal in spherical representation

$$L_{\mu\mu}^{\alpha\beta}(B, E) = \delta_{\mu\mu} L_{\mu\mu}^{\alpha\beta}(B, E) . \quad (67)$$

Similarly, from a rotation of 180° around an axis perpendicular to the field axis, it follows that

$$L_{\mu\mu}^{\alpha\beta}(B, E) = L_{\mu\mu}^{\alpha\beta*}(-B, -E) , \quad (68)$$

which means that the real part of $L_{\mu\mu}^{\alpha\beta}$ is even and the imaginary part odd in the field.

Space inversion symmetry (not applicable to optically active gases) yields

$$L_{\mu\mu}^{\alpha\beta}(B, E) = L_{\mu\mu}^{\alpha\beta}(B, -E) , \quad (69)$$

which implies that in the electric field case odd-in-field coefficients vanish. Finally, from time reversal symmetry one obtains the Onsager-Casimir relations¹⁹⁾

$$L_{\mu\mu}^{\alpha\beta}(B, E) = L_{\mu\mu}^{\beta\alpha*}(-B, E) . \quad (70)$$

The saturation value of the field induced change in $L_{\mu\mu}^{\alpha\beta}$ is given by eq. (62). The quantities $\underline{\chi}^\alpha$ and $\underline{\chi}^\beta$ in this expression are assumed to be both either even or odd in the angular momentum operator \underline{J} (as we will see in eq. (80), couplings off-diagonal in p and q will be neglected). For $\underline{\chi}$ of more complicated nature the following remains valid for the separate even and odd parts of $\underline{\chi}$. The operator \mathcal{R}_d is, just as \mathcal{R} itself, a positive semidefinite operator since for any $\Phi = \Phi_0 + \Phi_1$, with $\Phi_0 \in \mathcal{K}_0$, $\Phi_1 \in \mathcal{K}_1$

$$\langle \Phi | \mathcal{R}_d \Phi \rangle = \langle \Phi_0 | \mathcal{R} \Phi_0 \rangle + \langle \Phi_1 | \mathcal{R} \Phi_1 \rangle \geq 0 . \quad (71)$$

Consequently, if the $\underline{\chi}$ are even-in- \underline{J} , so that $R\underline{\chi} = \underline{\chi}$, we have

$$\Delta L_{\mu\mu}^{\alpha\alpha}(\infty) , \Delta L_{\mu\mu}^{\beta\beta}(\infty) \leq 0 . \quad (72)$$

For $\underline{\chi}$ odd-in- \underline{J} on the contrary, when $R\underline{\chi} = -\underline{\chi}$, the saturation values will be larger than zero

$$\Delta L_{\mu\mu}^{\alpha\alpha}(\infty) , \Delta L_{\mu\mu}^{\beta\beta}(\infty) > 0 . \quad (73)$$

Let us now investigate the $\Delta L_{\mu\mu}^{\alpha\beta}$ for $\alpha \neq \beta$. For these quantities we shall derive a Schwartz inequality. For arbitrary a and b one has

$$\langle a\chi_\mu^\alpha + b\chi_\mu^\beta | \mathcal{R}_d^{-1}(a\chi_\mu^\alpha + b\chi_\mu^\beta) \rangle \geq 0 . \quad (74)$$

Thus, if

$$a = \langle \chi_{\mu}^{\beta} | \mathcal{R}_d^{-1} \chi_{\mu}^{\beta} \rangle^{\frac{1}{2}} \langle \chi_{\mu}^{\alpha} | \mathcal{R}_d^{-1} \chi_{\mu}^{\beta} \rangle^{\frac{1}{2}} \quad (75)$$

and

$$b = \langle \chi_{\mu}^{\alpha} | \mathcal{R}_d^{-1} \chi_{\mu}^{\alpha} \rangle^{\frac{1}{2}} \langle \chi_{\mu}^{\beta} | \mathcal{R}_d^{-1} \chi_{\mu}^{\alpha} \rangle^{\frac{1}{2}}, \quad (76)$$

(74) becomes a Schwarz inequality,

$$\langle \chi_{\mu}^{\alpha} | \mathcal{R}_d^{-1} \chi_{\mu}^{\alpha} \rangle \langle \chi_{\mu}^{\beta} | \mathcal{R}_d^{-1} \chi_{\mu}^{\beta} \rangle \geq \langle \chi_{\mu}^{\alpha} | \mathcal{R}_d^{-1} \chi_{\mu}^{\beta} \rangle \langle \chi_{\mu}^{\beta} | \mathcal{R}_d^{-1} \chi_{\mu}^{\alpha} \rangle. \quad (77)$$

Since $\underline{\chi}^{\alpha}$ and $\underline{\chi}^{\beta}$ are assumed to be both either even or odd-in- \underline{r} this inequality may (in both cases) be written as

$$\langle R\chi_{\mu}^{\alpha} | \mathcal{R}_d^{-1} \chi_{\mu}^{\alpha} \rangle \langle R\chi_{\mu}^{\beta} | \mathcal{R}_d^{-1} \chi_{\mu}^{\beta} \rangle \geq \langle R\chi_{\mu}^{\alpha} | \mathcal{R}_d^{-1} \chi_{\mu}^{\beta} \rangle \langle R\chi_{\mu}^{\beta} | \mathcal{R}_d^{-1} \chi_{\mu}^{\alpha} \rangle \quad (78)$$

and consequently

$$\Delta L_{\mu\mu}^{\alpha\alpha}(\infty) \Delta L_{\mu\mu}^{\beta\beta}(\infty) \geq [\Delta L_{\mu\mu}^{\alpha\beta}(\infty)]^2. \quad (79)$$

The equality holds if $\underline{\chi}^{\alpha}$ is proportional to $\underline{\chi}^{\beta}$, which implies that both microscopic fluxes couple to one and the same tensor (both microscopic fluxes produce the same polarization). Equation (79) is a generalization of the relation between thermal conductivity, diffusion and their cross effects derived by Eggermont, Vestner and Knaap²²).

9. The field dependence of phenomenological coefficients

In order to simplify the evaluation of the field dependence of phenomenological coefficients one usually makes the so-called spherical approximation in the calculation of the matrix elements of the tensors. The approximation consists in neglecting in eq. (44) all terms with $L \neq 0$

$$\langle \Phi_{\mu\nu}^{pq\delta} | \mathcal{R}_d \Phi_{\mu'\nu'}^{p'q'\delta'} \rangle = \delta_{\mu\mu'} \delta_{\nu\nu'} \delta_{pp'} \delta_{qq'} \delta_{\delta\delta'} \langle \nu \rangle \otimes_0(pq\delta, p'q'\delta'), \quad (80)$$

and it applies only if none of $p, p', q, q' = 0$. Its name is derived from the fact that for an isotropic (spherical) potential all terms with $L \neq 0$ vanish³²). These contributions, which measure the coupling between \underline{W} and \underline{J} , are assumed to be much smaller than the spherical $L = 0$ contribution. Thus one has

$$\langle \Phi_{\mu\nu}^{pqs} | (\mathcal{R} + iL) \Phi_{\mu'\nu'}^{p'q's} \rangle^* = \delta_{pp'} \delta_{qq'} \delta_{\mu\mu'} \delta_{\nu\nu'} [\langle \nu \rangle \mathcal{G}_0(pqs) + \frac{i}{n} \nu \langle P_s^2 \omega \rangle], \quad (81)$$

and (if we neglect couplings off-diagonal in s) the elements of the inverse operator $(\mathcal{R} + iL)^{-1}$ are now equal to the inverse of the matrix elements.

With the normalized microscopic fluxes of eq. (53) the expression for the change in the phenomenological coefficient (cf. eqs. (57), (58)) now becomes

$$\Delta L_{\mu\mu'}^{\alpha\beta} = k C^\alpha C^\beta \sum_{pqs} \langle \Phi_{\mu}^\alpha | \mathcal{R}_d^{-1} \mathcal{R}_{nd} \Phi_{\mu'}^{pqs} \rangle \cdot \langle \Phi_{\mu'}^{pqs} | [(\mathcal{R}_d + iL)^{-1} - \mathcal{R}_d^{-1}] \Phi_{\mu}^{pqs} \rangle^* \cdot \langle \Phi_{\mu}^{pqs} | \mathcal{R}_{nd} \mathcal{R}_d^{-1} \Phi_{\mu'}^\beta \rangle \quad (82)$$

(α and β stand for triplets of labels: n , zero and a label which characterizes the scalar factor, cf. eq. (53)). All possible pqs -polarizations have now been included. Application of eq. (44) and the spherical approximation yields

$$\Delta L_{\mu\mu'}^{\alpha\beta} = \delta_{\mu\mu'} k C^\alpha C^\beta \sum_{pqs} (-1)^{p+q+n} \Omega(pqn) \sum_{\kappa, \nu} \begin{pmatrix} p & q & n \\ \kappa & \nu & -\mu \end{pmatrix}^2 \times \sum_{i,j} S^{-1}(\alpha)_i S(\beta)_j \frac{1}{S_0(pqs)} \langle P_s^2 [1 + i \frac{\nu\omega}{n S_0(pqs)}]^{-1} - 1 \rangle S(pqs)_j S^{-1}(\beta)_i, \quad (83)$$

where the summation refers to tensors $\Phi_{\mu}^i, \Phi_{\mu'}^j \in \mathcal{K}_0$. The relative change may now be written in the familiar form

$$\frac{\Delta L_{\mu\mu'}^{\alpha\beta}}{L_{\mu\mu'}^{\alpha\beta}} = - \sum_{pqs} \psi_{pqs} (1 + \delta_{p1} \delta_{q2}) (-1)^{p+q+n} \Omega(pqn) \sum_{\kappa, \nu} \begin{pmatrix} p & q & n \\ \kappa & \nu & -\mu \end{pmatrix}^2 \langle P_s^2 [f(\nu \xi_{pqs}) + i g(\nu \xi_{pqs})] \rangle, \quad (84)$$

with the magnitude of the contribution of the pqs -polarization defined as

$$\psi_{pq\beta} = (1 - \frac{1}{2} \delta_{p1} \delta_{q2}) \frac{\sum_{i,j} S^{-1}(\alpha_i) S(\beta_i) S(pq\beta) S^{-1}(\beta_j)}{S^{-1}(\alpha_\beta) S_0(pq\beta)} \quad (85)$$

and the field parameter

$$\xi_{pq\beta} = \omega \frac{1}{n S_0(pq\beta)} \equiv \omega \tau_{pq\beta} . \quad (86)$$

In eqs. (84) and (85) factors containing Kronecker delta symbols have been incorporated in order to get ψ 's identical to the ones defined in previous papers. The field dependent functions are given by

$$f(x) = \frac{x^2}{1+x^2} \quad g(x) = \frac{x}{1+x^2} . \quad (87)$$

Examples of the field dependence (84) for linear molecules for $r = 1, 2$ and various values of pq can be found in refs. 33 and 34.

10. Mixtures

The microscopic state of a multi-component mixture of dilute gases with internal degrees of freedom is specified by the distribution f_k of each molecular species k . The time behaviour of the f_k is described by a system of Waldmann-Snider equations (1), where the collision terms now represent the rate of change of f_k resulting from binary collisions with particles of the same and of all other species. We write for the local equilibrium distribution

$$f_k^0 = n x_k \left(\frac{m_k}{2\pi kT} \right)^{\frac{3}{2}} \frac{1}{Z_{rot,k}} \exp \{ -W_k^2 - \epsilon_k \} , \quad (88)$$

where x_k is the mole fraction of component k . It is important to note here that the distribution has been normalized to $n x_k$ and not to n as in ref. 22. The latter choice for the normalization has previously lead to unnecessary complications in the formalism.

The reduced molecular velocity of species k , \underline{w}_k , is defined in the same way as for simple gases (cf. eq. (3)), with \underline{v} the bulk velocity of the mixture

$$\underline{v} = \frac{\sum_k x_k m_k \underline{v}_k}{\sum_k x_k m_k} \quad (89)$$

and $\underline{v}_k = \langle \underline{c}_k / x_k \rangle$ the average velocity of species k .

In the non-equilibrium state, each f_k is considered to be close enough to equilibrium that f_k can be written in the form

$$f_k = f_k^0 (1 + \phi_k) \quad (90)$$

The non-equilibrium average of a quantity A , which for each species is specified by A_k , is calculated according to

$$\langle A \rangle = \frac{1}{n} \sum_k \text{Tr} \int A_k^\dagger f_k d\underline{c}_k \quad (91)$$

In analogy to the case of a simple gas it is useful to introduce a Hilbert space of operators such as $A = (A_1, A_2, \dots)$ and $\phi = (\phi_1, \phi_2, \dots)$, with the scalar product

$$\langle A | \phi \rangle = \frac{1}{n} \sum_k \text{Tr} \int A_k^\dagger f_k^0 \phi_k d\underline{c}_k \quad (92)$$

The choice of notation will lead to final results of similar appearance as in the simple gas case. For the deviations ϕ_k we have the linearized system of equations

$$-\psi_k = n \sum_l \mathcal{R}_{kl} \phi_l, \quad (93)$$

or, in short

$$-\psi = n \mathcal{R} \phi. \quad (94)$$

The Waldmann-Snider collision operators \mathcal{R}_{kl} constitute a matrix \mathcal{R} of operators. It is to be noticed that each diagonal element \mathcal{R}_{kk} still contains contributions from binary collisions with molecules of species other than k . As has been done for simple gases, a formal solution of eq. (93) is given by

$$\phi_k = -\frac{1}{n} \sum_l (\mathcal{R}^{-1})_{kl} \psi_l, \quad (95)$$

with $(\mathcal{R}^{-1})_{kl}$ the kl -element of the inverse operator matrix \mathcal{R}^{-1} , defined on the non-hydrodynamic subspace. The hydrodynamic subspace is richer now; for a binary mixture, e.g., it is 6-dimensional, with a basis consisting of the arrays $(1,0)$, $(0,1)$, $(m_1 \underline{w}_1, m_2 \underline{w}_1)$ and (E_1, E_2) .

The macroscopic fluxes are averages of microscopic fluxes and may be written as

$$\underline{j}^\alpha = \sum_k \text{Tr} \int f_k [(\underline{c}_k - \underline{v}) Q_{\alpha,k}] d\underline{c}_k, \quad (96)$$

where $Q_{\alpha,k}$ is again a molecular quantity such as mass, momentum or energy. We now introduce microscopic fluxes

$$\underline{\psi}^{\alpha k} = k^{-1} (\underline{c}_k - \underline{v}) Q_{\alpha,k} \quad (97)$$

and rewrite eq. (96) in short hand notation as

$$\underline{j}^\alpha = nk \langle \underline{\psi}^\alpha | \phi \rangle^* \quad (98)$$

The inhomogeneous term ψ has the form

$$\psi = \sum_\beta \underline{\psi}^\beta \cdot \underline{X}^\beta, \quad (99)$$

which means that

$$\psi_k = \sum_\beta \underline{\psi}^{\beta k} \cdot \underline{X}^\beta. \quad (100)$$

Thus, if one combines eqs. (98), (95) and (99),

$$\underline{j}^\alpha = -k \sum_\beta \langle \underline{\psi}^\alpha | \mathcal{R}^{-1} \underline{\psi}^\beta \rangle^* \cdot \underline{X}^\beta, \quad (101)$$

so that

$$\underline{L}^{\alpha\beta} = k \langle \underline{\psi}^\alpha | \mathcal{R}^{-1} \underline{\psi}^\beta \rangle^*. \quad (102)$$

In analogy to the simple gas case we consider a set of tensors (cf.

eq. (39))

$$\underline{\Phi}^{pqslk} = \left(\frac{2^p}{p!}\right)^{\frac{1}{2}} [\underline{W}_k]^p [\underline{J}_k]^q P_{s,k} . \quad (103)$$

In Hilbert space formulation, $\underline{\Phi}^{pqslk}$ may be considered as an array consisting of zeros except for component k , which has the value indicated in (103). These tensors then satisfy the orthogonality relation

$$\langle \Phi_{\mu\nu}^{pqslk} | \Phi_{\mu'\nu'}^{p'q's'l} \rangle = x_k \delta_{pp'} \delta_{qq'} \delta_{ss'} \delta_{kl} \delta_{\mu\mu'} \delta_{\nu\nu'} . \quad (104)$$

The normalization is to x_k instead of unity so as to have a concentration independent basis. The microscopic fluxes can now be written as a sum of such tensors

$$\underline{\Psi}^\alpha = \sum_k C^{\alpha lk} \underline{\Phi}^{\alpha lk} , \quad (105)$$

which is actually an array with the elements from (103) multiplied by factors $C^{\alpha lk}$. Consequently we can rewrite eq. (102) as a sum of matrix elements of the inverse collision operator

$$\underline{L}^{\alpha\beta} = \sum_{k,l} C^{\alpha lk} C^{\beta l'k} \langle \underline{\Phi}^{\alpha lk} | \mathcal{A}^{-1} \underline{\Phi}^{\beta l'k} \rangle^* . \quad (106)$$

For the matrix elements of the collision operator we write (cf. eq. (44))

$$\begin{aligned} \langle \Phi_{\mu\nu}^{pqslk} | \mathcal{A} \Phi_{\mu'\nu'}^{p'q's'l} \rangle &= \sum_{L,M} i^{p-p'+q-q'} (-1)^{L+p+q+\mu+\nu'} \sqrt{\Omega(pp'L) \Omega(qq'L)} \\ &\times \left(\begin{matrix} p & p' & L \\ -\mu & \mu' & -M \end{matrix} \right) \left(\begin{matrix} q & q' & L \\ -\nu & \nu' & M \end{matrix} \right) S_L \left(\begin{matrix} p & q & s \\ p' & q' & s' \end{matrix} \middle| \begin{matrix} k \\ l \end{matrix} \right) . \end{aligned} \quad (107)$$

The reduced matrix elements $S_L \left(\begin{matrix} p & q & s \\ p' & q' & s' \end{matrix} \middle| \begin{matrix} k \\ l \end{matrix} \right)$ depend upon the concentration and may be expressed in terms of concentration-independent cross sections according to^{22,35)}

$$S_L \left(\begin{matrix} p & q & s \\ p' & q' & s' \end{matrix} \middle| \begin{matrix} k \\ l \end{matrix} \right) = x_k x_{l'} v_{kl} \mathfrak{S}_L \left(\begin{matrix} p & q & s \\ p' & q' & s' \end{matrix} \middle| \begin{matrix} k \\ l \end{matrix} \right)_{kl} \quad (k \neq l) , \quad (108)$$

$$S_L \left(\begin{matrix} p & q & s \\ p' & q' & s' \end{matrix} \middle| \begin{matrix} k \\ k \end{matrix} \right) = x_k^2 v_{kk} \mathfrak{S}_L \left(\begin{matrix} p & q & s \\ p' & q' & s' \end{matrix} \middle| \begin{matrix} k \\ k \end{matrix} \right)_{kk} + x_k x_{l'} v_{kl} \mathfrak{S}_L \left(\begin{matrix} p & q & s \\ p' & q' & s' \end{matrix} \middle| \begin{matrix} p & q & s \\ p' & q' & s' \end{matrix} \right)_{kl} . \quad (109)$$

The cross section $\mathfrak{S}_L \left(\begin{matrix} p & q & s \\ p' & q' & s' \end{matrix} \middle| \begin{matrix} k \\ l \end{matrix} \right)_{kl}$ describes the coupling between a pqs -polarization of a molecule of species k and a $p'q's'$ -polarization of a molecule

of species l by collisions between species k and l , and v_{kl} is the corresponding average relative thermal speed

$$v_{kl} = \sqrt{\frac{8}{\pi} \frac{kT}{\mu_{kl}}} , \quad (110)$$

with μ_{kl} the reduced mass. Introduction of an external field requires the same modifications as in the simple gas case, i.e., \mathcal{R} is to be replaced by $\mathcal{R} + i\mathcal{L}$ (cf. section 6), hence

$$L_{\mu\mu}^{\alpha\beta} = k \langle \Psi_{\mu}^{\alpha} | (\mathcal{R} + i\mathcal{L})^{-1} \Psi_{\mu}^{\beta} \rangle^* = k \sum_{k,l} C^{\alpha 1 k} C^{\beta 1 l} \langle \Psi_{\mu}^{\alpha 1 k} | (\mathcal{R} + i\mathcal{L})^{-1} \Psi_{\mu}^{\beta 1 l} \rangle^* . \quad (111)$$

It is now obvious, that under the same conditions as before the general properties derived in section 8 will also be valid for mixtures. For the matrix elements of the Liouville operator we have

$$\langle \Phi_{\mu\nu}^{pqslk} | \mathcal{L} \Phi_{\mu'\nu'}^{p'q's'1l} \rangle = -\delta_{pp'} \delta_{qq'} \delta_{ss'} \delta_{kl} \delta_{\mu\mu'} \delta_{\nu\nu'} \frac{x_k}{n} \nu \langle p_{s,k}^2 \omega_k \rangle , \quad (112)$$

with the Larmor frequency ω_k as before.

11. Field dependence in a polyatomic gas-noble gas mixture

In this section a binary gas mixture, consisting of a polyatomic gas (species 1) and a noble gas (species 2) will be considered. As only component 1 has angular momentum, polarizations ($q \neq 0$) will only exist for this component. In order to evaluate expression (111) for $L_{\mu\mu}^{\alpha\beta}$, the same scheme as in the simple gas case is followed. First, the collision operator is split into a diagonal and a non-diagonal part. Then the inverse operator $(\mathcal{R} + i\mathcal{L})^{-1}$ is expanded in terms of \mathcal{R}_{nd} and the second-order contribution is calculated using the spherical approximation. The result for the relative change in the phenomenological coefficient will be of exactly the same form as before (eq. (84)), only the expression for ψ_{pqs} will be more complicated

$$\psi_{pqs} = \frac{\sum_{k,l=1,2} \sum_{i,j} S^{-1}(\alpha 1^k_i) S(pqs 1^1_i) S(pqs 1^1_j) S^{-1}(\beta 1^l_j)}{S_0(pqs 1^1) \sum_{k,l=1,2} S^{-1}(\alpha 1^k_l)} . \quad (113)$$

In approximating the elements S^{-1} of the inverse operator by matrix inversion one has to keep in mind that the basis functions used are not normalized to unity, cf. eqs. (103) and (104). The final results can be expressed in terms of concentration independent cross sections by means of eqs. (108) and (109). Explicit expressions for ψ_{pq8} for some transport coefficients can be found in refs. 22 and 36.

12. The heat flux, the diffusion velocity and the viscous pressure tensor

In this section we will schematically summarize the expressions for the common vectorial and tensorial transport phenomena in simple gases and in binary mixtures.

a) Simple gases:

For simple gases we will treat thermal conductivity and viscous flow. The constitutive relations for the heat flux and for the symmetric traceless part of the viscous pressure tensor $\underline{\Pi}$, respectively, are given by

$$\underline{q} = - \underline{\lambda} \cdot \underline{\nabla} T, \quad (114)$$

$$\underline{\Pi} = -2 \underline{\eta} : \underline{\nabla} \underline{v}, \quad (115)$$

with $\underline{\eta}$ the viscosity tensor. These equations are special forms of the linear laws (13). At the end of this section the relations between the transport coefficients occurring in these equations and the phenomenological coefficients of the linear laws are given (see below). Explicit expressions for the quantities occurring in section 4 are given in table I for the two phenomena under consideration.

b) Binary gas mixtures:

In a binary gas mixture we also have to consider diffusion. Moreover, due to the fact that gradients in the concentration have the same vectorial character as a temperature gradient, also the cross effects of diffusion and

Table I

Fluxes j^α and forces \bar{x}^α , microscopic fluxes \bar{y}^α and normalized microscopic fluxes $\bar{\phi}^\alpha$ for simple gases in the case of heat flux ($\alpha = q$), momentum transport ($\alpha = \pi$) and diffusion ($\alpha = j$). The quantity Q_α is the "transported quantity" and $C^\alpha = \bar{y}^\alpha / \bar{\phi}^\alpha$. The constant π is defined as $\pi^2 \equiv 2\alpha_{ro} / \alpha k$.

α	Q_α	j^α	\bar{x}^α	\bar{y}^α	$\bar{\phi}^\alpha$	C^α
q	$kT(W^2 + \varepsilon_k)$	q	$\frac{\nabla T}{T^2}$	$T \sqrt{\frac{2kT}{m}} [W^2 - \frac{5}{2} + \varepsilon_k - \langle \varepsilon \rangle] \bar{W}$	$[\frac{5}{4}(1+\pi^2)]^{-\frac{1}{2}} [W^2 - \frac{5}{2} + \varepsilon_k - \langle \varepsilon \rangle] [\bar{W}]^1$	$\bar{\phi}^{10E} = T \sqrt{\frac{2kT}{m}} [\frac{5}{4}(1+\pi^2)]^{\frac{1}{2}}$
π	$\sqrt{2mkT} \bar{W}$	$\bar{\Pi} = \frac{\nabla p}{T}$	$\frac{\nabla p}{T}$	$2T \sqrt{\frac{W}{W}}$	$\sqrt{2} [\bar{W}]^2$	$\bar{\phi}^{20} = T \sqrt{2}$

Table II

Fluxes and forces, microscopic fluxes and normalized microscopic fluxes for binary gas mixtures ($k = 1, 2$).

α	$Q_{\alpha k}$	j^α	\bar{x}^α	$\bar{y}^{\alpha k}$	$\bar{\phi}^{\alpha k}$	$C^{\alpha k}$
q	$kT(W_k^2 + \varepsilon_k)$	q	$\frac{\nabla T}{T^2}$	$T \sqrt{\frac{2kT}{m_k}} [W_k^2 - \frac{5}{2} + \varepsilon_k - \langle \varepsilon_k \rangle] \frac{W_k}{m_k}$	$[\frac{5}{4}(1+\pi_k^2)]^{-\frac{1}{2}} [W_k^2 - \frac{5}{2} + \varepsilon_k - \langle \varepsilon_k \rangle] [\frac{W_k}{m_k}]^1$	$\bar{\phi}^{10E k} = T \sqrt{\frac{2kT}{m_k}} [\frac{5}{4}(1+\pi_k^2)]^{\frac{1}{2}}$
j	$\frac{(-1)^{k+1}}{x_k}$	$\bar{y} = \frac{\nabla p}{T}$	$\pi k \frac{\nabla p}{T}$	$\frac{(-1)^{k+1}}{x_k} \sqrt{\frac{2T}{m_k}} \frac{W_k}{m_k}$	$\sqrt{2} [\frac{W_k}{m_k}]^1$	$\bar{\phi}^{10I k} = \frac{(-1)^{k+1}}{x_k} \sqrt{\frac{2T}{m_k}}$
π	$\sqrt{2mkT} \frac{W_k}{m_k}$	$\bar{\Pi} = \frac{\nabla p}{T}$	$\frac{\nabla p}{T}$	$2T \sqrt{\frac{W_k}{m_k}}$	$\sqrt{2} [\frac{W_k}{m_k}]^2$	$\bar{\phi}^{20I k} = T \sqrt{2}$

thermal conductivity, called thermal diffusion and Dufour effect, may occur. The constitutive relations which describe these phenomena are

$$\underline{q} = - \underline{\lambda} \cdot \underline{\nabla T} - \frac{nkT}{x_1 x_2} \underline{\mathcal{D}} \cdot \underline{\nabla x_1}, \quad (116)$$

$$\underline{v_1} - \underline{v_2} = - \frac{1}{x_1 x_2 T} \underline{D_T} \cdot \underline{\nabla T} - \frac{1}{x_1 x_2} \underline{D} \cdot \underline{\nabla x_1}, \quad (117)$$

$$\underline{\Pi} = - 2 \underline{\eta} : \underline{\nabla v}, \quad (118)$$

where $\underline{v_1} - \underline{v_2}$ is the diffusion velocity, defined as

$$\underline{v_1} - \underline{v_2} = \left\langle \frac{\underline{c}_1}{x_1} \right\rangle - \left\langle \frac{\underline{c}_2}{x_2} \right\rangle \quad (119)$$

and where \underline{D} is the diffusion tensor, $\underline{D_T}$ the thermal diffusion tensor and $\underline{\mathcal{D}}$ the Dufour tensor. See table II for the various fluxes, forces, etc. By substituting the expressions of tables I and II into the equations of sections 4 and 10, we get explicit expressions for the phenomenological coefficients $\underline{L}^{\alpha\beta}$ of the linear laws. For the phenomenological coefficients of eqs. (116) through (118) we need the following relations

$$\underline{\lambda} = \frac{1}{T^2} \underline{L}^{qq}, \quad (120)$$

$$\underline{D_T} = \frac{x_1 x_2}{T} \underline{L}^{jq} = \frac{x_1 x_2}{T} \underline{L}^{qj} = \underline{\mathcal{D}}, \quad (121)$$

$$\underline{D} = x_1 x_2 n k \underline{L}^{jj}, \quad (122)$$

$$\underline{\eta} = \frac{1}{2T} \underline{L}^{\pi\pi}, \quad (123)$$

which can be found by comparing the gradients of eqs. (116) through (118) to the thermodynamic forces \underline{X}^α listed in the tables.

In conclusion we may state that we have presented in this chapter a survey

of the kinetic theory of non-uniform gases in the presence of external fields in a compact way. Some new aspects of this presentation are, in particular, a modified formalism for gas mixtures and the derivation of an inequality for the magnitudes of the field effects on thermal conductivity, thermal diffusion and diffusion.

References on page 101.

CHAPTER II

EXPERIMENTS ON THE VISCOSITY OF POLAR GASES IN THE PRESENCE OF MAGNETIC AND ELECTRIC FIELDS

1. Introduction

Experimental studies on the influence of external fields on transport properties of dilute polyatomic gases have been carried out extensively during the last decade (see, e.g., refs. 1-3). The occurrence of these so-called Senftleben-Beenakker effects is explained in the following way. A macroscopic gradient in a polyatomic gas not only produces an anisotropy in the velocity distribution but via collisions also anisotropies (or polarizations) in the angular momentum distribution. Such angular momentum dependent polarizations, which are produced in collisions because of the non-spherical intermolecular potential, can be partially destroyed by applying an external field which will cause the molecules to precess around the field direction. This in turn will alter the transport properties.

Polarizations constitute deviations of the molecular distribution f from the local Maxwellian f^0 . Their general form is given by $[\underline{W}]^p [\underline{J}]^q P_s$ (see chapter I), a tensor consisting of an irreducible tensor of rank p in the reduced molecular velocity \underline{W} and a normalized irreducible tensor of rank q in the angular momentum \underline{J} , multiplied by a scalar factor P_s depending on W^2 and J^2 . The index s characterizes the scalar factor.

The tensorial factors of the various polarizations observed in field effects are by now well known. For linear diamagnetic $^1\Sigma$ molecules the tensorial factor is directly related to the field dependence of the effect. The scalar factor however, on which we will concentrate in this chapter and which is less accessible experimentally, remains undetermined. This factor is usually

expanded into orthogonal polynomials and generally only the first polynomial is taken into account. The study of symmetric top molecules might give some information since for these molecules, in contrast to linear ${}^1\Sigma$ molecules, the precession frequencies depend on the rotational state. For such a study experiments on the viscosity are preferable to other transport properties for the following reasons. Earlier experiments showed that in viscous flow only one type of angular momentum dependent polarization plays a role for most gases. A disentanglement of contributions from various polarizations is therefore not needed and a straightforward analysis of the scalar factor is possible. An additional advantage is gained by the fact that the polarization observed in viscosity experiments is a polarization with irreducible tensorial part $[\underline{J}]^2$. Other observed polarizations have more than one irreducible part and therefore a more complicated decay mechanism.

So far, for the scalar factor P (since in this chapter only the polarization produced by viscous flow is considered the index of P will be omitted) of the $[\underline{J}]^2$ type of polarization, two possible choices have been considered⁴):

1) $P = 1$:

since the tensor $[\underline{J}]^2$ is normalized only the orientation of the angular momentum plays a role ("normalized"),

$$2) P = \frac{\underline{J}^2 - \frac{3}{4}}{\langle \underline{J}^2 (\underline{J}^2 - \frac{3}{4}) \rangle^{\frac{1}{2}}} :$$

\underline{J} is treated in analogy to \underline{W} , i.e., magnitude as well as orientation are considered and the tensor polarization essentially has the form $[\underline{J}]^2$ ("unnormalized"). Henceforth this choice will shortly be denoted by $P \sim \underline{J}^2$.

Experiments on the influence of a magnetic field on the viscosity of some symmetric top molecules have already been carried out by Van Ditzhuyzen⁴). Similar experiments were carried out in an electric field⁵⁻⁷). Unfortunately it was not possible from these measurements to determine the exact form of polarization. The results seemed to favour slightly the so-called unnormalized form, but an unambiguous choice could not be made. In this respect a comparison between magnetic and electric field effects looks more promising. The underlying reason is that the spread in precession frequencies that occurs for symmetric top molecules in an electric field is different from that in a magnetic field (see section 2). The differences in the shapes of the resulting field

effect curves are rather subtle however, which makes it desirable to perform the experiments in one apparatus in order to eliminate systematic errors.

The following section gives the theoretical expressions, then follows a description of the experimental set-up in sections 3 and 4, and finally the results are presented and discussed in sections 5 and 6.

2. Theory

Theoretical expressions for the influence of external fields on viscosity have been derived by McCourt and Snider⁸⁾ and Kagan⁹⁾. In this section we will only deal with the relevant expressions and for a detailed outline of the theory one is referred to chapter I.

The polarization observed in viscosity experiments^{10-12,4)} is a tensor polarization with tensorial factor $[\underline{J}]^2$. The only exception known so far is formed by NH_3 and ND_3 where a $[\underline{M}]^2 [\underline{J}]^1$ -polarization plays a dominant role. If we restrict ourselves to the cases where only the $[\underline{J}]^2$ -polarization is present, the spherical components of the viscosity tensor change in the presence of a magnetic field according to

$$\frac{\Delta \eta_{\mu}}{\eta} = - \frac{\mathfrak{G}^2(20)_{02\pi}}{\mathfrak{G}(20) \mathfrak{G}(02\pi)} \langle P^2 [f(\mu \xi_{02\pi}) + ig(\mu \xi_{02\pi})] \rangle, \quad (1)$$

where the field-dependent functions are

$$f(x) = \frac{x^2}{1+x^2}, \quad g(x) = \frac{x}{1+x^2}, \quad (2)$$

and the field parameter

$$\xi_{02\pi} = \frac{\omega}{n < v > \mathfrak{G}(02\pi)} \equiv \omega \tau_{02\pi}. \quad (3)$$

For even-in-field coefficients this reduces to

$$\frac{\eta_{\mu}^{+} - \eta_{\mu}^{-}(0)}{\eta(0)} = \text{Re} \frac{\Delta \eta_{\mu}}{\eta} = - \frac{\mathfrak{G}^2(20)_{02\pi}}{\mathfrak{G}(20) \mathfrak{G}(02\pi)} \langle P^2 f(\mu \xi_{02\pi}) \rangle. \quad (4)$$

Here, $\sigma_{02\pi}^{20}$ and $\sigma(02\pi)$ are effective cross sections for the production and decay of the 02π -polarization as defined in chapter I, $\sigma(20)$ a cross section related to the field free viscosity $\eta(0)$, $\langle v \rangle$ the average thermal speed and ω the Larmor frequency.

For isotropic systems in an electric field, coefficients which are odd in the field vanish due to the fact that the electric field is a polar vector. The change in the even-in-field coefficients is given by eq. (4). Thus both magnetic and electric field effects are described by eq. (4), yet with different precession frequencies. For symmetric top molecules in magnetic and electric fields those frequencies are given by

$$\omega_B = \frac{g_{\perp} \mu_N}{\hbar} \left[1 + \frac{g_{\parallel} - g_{\perp}}{g_{\perp}} \frac{K^2}{J(J+1)} \right] B \quad (5)$$

and

$$\omega_E = \frac{\mu_e}{\hbar} \frac{K}{J(J+1)} E, \quad (6)$$

respectively; g_{\perp} and g_{\parallel} are the rotational g -factors perpendicular and parallel to the figure axis, μ_N the nuclear magneton, μ_e the electric dipole moment of the molecule, and J and K the rotational quantum numbers corresponding to the angular momentum \underline{J} and its projection upon the figure axis J_{\parallel} , respectively. The equilibrium average of any angular momentum dependent quantity A is defined by the expression

$$\langle A(J, K) \rangle = \frac{\sum_{J=0}^{\infty} \sum_{K=-J}^{K=+J} A(J, K) (2J+1) \exp \left\{ -\frac{\hbar^2}{2I_{\perp} kT} [J(J+1) + \left(\frac{I_{\perp}}{I_{\parallel}} - 1\right) K^2] \right\}}{\sum_{J=0}^{\infty} \sum_{K=-J}^{K=+J} (2J+1) \exp \left\{ -\frac{\hbar^2}{2I_{\perp} kT} [J(J+1) + \left(\frac{I_{\perp}}{I_{\parallel}} - 1\right) K^2] \right\}}, \quad (7)$$

which is to be applied in eqs. (1) and (4), and where the I are the moments of inertia of the molecule.

From eqs. (5) and (6) it follows that for symmetric top molecules the precession frequency around the field direction depends on the rotational (J, K) -state of the molecule. For the magnetic field case the spread in precession frequencies depends on the difference between g_{\perp} and g_{\parallel} and is usually small⁴). For the electric field case, the spread is necessarily large, since the precession frequency is proportional to $K/J(J+1)$ and vanishes for $K = 0$, irrespective of the value of the electric dipole moment of the molecule. The field dependence of the viscosity coefficients for symmetric top molecules

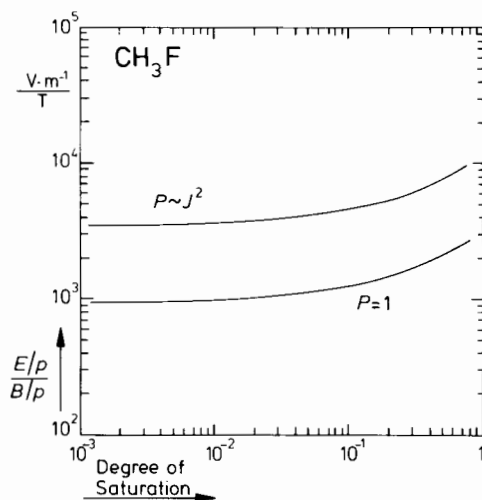


Fig. 1 The calculated ratio of E/p to B/p for the η_1^+ viscosity coefficient of CH_3F plotted as a function of the degree of saturation of the effect (see text). Two possible choices of the scalar factor P of the $[\underline{J}]^2$ -polarization are shown.

will be given by a weighted sum of contributions from molecules with different precession frequencies. The weight factor is a product of the Maxwellian weight of the rotational state and the scalar factor P of the tensor polarization, as can be seen from eqs. (1) and (4). The difference in behaviour between magnetic and electric field effects, due to the difference in the spread of precession frequencies, makes a comparison of the two types of measurements a powerful tool in the discrimination between different forms of P . This is illustrated in fig. 1 where the calculated ratio of E/p to B/p for the η_1^+ coefficient of CH_3F is plotted as a function of the degree of saturation (i.e., the ratio of the change in the coefficient at the current field to the saturation value). There is a large difference between the curves calculated for the two different choices of P in use so far.

It should be stressed that two assumptions have been made in the derivation of eq. (1). First, the spread in relaxation times $\tau_{02\pi}$ is neglected, i.e., a state-averaged cross section is used. Secondly, contributions from other polarizations are assumed to be absent. This last assumption can readily be checked experimentally if two different coefficients η_1^+ and η_2^+ are measured. When only a $[\underline{J}]^2$ -polarization is present, the ratio of the "positions" B/p of the two coefficients should result in a horizontal line $(B/p)_1 / (B/p)_2 = 2$, see eq. (4) and, e.g., fig. 4.

3. Description of the experimental set-up

For accurate measurements of small changes in the viscosity an apparatus consisting of four identical capillaries of rectangular cross section arranged in a Wheatstone bridge is appropriate. Fig. 2a shows a schematic view of the apparatus, which is very similar to the one used by Van Ditzhuyzen⁴). The capillaries (length $l = 60$ mm, width $w = 10$ mm, thickness $t = 0.5$ mm), consist of two gold coated brass plates held apart by pyrex spacers, see fig. 2b. The gold coating minimizes adsorption effects and protects the optically polished surfaces of the plates against corrosive gases.

For measurements in electric fields a voltage difference (up to 1 kV) is applied to the plates of the pair of capillaries c_1 and c_4 (or the pair c_2 and c_3). The change in viscosity is then given by a ratio of pressure differences,

$$2 \frac{p_C(E) - p_D(E)}{p_A - p_B} = - \frac{\Delta\eta_1^+(E)}{\eta} \quad (8)$$

The subscripts A,B,C and D denote the corresponding points of the bridge as shown in fig. 2a.

For measurements in magnetic fields the apparatus is placed in the 0.1 m room temperature bore of a 7.6 T superconducting magnet (homogeneity 99%). In order to determine more than one component of the viscosity tensor a design as shown in fig. 2c was chosen. By positioning either the pair c_1 and c_4 (position I) or the differently orientated pair c_2 and c_3 (position II) in the field centre, two different components of the viscosity tensor can be measured. According to Hulsman et al.¹³) the field induced imbalance of the bridge is now related to changes in the viscosity by

$$2 \frac{p_C(B) - p_D(B)}{p_A - p_B} = - \frac{\Delta\eta_1^+(B)}{\eta} \quad (\text{position I}) \quad (9)$$

$$2 \frac{p_D(B) - p_C(B)}{p_A - p_B} = - \frac{\Delta\eta_2^+(B)}{\eta} \quad (\text{position II}). \quad (10)$$

Thus three different measurements can be performed in one apparatus. For optimum temperature stability the apparatus is put in a vacuum jacket, which is

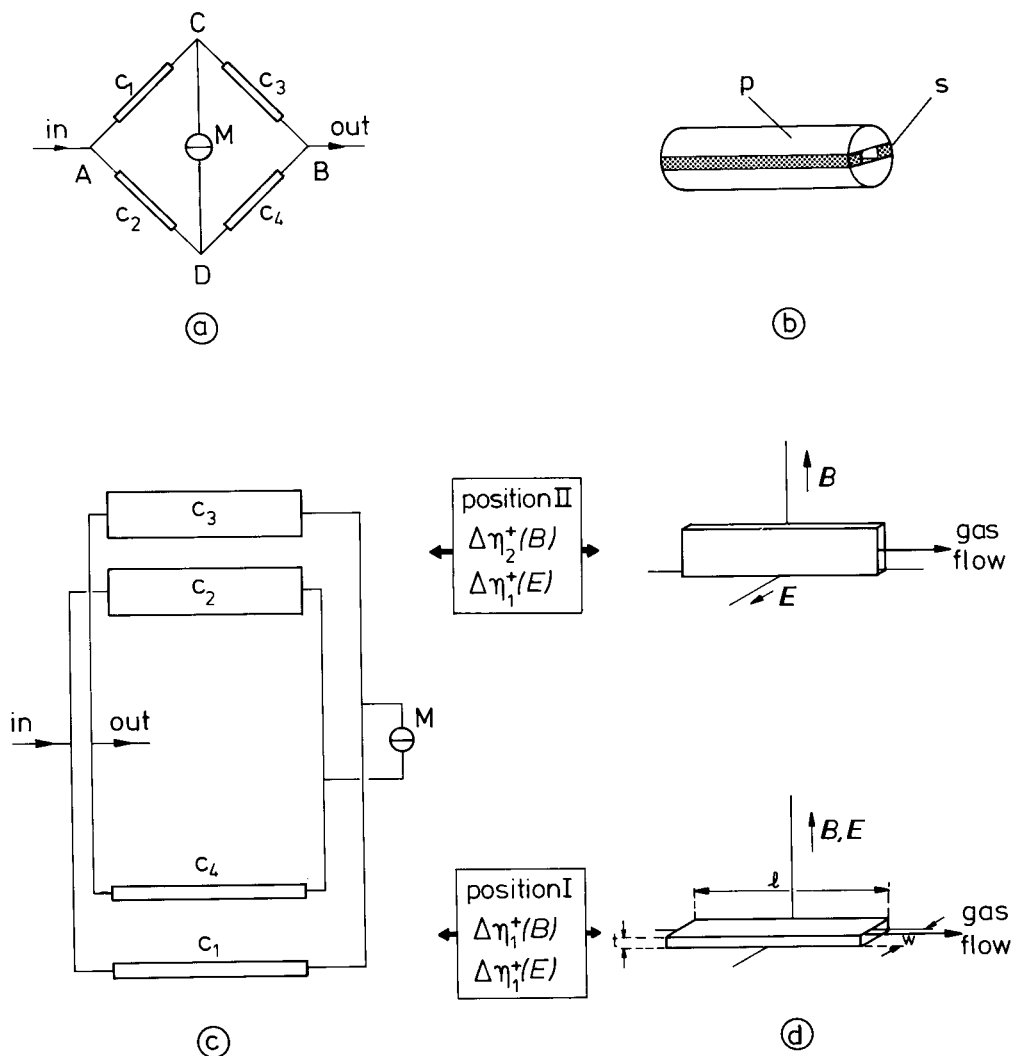


Fig. 2 The apparatus for the measurement of $\Delta\eta_1^+$ and $\Delta\eta_2^+$ in magnetic and $\Delta\eta_1^+$ in electric fields.

- Schematic diagram of the Wheatstone bridge consisting of four identical capillaries. M = differential manometer, c_1 , c_2 , etc. = capillaries.
- View of one of the capillaries. s = pyrex spacer, p = gold coated plate.
- The arrangement of the capillaries in the apparatus. Either the pair c_1 and c_4 (position I) or the pair c_2 and c_3 (position II) is positioned in the centre of the vertical magnetic field. Distance between upper and lower pair of capillaries: 0.62 m.
- The orientation of the capillaries with respect to the fields. Dimensions of the capillaries: $l = 60$ mm, $w = 10$ mm, $t = 0.5$ mm.

temperature controlled by a thermostat. The pressure difference $p_C - p_D$ is measured using a differential capacitance manometer (sensitivity: 10^{-4} Pa). The pressure drops $p_A - p_C$ and $p_C - p_B$ are measured with oil manometers. The resolving power of the entire system was found to be such that at the higher pressures relative changes in the viscosity as small as $5 \cdot 10^{-6}$ could be detected.

4. Corrections

The relations between the observed pressure differences and changes in viscosity as given in eqs. (8) through (10) are strictly valid only under ideal conditions. In the actual experimental set-up various corrections have to be taken into account. Equations (8) through (10) then become

$$2 \frac{p_C(E) - p_D(E)}{p_A - p_B} \left\{ 1 + \frac{1}{8} \left(\frac{p_A - p_B}{p + K_\eta} \right)^2 \right\} = - \left\{ (1 - \epsilon_1) \frac{\Delta \eta_1^+(E)}{\eta} + \epsilon_1 \frac{\Delta \eta_2^+(E)}{\eta} \right\}, \quad (11)$$

$$2 \frac{p_C(B) - p_D(B)}{p_A - p_B} \left\{ 1 + \frac{1}{8} \left(\frac{p_A - p_B}{p + K_\eta} \right)^2 \right\} = - \left\{ (1 - \epsilon_1) \frac{\Delta \eta_1^+(B)}{\eta} + \epsilon_1 \frac{\Delta \eta_2^+(B)}{\eta} - \frac{\Delta \eta_2^+(\epsilon_2 B)}{\eta} \right\}, \quad (12)$$

$$2 \frac{p_D(B) - p_C(B)}{p_A - p_B} \left\{ 1 + \frac{1}{8} \left(\frac{p_A - p_B}{p + K_\eta} \right)^2 \right\} = - \left\{ (1 - \epsilon_1) \frac{\Delta \eta_2^+(B)}{\eta} + \epsilon_1 \frac{\Delta \eta_1^+(B)}{\eta} - \frac{\Delta \eta_1^+(\epsilon_2 B)}{\eta} \right\}. \quad (13)$$

The various corrections stem from

1) The expansion of the gas

The correction factor for this effect is¹⁴⁾

$$\frac{1}{8} \left(\frac{p_A - p_B}{p + K_\eta} \right)^2,$$

where K_η is the Knudsen correction for the field free viscosity and p the average pressure in the bridge. The values for K_η (see table I) have been calculated⁴⁾, except the one for $\text{CH}_3\text{F-He}$, which has been determined in the present experimental set-up.

2) The broadening due to the expansion of the gas

Since the viscosity is studied as a function of the field to pressure ratio, a spread in field functions will occur because of the pressure drop across the capillary. Care was taken as to regulate the flow in such a way that $\Delta p/p < 0.3$. The magnitude of this correction decreases with increasing field-to-pressure ratio and is negligible for

the region of interest.

3) Pressure drops at the entrance of and inside the capillaries

A correction factor for this effect is discussed in refs. 11 and 13. For the present apparatus this correction is of the order of 10^{-3} and is therefore neglected.

4) The finite width of the capillaries

This causes a small distortion in the flow profile. The correction ϵ_1 is determined by the dimensions t and w of the capillary¹³); in our case $\epsilon_1 = 1.6 \cdot 10^{-2}$.

5) The viscous resistance of entrance and exit leads, and

6) The zero field unbalance of the bridge

These corrections are of the order of 10^{-3} and are neglected.

7) Magnetic stray field effects on the pair of capillaries that are not in the field centre

The fraction of the magnetic field felt at 0.62 m from the field centre is $\epsilon_2 = 7.5 \cdot 10^{-3}$. The magnitude of the correction for these effects depend on the B/p region studied, being $1.5 \cdot 10^{-2}$ at most.

8) Magnetic stray field effects on the entrance and exit leads

The correction for these effects has been calculated using a simplified model for the field decay in the vertical direction¹⁴). The correction was found to be smaller than 10^{-3} and is therefore neglected.

9) Knudsen effects

These effects occur at low densities, when the mean free path of the molecules becomes of the same order of magnitude as the dimensions of the capillaries. Corrections must therefore be applied to the field free viscosity (see correction 1), to the magnitude $\Delta\eta/\eta$, and to the field-to-pressure ratio F/p ($F = B$ or E) of the field effects. These last two corrections are applied according to¹⁵)

$$\frac{\Delta\eta}{\eta} = \left(\frac{\Delta\eta}{\eta}\right)_m \left(1 + \frac{K}{p} \frac{\Delta\eta}{\eta}\right) \quad (14)$$

$$\frac{F}{p} = \left(\frac{F}{p}\right)_m \left(1 + \frac{K}{p} \frac{F}{p}\right)^{-1}, \quad (15)$$

where m stands for "measured at pressure p ". Values for the experimentally determined Knudsen parameters are listed in table I. The magnitudes of these corrections range from 2% to 60% for the pressures used.

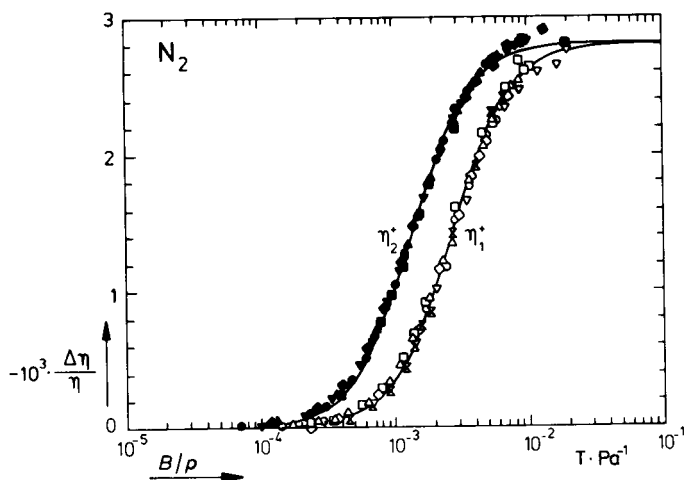


Fig. 3 $-\Delta\eta/\eta$ versus B/p for N_2 .

∇ 285 Pa, \square 604 Pa, \triangle 780 Pa, \times 785 Pa, \diamond 959 Pa, \circ 1265 Pa,
 \blacksquare 340 Pa, \blacklozenge 489 Pa, \blacktriangledown 635 Pa, \blacktriangle 968 Pa, \bullet 1232 Pa.

— : theoretical curve of eq. (4) scaled to fit the experimental points. For linear molecules the precession frequency is independent of the molecular rotational state and hence the form of the scalar factor of the polarization does not play a role in the shape of the curve. The saturation value is $2.81 \cdot 10^{-3}$ and the half field-to-pressure ratio for η_1' is 2.6 mT/Pa.

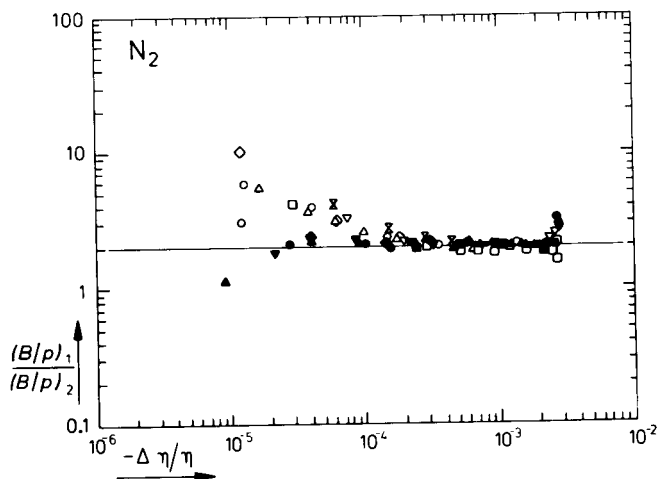


Fig. 4 $[J]^2$ -polarization test from the magnetic field measurements for N_2 .

The ratio of the positions of the two curves from fig. 3 are plotted as a function of the magnitude of the effect. For a $[J]^2$ -type of polarization one expects a value 2 (see line). The symbols for the various pressure runs are the same as in fig. 3. The average of the data points is 2.0 ± 0.1 .

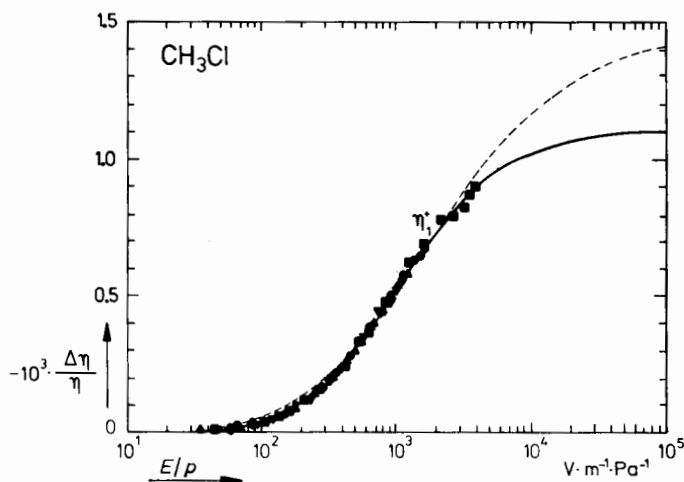


Fig. 5 $-\Delta\eta/\eta$ versus E/p for CH_3Cl .

■ 174 Pa, ● 426 Pa, ▲ 553 Pa, ▼ 628 Pa, ◆ 673 Pa, ⋈ 870 Pa.

--- : theoretical curve of eq. (4) for $P = 1$,

— : theoretical curve of eq. (4) for $P \sim E^2$.

The theoretical curves are scaled to fit the experimental points. The choices $P = 1$ and $P \sim E^2$ yield the saturation values 1.43 and 1.10, and the half saturation field-to-pressure ratios 1600 and 1000 $\text{V}\cdot\text{m}^{-1}/\text{Pa}$, respectively.

5. Experimental results

Experiments were carried out at room temperature on the linear molecule N_2 , the prolate molecules CH_3Cl and CH_3F , the mixture CH_3F -He and the oblate molecule PF_3 . All gases were obtained commercially. The purities of the gases were all better than 99%. Some data of the various molecules are listed in table II.

The analysis of measured data begins with the correction for the expansion of the gas (correction 1). Next, Knudsen corrections are applied to the individual pressure runs, using eqs. (14) and (15). The Knudsen correction parameters are listed in table I. For CH_3F the Knudsen parameters for the electric and the magnetic field effect were found to be different. This discrepancy is probably caused by the experimental uncertainty in the determination of the saturation values of the various pressure runs for this gas. Also, contributions from rarefied gas effects^{16,17)} or wall effects^{18,19)} may be responsible. Since the experimental Knudsen constants listed in table I contain both the correction for real Knudsen effects and possibly also for other $1/p$ -effects, they should be regarded only as a tool for obtaining the zero mean free path

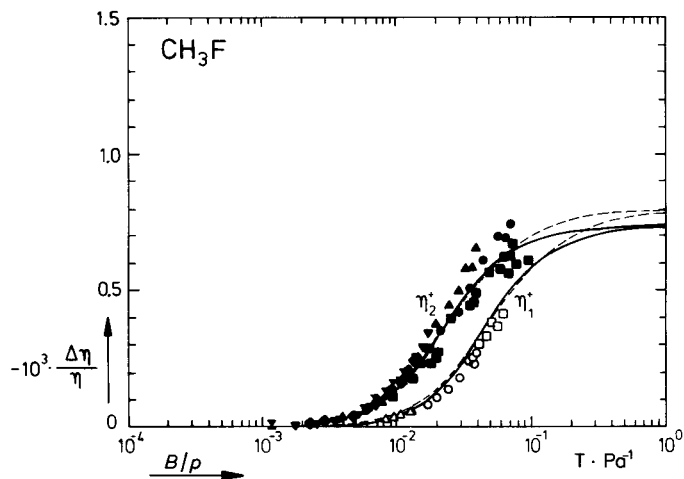


Fig. 6 $-\Delta\eta/\eta$ versus B/p for CH_3F .

□ 92 Pa, ○ 173 Pa, △ 526 Pa,
 ■ 197 Pa, ● 273 Pa, ▲ 301 Pa, ▼ 590 Pa, ◆ 805 Pa, ⌘ 622 Pa.

--- : theoretical curve of eq. (4) for $P = 1$,

— : theoretical curve of eq. (4) for $P \sim \sqrt{2}$.

The theoretical curves are scaled to fit the experimental points. The choices $P = 1$ and $P \sim \sqrt{2}$ yield the saturation values 0.81 and $0.74 \cdot 10^{-3}$, and the half saturation field-to-pressure ratios (for η_1^*) 52 and 46 mT/Pa , respectively.

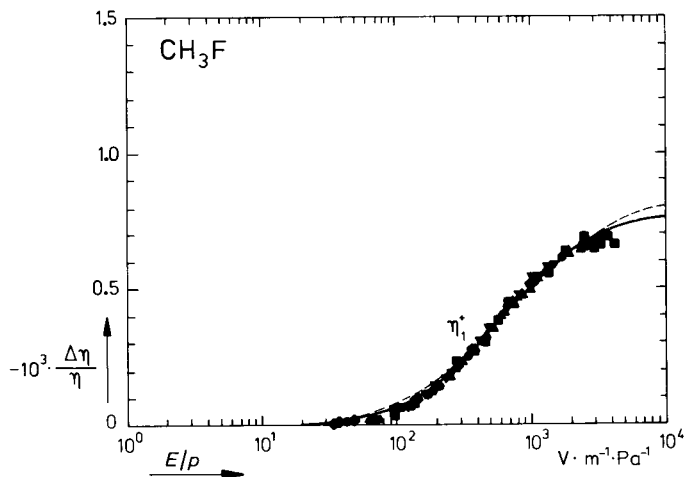


Fig. 7 $-\Delta\eta/\eta$ versus E/p for CH_3F .

■ 69 Pa, ● 88 Pa, ▲ 170 Pa, ▼ 419 Pa, ◆ 488 Pa, ⌘ 1074 Pa.

--- : theoretical curve of eq. (4) for $P = 1$,

— : theoretical curve of eq. (4) for $P \sim \sqrt{2}$.

The theoretical curves are scaled to fit the experimental points. The choices $P = 1$ and $P \sim \sqrt{2}$ yield the saturation values 0.83 and $0.77 \cdot 10^{-3}$, and the half saturation field-to-pressure ratios 690 and $590 \text{ V}\cdot\text{m}^{-1}/\text{Pa}$, respectively.

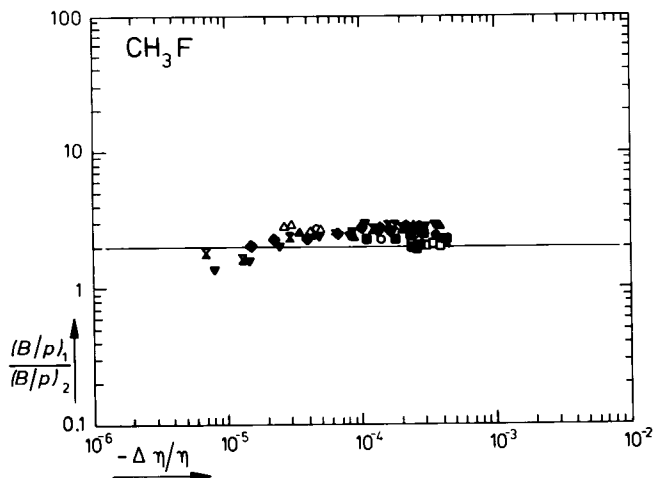


Fig. 8 $[J]^2$ -polarization test from the magnetic field measurements for CH_3F . The ratio of the positions of the two curves from fig. 6 are plotted as a function of the magnitude of the effect. For a $[J]^2$ -type of polarization one expects a value 2 (see line). The symbols for the various pressure runs are the same as in fig. 6. The average of the data points is 2.4 ± 0.3 .

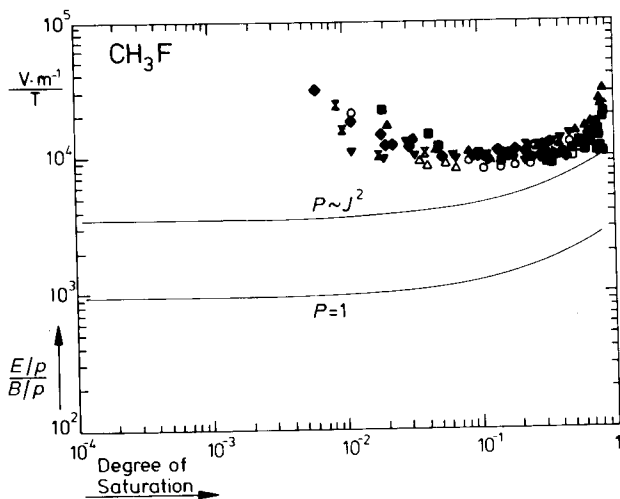


Fig. 9 Test on the scalar factor of the polarization from the magnetic and electric field measurements for CH_3F . The values of $(E/p)/(B/p)$ (for η_1^+) are plotted as a function of the degree of saturation. The symbols for the various pressure runs are the same as in figs. 6 and 7. Theoretical curves for two different choices of P for a $[J]^2$ -polarization are shown.

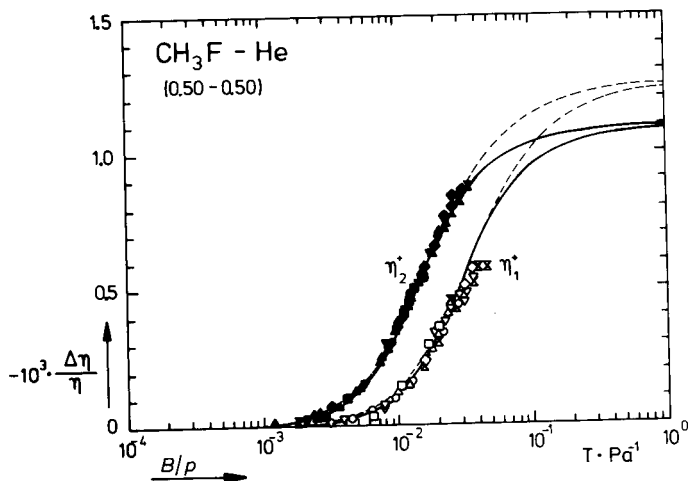


Fig. 10 $-\Delta\eta/\eta$ versus B/p for an equimolar CH_3F -He mixture.

\times 101 Pa, \diamond 142 Pa, ∇ 150 Pa, \triangle 186 Pa, \circ 196 Pa, \square 310 Pa,
 \boxtimes 155 Pa, \bullet 187 Pa, \blacktriangledown 216 Pa, \blacktriangle 260 Pa, \bullet 360 Pa, \blacksquare 490 Pa.

---: theoretical curve of eq. (4) for $P = 1$,

—: theoretical curve of eq. (4) for $P \sim \sqrt{2}$.

The theoretical curves are scaled to fit the experimental points. The choices $P = 1$ and $P \sim \sqrt{2}$ yield the saturation values 1.25 and $1.09 \cdot 10^{-3}$, and the half saturation field-to-pressure ratios (for η_1^*) 37 and 31 mT/Pa, respectively.

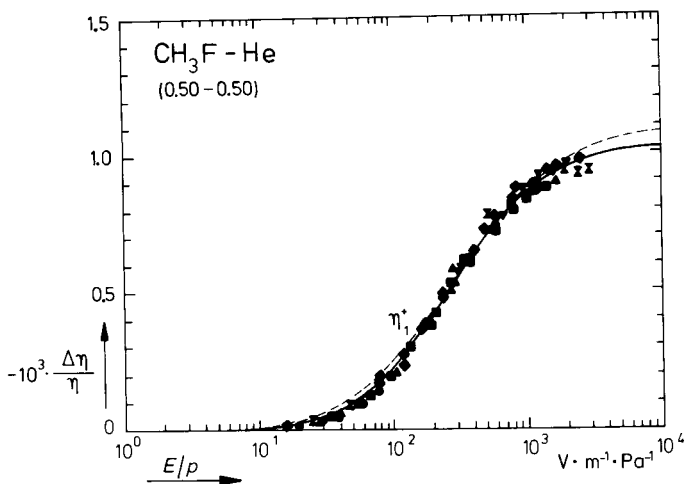


Fig. 11 $-\Delta\eta/\eta$ versus E/p for an equimolar CH_3F -He mixture.

\boxtimes 150 Pa, \bullet 190 Pa, \blacktriangledown 260 Pa, \blacktriangle 310 Pa, \bullet 454 Pa, \blacksquare 490 Pa.

---: theoretical curve of eq. (4) for $P = 1$,

—: theoretical curve of eq. (4) for $P \sim \sqrt{2}$.

The theoretical curves are scaled to fit the experimental points. The choices $P = 1$ and $P \sim \sqrt{2}$ yield the saturation values 1.08 and $1.03 \cdot 10^{-3}$, and the half saturation field-to-pressure ratios 300 and 260 $\text{V} \cdot \text{m}^{-1}/\text{Pa}$, respectively.

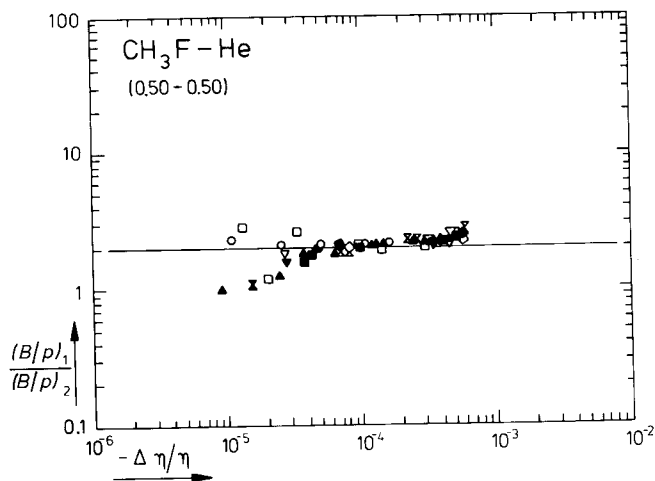


Fig. 12 $[j]^2$ -polarization test from the magnetic field measurements for an equimolar $\text{CH}_3\text{F-He}$ mixture. The ratio of the positions of the two curves from fig. 10 is plotted as a function of the magnitude of the effect. For a $[j]^2$ -type of polarization one expects a value 2 (see line). The symbols for the various pressure runs are the same as in fig. 10. The average of the data points is 2.2 ± 0.2 .

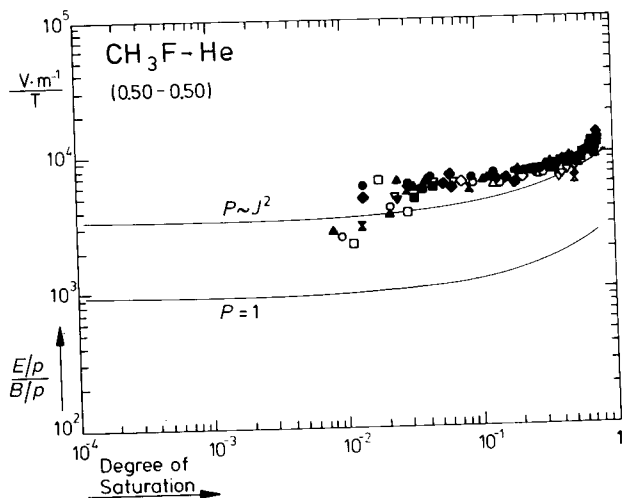


Fig. 13 Test on the scalar factor of the polarization from the magnetic and electric field measurements for an equimolar $\text{CH}_3\text{F-He}$ mixture. The values of $(E/p)/(B/p)$ (for η_1^+) are plotted as a function of the degree of saturation. The symbols for the various pressure runs are the same as in figs. 10 and 11. Theoretical curves for two different choices of P for a $[j]^2$ -polarization are shown.

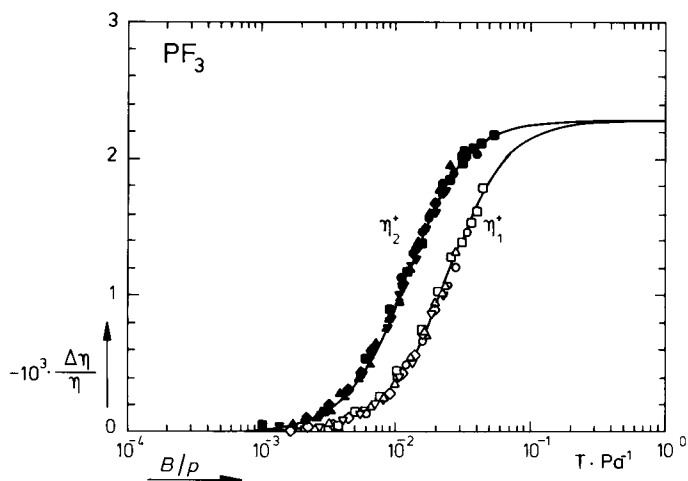


Fig. 14 $-\Delta\eta/\eta$ versus B/p for PF_3 .

□ 118 Pa, ○ 162 Pa, △ 203 Pa, ▽ 254 Pa, ◇ 305 Pa,
■ 93 Pa, ● 143 Pa, ▲ 182 Pa, ▼ 244 Pa, ◆ 310 Pa, X 330 Pa.

The curve of eq. (4) has been scaled to fit the experimental points. For this gas the two curves corresponding to $P = 1$ and $P \sim \underline{g}^2$ coincide. The saturation value is $2.27 \cdot 10^{-3}$ and the half saturation field-to-pressure ratio for η_1^+ is 24 mT/Pa.

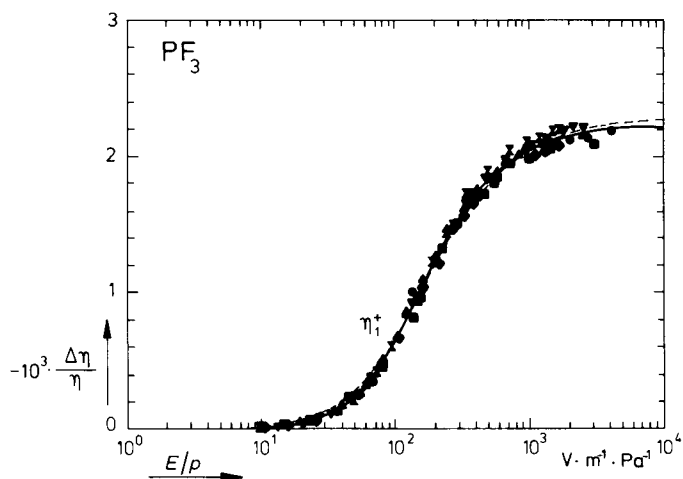


Fig. 15 $-\Delta\eta/\eta$ versus E/p for PF_3 .

■ 99 Pa, ● 114 Pa, ▲ 208 Pa, ▼ 252 Pa, ◆ 333 Pa, X 376 Pa.

--- : theoretical curve of eq. (4) for $P = 1$,

— : theoretical curve of eq. (4) for $P \sim \underline{g}^2$.

The theoretical curves are scaled to fit the experimental points. The choices $P = 1$ and $P \sim \underline{g}^2$ yield the saturation values 2.28 and $2.23 \cdot 10^{-3}$, and the half saturation field-to-pressure ratios 190 and $180 \text{ V}\cdot\text{m}^{-1}/\text{Pa}$, respectively.

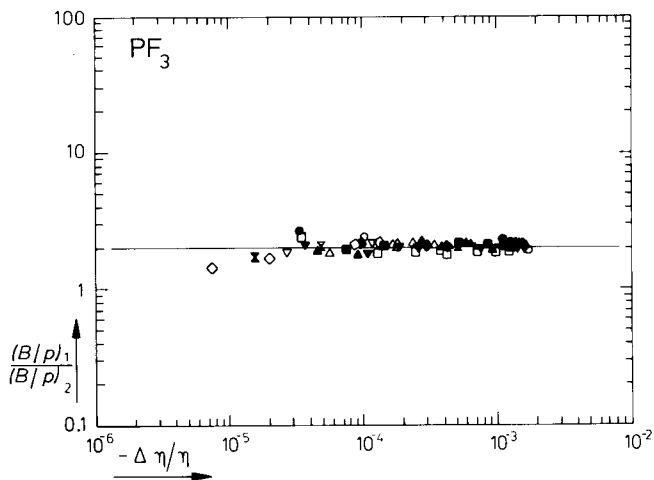


Fig. 16 $[J]^2$ -polarization test from the magnetic field measurements for PF_3 . The ratio of the positions of the two curves from fig. 14 are plotted as a function of the magnitude of the effect. For a $[J]^2$ -type of polarization one expects a value 2 (see line). The symbols for the various pressure runs are the same as in fig. 14. The average of the data points is 2.06 ± 0.14 .

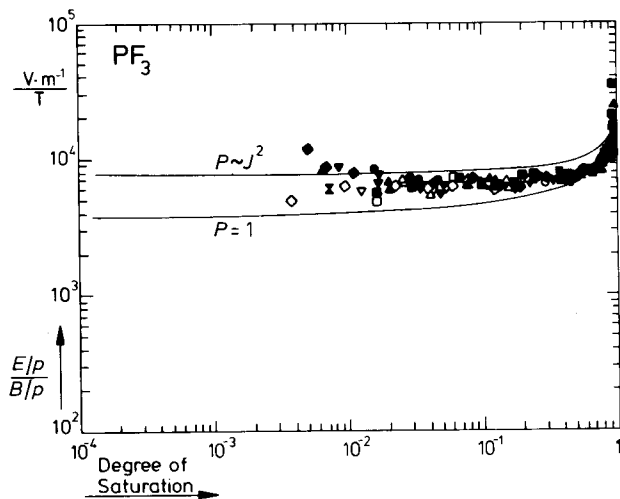


Fig. 17 Test on the scalar factor of the polarization from the magnetic and electric field measurements for PF_3 . The values of $(E/p)/(B/p)$ (for η_1^+) are plotted as a function of the degree of saturation. The symbols for the various pressure runs are the same as in figs. 14 and 15. Theoretical curves for two different choices of P for a $[J]^2$ -polarization are shown.

limit. After this extrapolation corrections 4 and 7 are applied and a check on the $[J]^2$ -polarization is performed by plotting the ratio of $(B/p)_1$ and $(B/p)_2$ as a function of $\Delta\eta/\eta$, see e.g. fig. 4. If this ratio differs from the theoretical value 2, also another polarization is present and further investigation of the $[J]^2$ -polarization is unreliable for our purpose.

Finally some tests on the scalar factor of the $[J]^2$ -polarization are performed. First the individual magnetic and electric field measurements and theoretical curve-fit procedures are used to determine whether it is possible to make a choice of the scalar factor based on the separate curves. Then a combined fit of magnetic and electric field measurements is made (i.e., using the same parameters for both curves). As pointed out in section 2, an elegant way of showing the result of this fit is obtained by plotting in one single graph for the measurements the ratio of B/p and E/p as a function of the degree of saturation, see e.g., fig. 17. In determining B/p for η_1^+ the values for η_2^+ were also employed by shifting them along the B/p axis by a factor 2.

Note that the saturation value for the electric field effect is generally lower than the one for the magnetic field effect, since in the electric field case the molecules for which $K = 0$ do not contribute to the effect (cf. eq. (6)).

Experimental results for the magnetic and electric field dependence of the relative change in the coefficients η_1^+ and η_2^+ are shown in figs. 3 through 17. Some experimental values are listed in table III.

Table I

The Knudsen correction parameters for η , $\Delta\eta$, B/p and E/p as found in this experiment ($T = 300$ K), together with literature data on the field free viscosity. The data in parentheses are calculated according to ref. 4.

gas	K_η (Pa)	$K_{\Delta\eta(B)}$ (Pa)	$K_{\Delta\eta(E)}$ (Pa)	$K_{B/p}$ (Pa)	$K_{E/p}$ (Pa)	η (10^{-6} Pa·s)
N ₂	(81)	146	-	62	-	17.8
CH ₃ Cl	(36)	-	64	-	12	10.7
CH ₃ F	(46)	20	63	19	14	11.0
CH ₃ F-He (0.50-0.50)	94	106	163	48	57	32.5
PF ₃	(44)	66	66	31	31	16.9

Table II

Molecular constants (SI units): the rotational temperature $\hbar^2/2kI_{\perp}$, the ratio of moments of inertia I_{\parallel}/I_{\perp} , rotational g -factors, the electric dipole moment μ_e , the mean electric polarizability $\bar{\alpha}$ and its anisotropic part $\alpha^{\parallel} - \alpha^{\perp}$. The symbols \parallel and \perp refer to directions parallel and perpendicular to the molecular axis of symmetry. Most data are taken from refs. 4 and 21.

gas	$\frac{\hbar^2}{2kI_{\perp}}$ (K)	I_{\parallel}/I_{\perp}	g_{\perp}	g_{\parallel}	μ_e (10^{-30} C·m)	$\bar{\alpha}$ (10^{-40} F·m ²)	$\alpha^{\parallel} - \alpha^{\perp}$ (10^{-40} F·m ²)
N ₂	2.9	0	-0.278		0	1.97	+0.77
CH ₃ Cl	0.63	0.086	-0.0163	+0.305	6.23	5.14	+1.8
CH ₃ F	1.2	0.166	-0.062	+0.265	6.20	2.93	+0.36
PF ₃	0.38	1.61	-0.0659	-0.081	3.44	4.59	-0.70

Table III

Results of the numerical analysis of data on the magnetic and electric field effects on the viscosity ($T = 300$ K). The saturation values $(\Delta n/n)_{\text{sat}}$ and the half saturation field to pressure ratios $(B/p)_{\frac{1}{2}}$ and $(E/p)_{\frac{1}{2}}$ of n_1^+ follow from a least square fit of the curves of eq. (4) to the data points. The first columns refer to $P = 1$ and the second ones to $P \sim \sqrt{2}$. The indices 1 and 2 refer to n_1^+ and n_2^+ , respectively.

gas	MAGNETIC					ELECTRIC			
	$10^3 \cdot (\Delta n/n)_{\text{sat}}$		$(\frac{B}{p})_{\frac{1}{2}}$		$\langle \frac{(B/p)_1}{(B/p)_2} \rangle$	$10^3 \cdot (\frac{\Delta n}{n})_{\text{sat}}$		$(\frac{E}{p})_{\frac{1}{2}}$	
			(mT/Pa)					(V·m ⁻¹ /Pa)	
N ₂	-2.8	-2.8	2.6	2.6	2.0 ± 0.1	-	-	-	-
CH ₃ Cl	-	-	-	-	-	-1.4	-1.1	1500	1000
CH ₃ F	-0.8	-0.7	52	46	2.4 ± 0.3	-0.8	-0.8	690	590
CH ₃ F-He (0.50-0.50)	-1.3	-1.1	37	31	2.2 ± 0.2	-1.1	-1.0	300	260
PF ₃	-2.27	-2.27	24	24	2.06 ± 0.14	-2.28	-2.23	190	180

6. Discussion

In this section we will discuss the results presented in the previous section.

1) N_2 (figs. 3 and 4)

These measurements were carried out as a check on the apparatus. As must be expected, no electric field effect was found. The results for the magnetic field effects on η_1^+ and η_2^+ reproduce the ones obtained by Hulsman¹³). Fig. 4 shows the ratio of the field-to-pressure ratios of the two coefficients as a function of the relative change in the viscosity. This ratio should be precisely 2 if only a $[\underline{J}]^2$ -type of polarization is present. From this graph one can conclude that within the experimental error no polarization other than a $[\underline{J}]^2$ -polarization contributes to the effect for N_2 .

2) CH_3Cl (fig. 5)

The electric field measurements for this gas are very well described with a $[\underline{J}]^2$ ($P \sim \underline{J}^2$) polarization. As we will see below this type of agreement is not sufficient for a decisive conclusion concerning the scalar factor. No magnetic field effect could be measured due to the small g -factor and thus there is no proof that no other than a $[\underline{J}]^2$ -type of polarization is present for this gas.

3) CH_3F (figs. 6 through 9)

Measurements were performed on the molecule CH_3F , because of the large difference in position of the effect between the two cases $P = 1$ and $P \sim \underline{J}^2$ for this gas (see the theoretical curves in fig. 1).

Unfortunately the position of the effect proved to be such that it was not possible to measure the magnetic field effect up to high degrees of saturation. Even though the experimental uncertainty is rather large, it is clear that the distance between the two curves is systematically larger than a factor 2. This is shown in fig. 8, where this distance is plotted as a function of the magnitude of the effect. Apparently the effect cannot be described with a single $[\underline{J}]^2$ -type of polarization.

Fig. 9 shows that, as expected from the presence of other polarizations, a simultaneous fit of both magnetic and electric data points fails.

According to Snider et al.²⁰), in first-order distorted-wave Born

approximation a dipole-dipole interaction can, for symmetric top molecules, produce a $[\underline{W}]^2[\underline{J}]^1$ -polarization, but no appreciable $[\underline{J}]^2$ -polarization, which is generally due to P_2 -terms in the molecular interaction. Performing the same calculations as Snider did for NH_3 and ND_3 ²⁰) for the production cross sections of CH_3F one indeed finds that for CH_3F not only a $[\underline{J}]^2$ -polarization but also a $[\underline{W}]^2[\underline{J}]^1$ -polarization can be expected in viscous flow.

4) CH_3F -He (0.50-0.50) (figs. 10 through 13)

Measurements of an equimolar CH_3F -He mixture were performed for several reasons. In the first place dilution of CH_3F with He diminishes the dipole-dipole interaction and therefore also the contribution from the $[\underline{W}]^2[\underline{J}]^1$ -polarization. Secondly, since the sign of contributions from odd-in- \underline{J} polarizations is different from the one of even-in- \underline{J} polarizations, the effect is expected to increase. This would also improve the experimental accuracy. Thirdly, the position of the effect shifts towards lower B/p and E/p values, due to the fact that the decay time of the polarization, which is rather short for dipole-dipole interaction, becomes larger. This shift creates the possibility to measure up to high degrees of saturation, which results in a much higher accuracy of the analysis.

The data indeed show a higher saturation value and a lower half saturation field-to-pressure ratio and thus a higher accuracy. The ratio between the positions of the field effects for the two coefficients is now considerably closer to the value 2 (the average for the data points is 2.2 ± 0.2). Consequently, the contribution from other polarizations is clearly diminished with respect to the case of pure CH_3F (cf. figs. 8 and 12).

The magnetic field measurements are described somewhat better than for pure CH_3F by both the $P = 1$ and the $P \sim \underline{J}^2$ curve (see fig. 10).

The electric measurements are described better with a $[\underline{J}]^2$ -polarization with scalar factor $P \sim \underline{J}^2$ (see fig. 11). The same holds for the simultaneous fit of magnetic and electric measurements, see fig. 13. The ratio of E/p and B/p values is however systematically larger than the theoretical values for $P \sim \underline{J}^2$. In view of the still detectable presence of polarizations of other tensorial type, no definitive conclusions concerning P can be drawn.

5) PF_3 (figs. 14 through 17)

Since this oblate molecule has a small dipole moment it is expected to show only the contribution from a $[\underline{J}]^2$ -type of polarization. Earlier

measurements by Van Ditzhuyzen moreover showed that the viscomagnetic effect for PF_3 is very large⁴). Therefore it was decided to perform measurements on the gas PF_3 , which would hopefully yield the decisive information. Indeed, the ratio between the positions of the magnetic field effects (see fig. 16) is now precisely 2. At first glance both the magnetic and the electric field measurements seem to show a perfect $[\underline{J}]^2$ ($P \sim \underline{J}^2$) behaviour (see figs. 14, 15 and 16). A simultaneous fit however, fails again (see fig. 17): neither description satisfies the experimental points.

In conclusion we can say that neither possibility for the scalar factor of the $[\underline{J}]^2$ -polarization mentioned in section 1, namely $P = 1$ or $P \sim \underline{J}^2$, describes the experimental results very well. This is especially emphasized by the measurements of PF_3 , where no complications of other nature arise. These last measurements are accurate and no tensorial type other than the $[\underline{J}]^2$ -type of polarization is present. Probably one should not limit oneself to the two choices of P mentioned in section 1, but also allow a more complicated form of the scalar factor, e.g. a combination of these two possibilities. The present experimental results, however, do not allow a more profound quantitative analysis of the scalar factor of the polarization, taking into account more than one of the possibilities studied in this chapter.

References on page 102.

CHAPTER III

EXPERIMENTS ON THE INFLUENCE OF A MAGNETIC FIELD ON DIFFUSION IN N₂-NOBLE GAS MIXTURES

1. Introduction

The influence of external magnetic and electric fields on the transport properties of dilute polyatomic gases has been studied extensively during the last two decades¹⁻⁷). So far the magnetic field effects on shear viscosity⁸⁻¹³) and thermal conductivity¹⁴⁻¹⁹) have been measured for various kinds of molecules. It was found that a velocity gradient predominantly creates a polarization with tensorial character $[\underline{J}]^2$ ($[\underline{J}]^q$ is a normalized irreducible tensor of rank q formed from the angular momentum \underline{J}), whereas a temperature gradient predominantly produces a polarization of the type $[\underline{W}]^1[\underline{J}]^2$ ($[\underline{W}]^p$ is an irreducible tensor of rank p in the reduced molecular velocity \underline{W}). Similar experiments have been carried out in electric fields²⁰⁻²⁵). For mixtures of polyatomic gases and noble gases the magnetic field effect on the cross phenomena, thermal diffusion and its reciprocal effect, the Dufour effect, were investigated. These measurements successfully confirmed for the first time an Onsager relation in the presence of a magnetic field²⁶⁻²⁸). Attempts to complete the set of measurements with data on the field effect on diffusion have failed so far²⁹). In this paper the existence of such an effect will be verified and results for N₂-noble gas mixtures will be presented.

Measurements of the magnetic field effect on diffusion are interesting in two ways. In the first place these measurements yield information on non-equilibrium polarizations produced by a concentration gradient. Furthermore, data on the field effect on diffusion would give the possibility to perform a final check of the theoretical description, using a relation between the field

effects on diffusion, thermal diffusion and thermal conduction. In this way additional information will be obtained concerning the scalar structure of polarizations. Some details of the theoretical description can be found in the following section. In sections 3 and 4 the experimental set-up is described and in sections 5 and 6 the results are presented and discussed.

2. Theory

In this section theoretical expressions relevant for the magnetic field effect on diffusion will be given. For a survey and detailed explanation the reader is referred to chapter I and to ref. 30.

In a binary gas mixture a gradient in the concentration generates a particle flux. In the absence of external forces and pressure and temperature gradients the flux of species 1 in the field-free case is given by:

$$\underline{j}_1 = -n D \underline{\nabla} x_1, \quad (1)$$

where n is the total number density, x_1 is the mole fraction of species 1 and D is the diffusion coefficient. In a magnetic field \underline{B} this transport coefficient has to be replaced by a tensor:

$$\underline{j}_1 = -n \underline{D} \cdot \underline{\nabla} x_1. \quad (2)$$

Spatial symmetry considerations require that the diffusion tensor takes the form

$$\underline{D} = \begin{pmatrix} D^\perp & -D^{\text{tr}} & 0 \\ D^{\text{tr}} & D^\perp & 0 \\ 0 & 0 & D^\parallel \end{pmatrix}, \quad (3)$$

if the field is in the z -direction. The diagonal elements are even in the field whereas the off-diagonal element D^{tr} is odd.

The polarizations depending on the angular momentum \underline{J} , observed in experiments on the influence of a magnetic field on thermal conductivity and thermal diffusion, are of the type $[\underline{H}]^1[\underline{J}]^2$ and $[\underline{H}]^1[\underline{J}]^1$. If one takes into account these two polarizations, the elements of the diffusion tensor for a

polyatomic gas-noble gas mixture change according to

$$\frac{D^{+r}}{D} = -\psi_{12}[g(\xi_{12}) + 2g(2\xi_{12})] + \psi_{11}g(\xi_{11}) , \quad (4)$$

$$\frac{\Delta D^{\perp}}{D} = \frac{D^{\perp}(B) - D^{\perp}(0)}{D} = -\psi_{12}[f(\xi_{12}) + 2f(2\xi_{12})] + \psi_{11}f(\xi_{11}) , \quad (5)$$

$$\frac{\Delta D^{\parallel}}{D} = \frac{D^{\parallel}(B) - D^{\parallel}(0)}{D} = -2\psi_{12} f(\xi_{12}) + 2\psi_{11}f(\xi_{11}) , \quad (6)$$

with the field functions

$$f(x) = \frac{x^2}{1+x^2} , \quad g(x) = \frac{x}{1+x^2} , \quad (7)$$

and the field parameter

$$\xi_{pq} = \frac{g\mu_N kT}{\hbar [x_1 v_{11} \mathfrak{S}(\underline{pqj}|\underline{1})_{11} + x_2 v_{12} \mathfrak{S}(\underline{pqj}|\underline{1})_{12}]} \frac{B}{p} . \quad (8)$$

Here g is the rotational g -factor of the polyatomic molecule, μ_N the nuclear magneton, $\langle v \rangle$ a relative thermal speed and the $\mathfrak{S}(\underline{pqj}|\underline{1})_{kl}$ effective cross sections governing the decay due to the collisions of species k and l (1 = polyatomic gas, 2 = noble gas) of the \underline{pqj} -polarization (rank p in \underline{W} , rank q in \underline{J} and scalar factor characterized by j). For the magnitude of the contributions from the polarizations we can write down

$$\psi_{pq} = \frac{(1 - \frac{1}{2}\delta_{p1}\delta_{q2})x_2 v_{12} \mathfrak{S}^2(\underline{10}|\underline{1})_{12}}{\mathfrak{S}(\underline{10}|\underline{1})_{12} [x_1 v_{11} \mathfrak{S}(\underline{pqj}|\underline{1})_{11} + x_2 v_{12} \mathfrak{S}(\underline{pqj}|\underline{1})_{12}]} , \quad (9)$$

where $\mathfrak{S}(\underline{10}|\underline{1})_{12}$ describes the production of the \underline{pqj} -polarization in a concentration gradient due to collisions between species 1 and 2 and $\mathfrak{S}(\underline{10}|\underline{1})_{12}$ the field free diffusion.

In the derivation of eqs. (4) through (6) the approximation has been made that the irreducible tensor parts of $[\underline{W}]^1[\underline{J}]^2$ and $[\underline{W}]^1[\underline{J}]^1$ all have the same decay time. This approximation is strictly valid for a spherical potential³¹⁾ and is therefore generally referred to as the "spherical approximation". Measurements of the field effects on thermal diffusion and thermal conductivity showed that the spherical approximation yields a satisfactory description of the experimental results²⁶⁾.

In chapter I it was shown (cf. chapter I, eq. (79)) that for the field induced change in the generalized phenomenological coefficients L

$$\Delta L_{\mu\mu}^{\dot{j}\dot{j}}(\infty) \Delta L_{\mu\mu}^{qq}(\infty) = [\Delta L_{\mu\mu}^{\dot{j}q}(\infty)]^2, \quad (10)$$

if one assumes that in the three experiments the same polarization is present. In our case $L^{\dot{j}\dot{j}}$ is the diffusion coefficient, L^{qq} the thermal conductivity coefficient and $L^{\dot{j}q}$ the coefficient of the cross effect, thermal diffusion. Using the relation between these generalized phenomenological coefficients and the usual transport coefficients D , λ and D_T (cf. chapter I, eqs. (120) through (123)), and the relations

$$\lim_{B \rightarrow \infty} \frac{\Delta D}{D} = c \psi_{pq}^T, \quad \lim_{B \rightarrow \infty} \frac{\Delta \lambda}{\lambda} = c \psi_{pq}^\lambda, \quad \lim_{B \rightarrow \infty} \frac{\Delta D}{D} = c \psi_{pq}^D, \quad (11)$$

with c a numerical constant (cf. e.g., eqs. (4) through (6)), we can rewrite eq. (10) as

$$(\psi_{pq}^T)^2 = \frac{x_1 x_2 \lambda}{n k D} \psi_{pq}^D \psi_{pq}^\lambda. \quad (12)$$

This is the relation which was established by Eggermont et al.³⁰⁾ on the basis of the above stated assumption, using explicit expressions for the ψ 's. As we have seen in chapter I the equality has in general to be replaced by an inequality. If more than one single type of polarization is produced and there is no coupling between these polarizations, the relation between the field effects on thermal conduction, thermal diffusion and diffusion (12) remains still valid for the contributions from each type separately. Substitution of data on the magnetic field effect on thermal conduction and thermal diffusion into this relation show that a (small) magnetic field effect on diffusion should exist (see e.g. ref. 26). The measurement of such an effect would therefore be an interesting direct test of the description.

3. Description of the experimental set-up

For the accurate determination of small effects, such as the magnetic field effect on diffusion, measurements of transverse effects (which occur only in the presence of a magnetic field) are indicated. The central part of the apparatus is formed by a capillary of rectangular cross section (see fig. 1; dimensions: length $l = 60$ mm, width $w = 20$ mm, thickness $t = 0.7$ mm; material: brass). Across the length of this capillary a concentration gradient is set up by connecting each end to a 50 l bulb containing one of the components of the mixture to be measured. Under the influence of a magnetic field \underline{B} a transverse particle flow is produced (cf. eq. (2), let $\underline{B} = (0,0,B)$ and $\underline{\nabla x} = (\nabla x, 0, 0)$):

$$j_1^{tr} = j_{1,y} = -nD^{tr} \nabla x_1 . \quad (13)$$

This flow gives rise to a small concentration difference δx across the width of the capillary. For the set-up of fig. 1 one has in the stationary state

$$\delta x = \frac{w}{l} \frac{D^{tr}}{D} \Delta x , \quad (14)$$

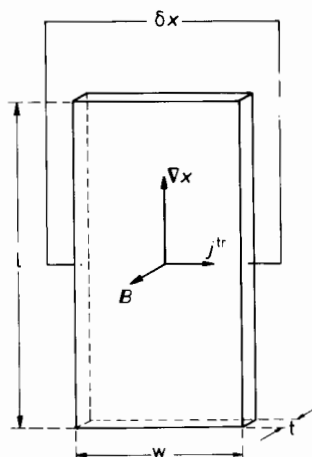


Fig. 1 Schematic diagram of the apparatus for the measurement of the magnetic field effect on diffusion. The dimensions are : $l = 60$ mm, $w = 20$ mm and $t = 0.7$ mm. The field orientation is the one for the measurement of D^{tr} . The indicated directions for ∇x and j^{tr} are those for N_2 in a N_2 -noble gas mixture. The cells for measuring the transverse concentration difference δx are located at 0.75 m from the field centre. In the absence of a magnetic field $j^{tr} = 0$.

where $\Delta x = l \nabla x$ is the applied concentration difference.

In order to be able to disentangle the contributions of the various polarizations, data on at least two independent elements (or combinations of elements) of the diffusion tensor are required. For this purpose the apparatus was designed in such a way that the orientation of the magnetic field with respect to the gradient can be changed. In the case of the orientation shown in fig. 2 (let $\underline{B} = (0,0,B)$ and $\underline{\nabla}x = (0, -\frac{1}{2}\sqrt{2} \nabla x, \frac{1}{2}\sqrt{2} \nabla x)$) also a transverse particle flow

$$j_1^{tr} = \frac{1}{2}\sqrt{2} (j_{1,y} + j_{1,z}) = -\frac{1}{2} n(D'' - D^\perp) \nabla x_1 \quad (15)$$

will occur due to the fact that D'' is not equal to D^\perp (and thus j'' differs from j^\perp). The concentration difference across the width of the capillary is then given by

$$\delta x = \frac{1}{2} \frac{w}{l} \frac{D'' - D^\perp}{D} \Delta x. \quad (16)$$

The transverse concentration differences, which occur under both orientations (typical value $1 * 10^{-5}$), are detected by measuring the difference in heat conductivity between the gas mixtures at both sides of the capillary, using a matched pair of katharometer type thermistors (bead size: 1 mm; bead temperature: 8 K above ambient temperature) arranged in a Wheatstone bridge.

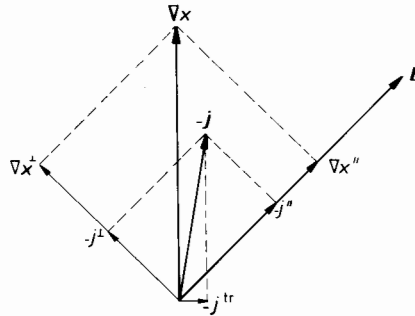


Fig. 2 The field orientation for measuring the difference between the two longitudinal diffusion coefficients D'' and D^\perp . Note that the magnetic field \underline{B} now lies in the plane of drawing and makes an angle of 45° with the concentration gradient $\underline{\nabla}x$. In the absence of a magnetic field $D'' = D^\perp$, consequently $j'' = j^\perp$ and thus $j^{tr} = 0$.

For optimum stability the measuring cells containing these thermistors are located in one single thermally isolated copper block, which is kept at constant temperature by means of a thermoelectric heat pump. To avoid effects of magnetic stray fields on the thermistors this block is placed at 0.75 m from the field centre inside a double magnetic shield of Netic S3 alloy. A high sensitivity is attained: in a N_2 -He mixture concentration differences as small as $2 \cdot 10^{-7}$ can still be detected. In a similar way also the applied concentration gradient, which slowly decays (relaxation time approximately 2 hours for N_2 -Ar at $p = 250$ Pa), is monitored. The capillary and the detection section are placed inside a vacuum jacket, while the bulbs and the leads are stabilized with water from a thermostat.

The differences in thermal conductivity are related to concentration differences by calibrating them with mixtures of known composition. To ensure reproducibility, the pressures of the mixtures introduced in the apparatus are compared to a reference pressure using a high accuracy differential capacitance manometer.

4. Experimental checks and corrections

Several corrections have to be applied to the expressions in eqs. (14) and (16) in order to take into account the non-ideal experimental conditions. First of all, as in Hall experiments, the ends of the capillary have a short-circuiting effect on the transverse flow. To account for this effect, which vanishes when $l \gg w$, a correction³²⁾ $\epsilon = 2 \cdot 10^{-2}$ has been incorporated. Equations (14) and (16) then read

$$\left(\frac{\Delta D}{D}\right)_m = (1 + \epsilon) \frac{1}{w} \frac{\delta x}{\Delta x}, \quad (17)$$

where m stands for "measured at pressure p".

Secondly, Knudsen effects have to be taken into account. These effects occur because at low pressures the mean free path of the molecules becomes comparable to the thickness of the capillary. The corrections for these effects on the magnitude and the position of the field effect are applied to the individual pressure runs according to¹⁶⁾

$$\left(\frac{\Delta D}{D}\right) = \left(\frac{\Delta D}{D}\right)_m \left[1 + \frac{K}{p}\right] \quad (18)$$

and

$$\left(\frac{B}{p}\right) = \left(\frac{B}{p}\right)_m \left[1 + \frac{K_p}{p}\right]^{-1}, \quad (19)$$

where the K are the Knudsen correction coefficients. The values of K_{AD} and K_p , resulting from a linear fit of the experimental values of $(D^{tr}/D)^{-1}_{max}$ and $(B/p)_{max}$ as a function of $1/p$ respectively, are listed in table I.

As we are dealing with rather small effects, a number of consistency tests were performed in order to be sure that no systematic errors are present. It was verified that

- 1) no field effect occurs in noble gases,
- 2) no field effect occurs at zero gradient,
- 3) the field effect is proportional to the magnitude of the applied gradient,
- 4) the field effect is proportional to the geometrical factor $1/w$ (see section 5),
- 5) D^{tr} is odd in the field and
- 6) $D^{||} - D^{\perp}$ is even, and that
- 7) the sign of the effect is in accordance with theory (positive ψ , cf. eqs. (2) through (6) and figs. 1 and 2).

5. Experimental results

Experiments have been carried out for N_2 -He, N_2 -Ne and N_2 -Ar mixtures at room temperature. The effect has been studied as a function of the noble gas concentration.

The experimental data and the results of the data analysis are listed in table I. Some of the systems investigated are illustrated in figs. 3 through 5. The theoretical curves of eqs. (4) through (6) have been fitted to the experimental points using the ψ 's and the ξ 's as adjustable parameters. As one can see, the field dependence of the data points is in perfect agreement with the theoretical behaviour. Analogous to the results of the magnetic field effect on thermal diffusion²⁶), the measurements can very well be described using one single $[W]^1[J]^2$ -polarization in the case of N_2 -He, but for N_2 -Ne and N_2 -Ar also a second polarization of the type $[W]^1[J]^1$ has to be taken into account.

In fig. 6 the quantity $B/p\xi_{12}$, which is related to the position of the effect, is plotted as a function of the noble gas concentration. It is clear from these graphs that this quantity depends linearly on the concentration in agreement with eq. (8). The lines are fitted to the data points in such a way that they extrapolate to the same value for pure N_2 . Extrapolations to $x_2 = 0$ and 1 yield values for the two decay cross sections occurring in eq. (8), see table II.

Using eq. (9) and the values for $\mathfrak{G}\left(\begin{smallmatrix} 10 & 1 \\ 10 & 1 \end{smallmatrix}\right)_{12}$, which follow from data on the field-free diffusion coefficient, one can now determine the production cross sections for the diffusion for each concentration studied. The results are shown in fig. 7. Since cross sections do not depend on the concentration the data points should lie on a straight horizontal line, which is indeed found.

We will now compare the present results with data on the field influence on thermal conduction¹⁸⁾ and thermal diffusion²⁶⁾. As far as the position along the B/p axis is concerned these results showed some discrepancies for N_2 -Ne and N_2 -Ar, see fig. 6. If compared now also to the present results, the discrepancies become even more significant: differences up to 30% occur whereas the experimental error equals 10% at most (cf. fig. 6 and table IV).

No agreement at all is found when we combine the magnitudes ψ of the magnetic field effects on thermal conduction, thermal diffusion and diffusion in order to test relation (12), see table III. The contributions from the $[\underline{w}]^1[\underline{j}]^2$ -polarization to the observed effects for N_2 -Ar and N_2 -Ne are larger than the predicted values by approximate factors of 4 and 3 respectively. Even in the case of N_2 -He where no other polarization contributes to the effects and one therefore directly can compare the magnitudes of the various field effects, the field effect on diffusion is approximately twice as large as expected.

It was extensively verified that these discrepancies are not due to systematic experimental errors by performing many experimental checks (see section 4). Measurements have also been performed in an apparatus with different dimensions ($l = 60$ mm, $w = 10$ mm and $t = 1.4$ mm) for an equimolar N_2 -Ar mixture. Due to the smaller signal ($l/w = 1/6$ instead of $1/3$) the accuracy was lower than for the previous apparatus, but within the accuracy limits, these measurements reproduced the earlier obtained results (cf. table I).

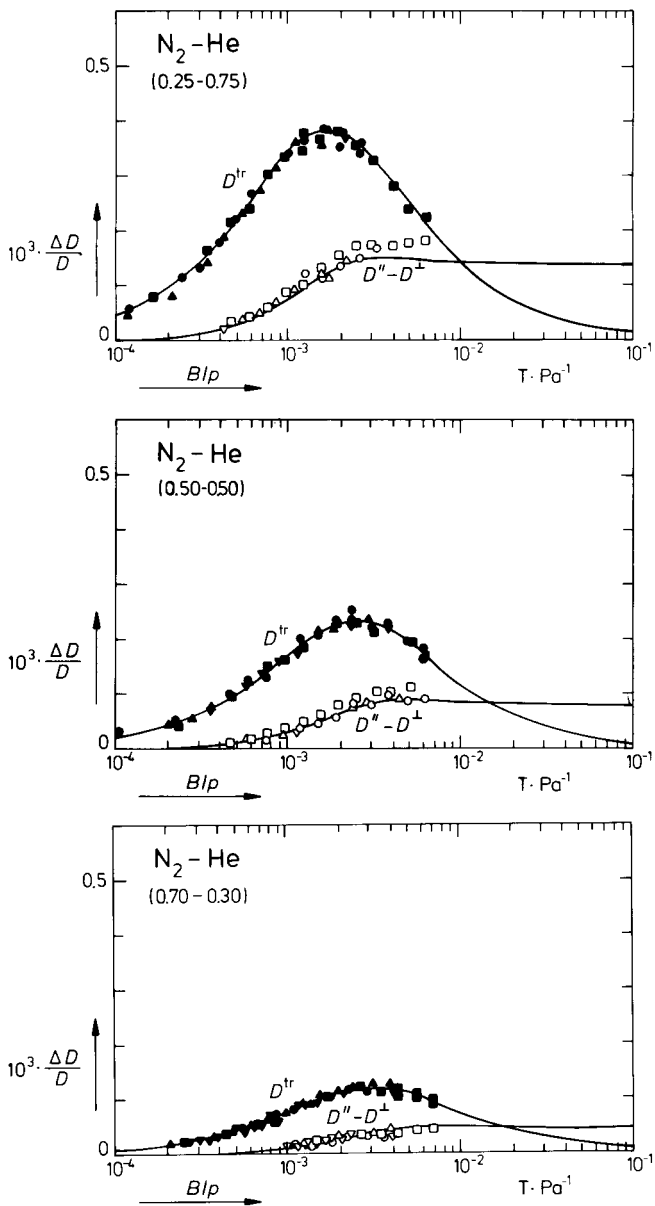


Fig. 3 Experimental results for N_2 -He at 300 K for three noble gas concentrations:

$x_2 = 0.75$: \square \blacksquare 269 Pa, \circ \bullet 534 Pa, \triangle \blacktriangle 934 Pa, ∇ \blacktriangledown 934 Pa,

$x_2 = 0.50$: \square \blacksquare 284 Pa, \circ \bullet 291 Pa, \triangle \blacktriangle 560 Pa, ∇ \blacktriangledown 941 Pa,

$x_2 = 0.30$: \square \blacksquare 271 Pa, \circ \bullet 548 Pa, \triangle \blacktriangle 552 Pa, ∇ \blacktriangledown 967 Pa.

The drawn lines are the theoretical curves of eqs. (4) through (6) scaled to fit the experimental points. The fit parameters are

$\psi_{12} = 2.7, 1.6, 0.83 \cdot 10^{-4}$ and $B/p\bar{\epsilon}_{12} = 2.8, 3.9, 4.9$ mT/Pa respectively, with $\psi_{11} = 0$.

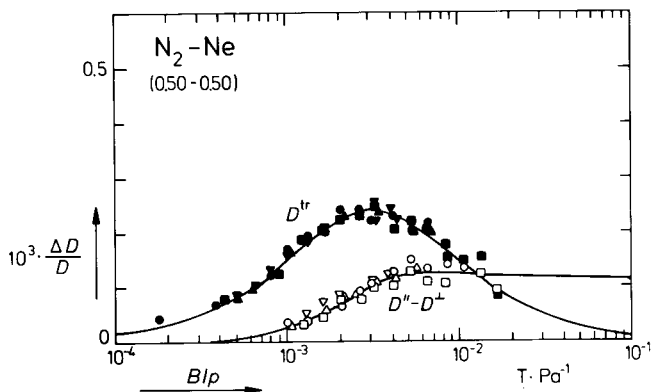


Fig. 4 Experimental results for N_2 -Ne (0.50-0.50) at 300 K.

□■ 134 Pa, ○● 189 Pa, △▲ 293 Pa, ▽▼ 547 Pa.

The drawn lines are the theoretical curves of eqs. (4) through (6) scaled to fit the experimental points. The fit parameters are

$$\psi_{12} = 1.9 \cdot 10^{-4}, B/p\xi_{12} = 4.9 \text{ mT/Pa}, \psi_{11} = 0.53 \cdot 10^{-4}, B/p\xi_{11} = 3.0 \text{ mT/Pa}.$$

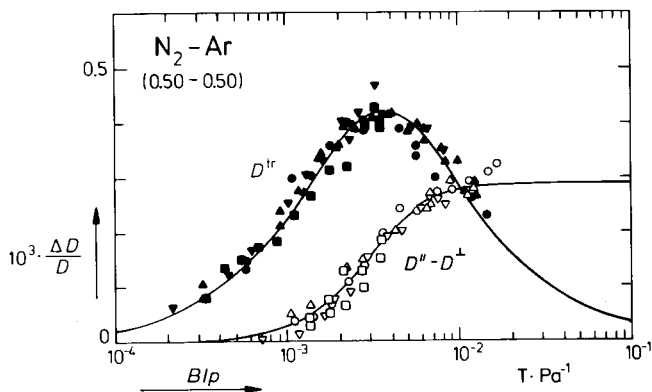


Fig. 5 Experimental results for N_2 -Ar (0.50-0.50) at 300 K.

○● 137 Pa, △▲ 190 Pa, ▽▼ 270 Pa, □■ 586 Pa.

The drawn lines are the theoretical curves of eqs. (4) through (6) scaled to fit the experimental points. The fit parameters are

$$\psi_{12} = 3.7 \cdot 10^{-4}, B/p\xi_{12} = 6.5 \text{ mT/Pa}, \psi_{11} = 2.2 \cdot 10^{-4}, B/p\xi_{11} = 6.1 \text{ mT/Pa}.$$

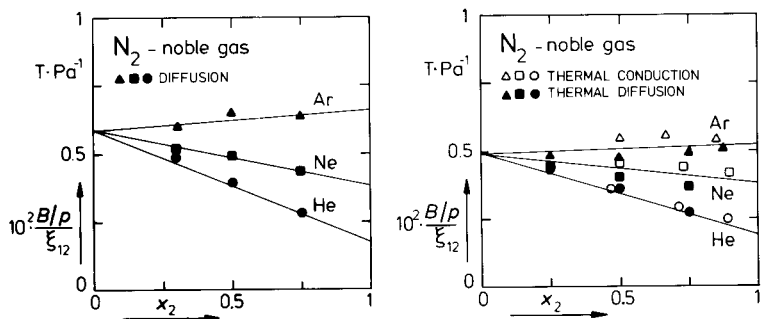


Fig. 6 The position of the magnetic field effect for N_2 -noble gas mixtures as a function of the mole fraction of the noble gas. Left: field effect on diffusion. Right: field effects on thermal conduction¹⁸⁾ (open symbols) and thermal diffusion²⁶⁾ (closed symbols).

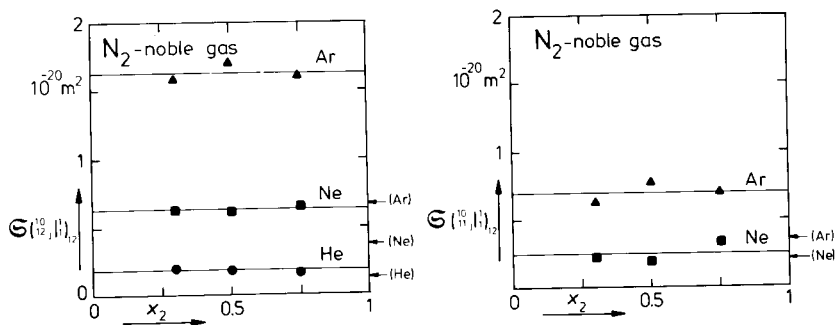


Fig. 7 The production cross section for the $[W]^1[U]^2$ -polarization and the $[W]^1[U]^1$ -polarization for N_2 -noble gas mixtures versus the mole fraction of the noble gas. The arrows indicate the values predicted from the combined results of experiments on thermal conduction and thermal diffusion using eq. (12).

6. Discussion

The experimental results presented in the previous section clearly show, if we exclude systematic experimental errors, that the theoretical description fails in certain aspects. Summarizing we come to the following conclusions:

- 1) If we look at each set of measurements separately (i.e., thermal conduction or thermal diffusion or diffusion), everything is internally consistent: field and concentration dependence agree perfectly well with theory.
- 2) If we compare the results of the three sets of measurements using relation (12), small discrepancies occur for the positions of the effect, while inadmissibly large discrepancies occur for the magnitude.
- 3) Whereas for N_2 -Ar and N_2 -Ne the results for the ψ 's and ξ 's follow from a complicated 4-parameter fit and may therefore be inaccurate, for N_2 -He only one polarization contributes to the effect and the "raw" experimental data can directly be used for a comparison. Even in this simple case no agreement is found.

Table I

Experimental results for N_2 -noble gas mixtures ($T = 300$ K).

gas	x_2	$10^3 \cdot \left(\frac{D^{tr}}{D}\right)_{\max}$	$\left(\frac{B}{p}\right)_{\max}$	K_Δ	K_p	$10^3 \cdot \psi_{12}$	$B/p\xi_{12}$	$10^3 \cdot \psi_{11}$	$B/p\xi_{11}$
			(mT/Pa)	(Pa)	(Pa)		(mT/Pa)		(mT/Pa)
N_2 -He	0.30	0.12	3.0	11	22	0.084	4.9	< 0.002	-
	0.50	0.23	2.4	40	37	0.16	3.9	< 0.002	-
	0.75	0.39	1.7	19	84	0.27	2.8	< 0.002	-
N_2 -Ne	0.30	0.15	3.1	< 5	< 5	0.11	5.1	0.028	4.4
	0.50	0.24	3.1	< 5	< 5	0.19	4.9	0.053	3.0
	0.75	0.41	2.5	16	15	0.35	4.4	0.19	3.8
N_2 -Ar	0.30	0.23	3.5	64	< 5	0.20	6.0	0.11	4.5
	0.50	0.43	3.6	77	< 5	0.37	6.5	0.21	6.1
	0.75	0.59	3.5	39	< 5	0.50	6.3	0.27	6.0
N_2 -Ar*)	0.50	0.39	3.4	44	< 5				

*) Measured in a different apparatus: $l = 60$ mm, $w = 10$ mm and $t = 1.4$ mm.

Table II

Effective cross sections for the production and decay of the polarizations in diffusing N_2 -noble gas mixtures. The values in parentheses are calculated from the results of thermal conduction¹⁸⁾ and thermal diffusion²⁶⁾ measurements, using relation (12).

gas	$\sigma_{12j 1}^{10j 1} \quad \sigma_{11j 1}^{10j 1}$				$\sigma_{12j 1}^{12j 1} \quad \sigma_{12j 1}^{12j 1} \quad \sigma_{11j 1}^{11j 1} \quad \sigma_{11j 1}^{11j 1}$			
	(10^{-20} m^2)				(10^{-20} m^2)			
N_2 -He	0.18 (0.12)	<0.01 (<0.01)			7.4 (8.7)	48 (41)	- -	- -
N_2 -Ne	0.63 (0.37)	0.24 (0.18)			28 (29)	48 (41)	23 (39)	35 (16)
N_2 -Ar	1.4 (0.66)	0.69 (0.34)			58 (47)	48 (41)	60 (26)	35 (16)

Table III

Comparison of the present results with the predictions from thermal conduction and thermal diffusion, using relation (12), for $x_2 = 0.5$.

gas	$10^3 \cdot \psi_{12}^\lambda$	$10^3 \cdot \psi_{12}^\tau$	$10^3 \cdot \psi_{12}^D$	$10^3 \cdot \psi_{12}^D_{calc}$
N_2 -He	1.4	0.25	0.16	0.08
N_2 -Ne	2.5	0.38	0.19	0.08
N_2 -Ar	1.9	0.37	0.37	0.10

Apparently the assumption which underlies the relation between the three effects, namely that the same polarization is produced in the three cases (see section 2), is not justified. From the dependence of field effects on the orientation of the field with respect to the gradient we do however know, that the polarizations which give rise to the field effects under consideration all have the same tensorial character. Consequently their scalar factors, which have always been taken equal, must differ.

Let us now restrict ourselves to the case where just one tensorial type of polarization plays a role and consider two vectors $\underline{\Phi}^{12j}$ and $\underline{\Phi}^{12q}$, corresponding to the polarizations produced by concentration and temperature gradients respectively. These vectors, which have the same — known — tensorial factor, are normalized according to

$$\langle \underline{\Phi}^{12i} | \underline{\Phi}^{12i} \rangle = \underline{I} \quad (i = j, q), \quad (20)$$

where the brackets denote the usual scalar product in the Hilbert space of velocity and angular momentum dependent expansion functions, see chapter I, and \underline{I} is the unit tensor. The two functions $\underline{\Phi}^{12j}$ and $\underline{\Phi}^{12q}$ need not be orthogonal. Their scalar product is a diagonal tensor with elements which we will denote by a_{jq} :

$$\langle \underline{\Phi}^{12j} | \underline{\Phi}^{12q} \rangle = \underline{I} a_{jq}. \quad (21)$$

If the experimental results can be described with only one polarization, which is the case for the system N_2 -He, we may assume that $\underline{\Phi}^{12j}$ and $\underline{\Phi}^{12q}$ do not couple to any other polarization. The relation between the three field effects then takes the form (see appendix)

$$(\psi_{pq}^T)^2 = a_{jq}^2 \frac{x_1 x_2 \lambda}{n k D} \psi_{pq}^D \psi_{pq}^\lambda. \quad (22)$$

The possibilities for the value of a_{jq} are

- 1) $|a_{jq}| = 1$: This means that the vectors $\underline{\Phi}^{12j}$ and $\underline{\Phi}^{12q}$ coincide: $\underline{\Phi}^{12j} = \underline{\Phi}^{12q} = \underline{\Phi}^{12}$, the same polarization is produced and relation (12) should be valid (note that eq. (22) indeed reduces to eq. (12)).

- 2) $a_{jq} = 0$: The vectors $\underline{\Phi}^{12j}$ and $\underline{\Phi}^{12j}$ are now orthogonal. In such a case no field effect on the cross effects (thermal diffusion and the Dufour effect), would occur (cf. eq. (22)), which is contradicted by the experiments. If $a_{jq} = 0$, such field effects would only exist when the polarizations couple to each other. In order to reconcile the experimental data the cross section for such a coupling would have to be of the same order of magnitude as the decay cross sections of the polarizations. In turn, such a large off-diagonal cross section would give rise to a more complicated field dependence, which makes $a_{jq} = 0$ highly improbable.
- 3) $0 < |a_{jq}| < 1$: The vectors $\underline{\Phi}^{12j}$ and $\underline{\Phi}^{12q}$ are neither orthogonal nor identical. Due to the fact that the two polarizations now have a certain common component, also field effects on the cross effects will occur.

Equation (22) enables us to determine $|a_{jq}|$. The resulting values for this coefficient are listed in table IV. If there is no coupling between the polarizations their decay cross sections must be equal (see appendix). In order to check this, the half saturation field-to-pressure ratios are also listed. One should keep in mind that for N_2 -He the data are provided directly by the experiment, whereas for N_2 -Ne and N_2 -Ar a 4-parameter fit is needed to disentangle the contributions from polarizations of different tensorial type. All $|a_{jq}|$ should be smaller than unity, which is indeed found. The inequality derived in chapter I (Ch. I, eq. (79)) is thus experimentally confirmed. For N_2 -He the positions of the field effects coincide within the experimental error of 10%. For N_2 -Ne and N_2 -Ar larger differences between the positions of the $[\underline{W}]^1[\underline{J}]^2$ -contribution to the field effects occur. This may be due to inaccuracies in the determination of these positions. On the other hand, this might also be an indication that there is a slight coupling between the polarizations.

In conclusion we can say that the results of this experiment have shown that concentration and temperature gradients produce different polarizations. The tensorial factors of these polarizations are equal, consequently their scalar factors must be different. From a comparison of the results of the field effects on diffusion, thermal conduction and thermal diffusion the scalar product of these scalar factors has been determined. More information on their exact form can, however, not be obtained from the present experimental data.

Finally, the measurements yield numerical values for the production and the decay of the polarization produced by a concentration gradient, see table II.

References on page 103.

Table IV

Comparison between the measurements of the magnetic field effects on thermal conduction, thermal diffusion and diffusion. The values in parentheses are obtained by interpolation. The values for the field free diffusion coefficient are taken from ref. 33, the ones for the thermal conductivity coefficient from ref. 18. From these data the listed values for the scalar product a_{jq} are obtained (see eq. (22)).

gas	x_2	B/p^E_{12} (mT/Pa)			$10^3 \cdot \psi_{12}$			$\begin{matrix} D & \lambda \\ (10^{-4} \text{ m}^2 \cdot \text{s}^{-1}) & (\text{W} \cdot \text{m}^{-1} \cdot \text{K}^{-1}) \end{matrix}$		$ a_{jq} $
		D	λ	D_T	D	λ	D_T			
N ₂ -He	0.30	4.9	(4.4)	(4.2)	0.083	(2.3)	(0.17)	0.722	0.043	0.52
	0.50	3.9	3.7	3.5	0.16	1.4	0.25	0.722	0.058	0.51
	0.75	2.8	(2.9)	2.7	0.27	(0.66)	0.24	0.722	0.088	0.43
N ₂ -Ne	0.30	5.1	(5.0)	(4.4)	0.11	(3.2)	(0.26)	0.328	0.030	0.50
	0.50	4.9	4.7	4.0	0.19	2.5	0.38	0.328	0.034	0.48
	0.75	4.4	(4.3)	3.6	0.35	(1.4)	0.33	0.328	0.040	0.36
N ₂ -Ar	0.30	6.0	(5.4)	(4.8)	0.20	(2.7)	(0.32)	0.197	0.023	0.45
	0.50	6.5	5.4	4.7	0.37	1.9	0.37	0.197	0.021	0.39
	0.75	6.3	(5.3)	4.9	0.50	(0.89)	0.23	0.197	0.020	0.28

APPENDIX Derivation of a general relation between field effects

According to chapter I the saturation value of a phenomenological coefficient in an external field may be written as

$$\Delta L_{\mu\mu}^{\alpha\beta}(\infty) = -k \langle R \chi_{\mu}^{\alpha} | \mathcal{R}_d^{-1} \chi_{\mu}^{\beta} \rangle, \quad (\text{A.1})$$

with

$$\chi_{\mu}^{\alpha} = \mathcal{R}_{nd} \mathcal{R}_d^{-1} \psi_{\mu}^{\alpha}, \quad \chi_{\mu}^{\beta} = \mathcal{R}_{nd} \mathcal{R}_d^{-1} \psi_{\mu}^{\beta}. \quad (\text{A.2})$$

Here, \mathcal{R}_d and \mathcal{R}_{nd} are the diagonal and non-diagonal part of the linearized Waldmann-Snider collision operator, respectively, ψ^{α} and ψ^{β} are microscopic fluxes and R is the angular momentum reversal operator. We assume that each microscopic flux produces its own polarization, $\phi^{pq\alpha}$ and $\phi^{pq\beta}$ respectively, and that different polarizations do not couple. Thus

$$\langle R \chi^{\alpha} | = \langle \psi^{\alpha} \mathcal{R}_d^{-1} \mathcal{R}_{nd} | = \sum_i \langle \psi^{\alpha} | \mathcal{R}_d^{-1} \phi^i \rangle \langle \phi^i | \mathcal{R}_{nd} \phi^{pq\alpha} \rangle \langle \phi^{pq\alpha} | \equiv K^{\alpha} \langle \phi^{pq\alpha} | \quad (\text{A.3})$$

and similarly

$$| \chi^{\beta} \rangle = K^{\beta} | \phi^{pq\beta} \rangle. \quad (\text{A.4})$$

For the sake of simplicity we have omitted in these equations indices such as μ and ν , characterizing the spherical components. The two polarizations have the same tensorial factor (rank p in \underline{w} and q in \underline{J}), but possibly different scalar factors. For their scalar product we write

$$\langle \phi^{pq\alpha} | \phi^{pq\beta} \rangle = \alpha_{\alpha\beta}, \quad (\text{A.5})$$

so that

$$\begin{aligned} \Delta L^{\alpha\beta}(\infty) &= -k K^{\alpha} K^{\beta} \langle \phi^{pq\alpha} | \mathcal{R}_d^{-1} \phi^{pq\beta} \rangle = -k K^{\alpha} K^{\beta} \sum_i \langle \phi^{pq\alpha} | \phi^i \rangle \langle \phi^i | \mathcal{R}_d^{-1} \phi^{pq\beta} \rangle = \\ &= -k K^{\alpha} K^{\beta} \alpha_{\alpha\beta} \langle \phi^{pq\beta} | \mathcal{R}_d^{-1} \phi^{pq\beta} \rangle \end{aligned} \quad (\text{A.6})$$

and

$$\Delta L^{\beta\alpha}(\infty) = -k K^{\beta\alpha}_{KK} a_{\alpha\beta} \langle \Phi^{pq\alpha} | \mathcal{R}_d^{-1} \Phi^{pq\alpha} \rangle . \quad (\text{A.7})$$

From the Onsager relations (cf. chapter I) we now see that

$$\langle \Phi^{pq\alpha} | \mathcal{R}_d^{-1} \Phi^{pq\alpha} \rangle = \langle \Phi^{pq\beta} | \mathcal{R}_d^{-1} \Phi^{pq\beta} \rangle , \quad (\text{A.8})$$

which means that the decays of the two polarizations have to be equal. Furthermore we have

$$\Delta L^{\alpha\alpha}(\infty) = -k K^{\alpha\alpha}_{KK} \langle \Phi^{pq\alpha} | \mathcal{R}_d^{-1} \Phi^{pq\alpha} \rangle \quad (\text{A.9})$$

and

$$\Delta L^{\beta\beta}(\infty) = -k K^{\beta\beta}_{KK} \langle \Phi^{pq\beta} | \mathcal{R}_d^{-1} \Phi^{pq\beta} \rangle . \quad (\text{A.10})$$

Combination of eqs. (A.6) through (A.10) yield

$$\Delta L^{\alpha\alpha}(\infty) \Delta L^{\beta\beta}(\infty) = a_{\alpha\beta}^2 [\Delta L^{\alpha\beta}(\infty)]^2 , \quad (\text{A.11})$$

which is a generalization of eq. (10). Since $a_{\alpha\beta} \leq 1$, eq. (A.11) is in accordance with the inequality derived in chapter I (Ch. I, eq. (79)).

References on page 103.

CHAPTER IV

A COMPARISON OF DATA ON THE VISCOMAGNETIC EFFECT, FLOW BIREFRINGENCE AND DEPOLARIZED RAYLEIGH LINE BROADENING

1. Introduction

The results of the experiments described in the preceding two chapters have clearly shown that the structure of the polarizations is not as simple as one might hope. In order to obtain further information, existing data on the viscomagnetic effect, flow birefringence and depolarized Rayleigh line broadening will be reanalysed.

In experiments on the viscosity, it was observed that a velocity gradient predominantly creates a polarization of tensorial type $[\underline{J}]^2$ ($[\underline{J}]^q$ is a normalized irreducible tensor of rank q formed from the angular momentum operator \underline{J} , cf. chapter I). On the scalar dependence on the molecular angular momentum \underline{J} however, no explicit information can be obtained.

On the other hand, in a gas of optically anisotropic molecules (such as all linear molecules), a polarization of the type $[\underline{J}]^2$ causes birefringence due to the fact that the dielectric tensor is related to the non-equilibrium average of the tensor $[\underline{J}]^2$. Consequently measurements of flow birefringence also yield information on this type of polarization. Note that in the flow birefringence experiment the same polarization is present as in the viscosity experiment, but as we will see below the scalar factor of the polarization plays a different role in flow birefringence. Finally, further information may be obtained from the shape of the depolarized Rayleigh line, which is determined by the decay of the $[\underline{J}]^2$ -alignment. It will be shown in this chapter that from a systematic comparison of the results of the viscomagnetic effect, flow birefringence and depolarized Rayleigh line broadening information can be obtained on the scalar

factor of the $[\underline{J}]^2$ -polarization.

The tensor polarization of the angular momentum \underline{J} and the second rank tensor of the reduced molecular velocity \underline{W} are characterized by normalized tensors $\underline{\Phi}$, respectively

$$\underline{\Phi}^{02} = [\underline{J}]^2 = \sqrt{\frac{15}{2}} \frac{[\underline{J}]^2}{[\underline{J}^2(\underline{J}^2 - \frac{3}{4})]^{\frac{1}{2}}} , \quad (1)$$

$$\underline{\Phi}^{20} = \sqrt{2} [\underline{W}]^2 . \quad (2)$$

The polarization produced by a velocity gradient, with known tensorial factor $[\underline{J}]^2$ and unknown scalar part, will be represented by a normalized tensor $\underline{\Phi}^{02\pi} = \underline{\Phi}^{02} p_{\pi}$, where the index π refers to the pressure tensor.

The kinetic theory of dilute polyatomic gases, which has been derived in order to describe these effects¹⁻⁴), gives explicit expressions for the measured quantities in terms of matrix elements S of the Waldmann-Snider collision operator⁵). For these matrix elements the same symbolic notation as in chapter I is used, e.g.,

$$\langle \Phi_{\mu}^{02\pi} | R \Phi_{\mu}^{20} \rangle = S \begin{pmatrix} 20 \\ 02\pi \end{pmatrix} , \quad (3)$$

$$\langle \Phi_{\mu}^{02\pi} | R \Phi_{\mu}^{02\pi} \rangle = S(02\pi) , \quad (4)$$

$$\langle \Phi_{\mu}^{20} | R^{-1} \Phi_{\mu}^{02} \rangle = S^{-1} \begin{pmatrix} 20 \\ 02 \end{pmatrix} . \quad (5)$$

For simple gases the matrix elements S are expressed in terms of effective cross sections in the following way

$$S \begin{pmatrix} p & q & s \\ p' & q' & s' \end{pmatrix} = \langle v \rangle \Theta \begin{pmatrix} p & q & s \\ p' & q' & s' \end{pmatrix} , \quad (6)$$

with the average thermal speed

$$\langle v \rangle = \sqrt{\frac{16}{\pi m} kT} . \quad (7)$$

Although theoretical expressions are usually given in terms of cross sections, they will now be given in terms of matrix elements which is more convenient for subsequent extension to mixtures.

In the following sections the relevant theoretical details of the various experiments will be presented together with a comparison of the experimental results for linear molecules. Modifications for symmetric top molecules and mixtures can be found in the appendices. In section 7 the conclusions of this chapter are compared to the results of model calculations.

2. The viscomagnetic effect

The occurrence of field effects can easily be visualized as follows. In a polyatomic gas with macroscopic gradients, collisions produce anisotropies (polarizations) in the angular momentum distribution. Upon application of an external field, these polarizations will partially be destroyed due to precession of the molecular moments in the field. This affects subsequent collisions, and consequently the transport properties of the gas will change. Measurements of such field effects will therefore yield information on the polarizations. In this chapter we are interested in particular in the $[\underline{j}]^2$ -polarization, which has been observed in the magnetic field effect on viscosity. The viscomagnetic effect has been studied extensively experimentally for a large number of linear molecules⁶⁾ and symmetric top molecules^{7,8)}. Also the concentration and temperature dependence of the effect has been investigated^{9,10)}.

The results of these measurements show that, except for NH_3 and ND_3 , all measurements are very well described with just one single tensorial type of polarization ($[\underline{j}]^2$). This leads us to the following assumption.

There exists a complete orthonormal set \mathcal{B} of expansion functions $\underline{\phi}^{02i}$, containing $\underline{\phi}^{02\pi}$ (the polarization produced by a velocity gradient, whose exact form is still unknown), for which

$$\langle \phi_{\mu}^{20} | \mathcal{R} \phi_{\mu}^{02i} \rangle = \delta_{i\pi} S \left(\begin{smallmatrix} 20 \\ 02\pi \end{smallmatrix} \right) \quad (8)$$

and

$$\langle \phi_{\mu}^{02i} | \mathcal{R} \phi_{\mu}^{02i'} \rangle = \delta_{ii'} S(02i) \quad (9)$$

This means that the matrix element $S\left(\begin{smallmatrix} 20 \\ 02\pi \end{smallmatrix}\right)$, which represents the production of the polarization, is the only non-zero off-diagonal element. Consequently the viscomagnetic effect is determined by three matrix elements $S\left(\begin{smallmatrix} 20 \\ 02\pi \end{smallmatrix}\right)$, $S(02\pi)$ and $S(20)$. The saturation value of the magnetic field effect on viscosity, e.g., reads^{1,11,12)}

$$\left(\frac{\Delta\eta}{\eta}\right)_{\text{sat}} = - \frac{S\left(\begin{smallmatrix} 20 \\ 02\pi \end{smallmatrix}\right)^2}{S(20) S(02\pi)} . \quad (10)$$

The half saturation field to pressure ratio for n_1^+ is related to the decay of the tensor polarization by

$$\left(\frac{B}{p}\right)_{\frac{1}{2}} = \frac{\hbar}{g\mu_N kT} S(02\pi) , \quad (11)$$

where g is the rotational g -factor and μ_N the nuclear magneton. Finally the field free viscosity of the gas is given by

$$\eta = kT S^{-1}(20) . \quad (12)$$

Numerical values for the cross sections corresponding to the matrix elements occurring in eqs. (10), (11) and (12) have already been reported (see refs. 6, 9, 10 and 11; note however, that 02 in earlier papers stands for 02π , since scalar factors of polarizations have always been neglected). A number of results are listed in table I (simple gases) and in table II (mixtures).

3. Flow birefringence

A direct proof of the presence of a $[\underline{J}]^2$ -polarization is provided by observing flow birefringence in a gas of optically anisotropic molecules. In 1970 the first theoretical description of this phenomenon was given by Hess³⁾.

The optical properties of a gas are characterized by the dielectric tensor $\underline{\underline{\epsilon}}$, which is linked to the non-equilibrium average of the optical polarizability tensor $\underline{\underline{\alpha}}$. In particular we write down for the anisotropic (traceless) part

$$\underline{\underline{\epsilon}} = \frac{n}{\epsilon_0} (\alpha^{\parallel} - \alpha^{\perp}) <[\underline{u}]^2> , \quad (13)$$

Table I

Experimental results and some molecular constants for the simple gases studied in this chapter ($T = 300$ K). The molecular constants are taken from ref. 13. The flow birefringence (FBR) results are taken from ref. 15, the results from measurements of the viscomagnetic effect (VME) on n_1 from refs. 7 and 8, while the results presented for the depolarized Rayleigh line broadening (DPR) stem from a new analysis of the measurements of ref. 21, see text. The definition of the listed quantities is consistent with ref. 21

$$2\pi\Gamma = -\left[\frac{dC(t)}{dt}\right]_{t=0}, \quad 2\pi\tilde{\Gamma} = \left[\int_0^\infty C(t) dt\right]^{-1}, \quad 4\pi^2\Gamma_2 = \left[\frac{d^2C(t)}{dt^2}\right]_{t=0} - \left[\frac{dC(t)}{dt}\right]_{t=0}^2$$

The polarizability α is given in $F \cdot m^2$ signifying that the induced electric dipole moment is defined as $p \equiv \alpha E$.

gas	$\frac{h^2}{2kT_L}$ (K)	g_L μ_0 (10^{-30} Cm)	FBR $\alpha''-\alpha^L$ (10^{-40} F.m ²)(10^{-16} s)	VME $10^3 \cdot (\frac{\Delta n}{n})_{sat}$ $(\frac{E}{p})^{\frac{1}{2}}$ (mT/Pa) (10^{-6} Pa.s) $n(0)$	DPR $\frac{\Gamma}{n}$ $\frac{\tilde{\Gamma}}{n}$ (m ³ .mol ⁻¹ .s ⁻¹) (m ⁶ .mol ⁻² .s ⁻²)			
N ₂	2.9	-0.278	0	2.6	17.81	22.6	20.4	42
OCS	0.29	-0.0287	2.40	4.5	9.0	12.21	47.5	100
CO	2.8	-0.269	0.37	0.59	2.1	17.53	26.0	49
CO ₂	0.56	-0.0551	0	2.30	5.8	14.66	43.5	137
N ₂ O	0.60	-0.0761	0.53	3.3	7.6	14.6	-	-
HD	64.3	+0.663	0.0	0.33	1.63	10.7	6.30	3.1
nH ₂	85.3	+0.883	0	0.33	0.21	8.72	1.22	0.0
pH ₂	85.3	+0.883	0	0.33	0.36	8.72	1.30	0.1
nD ₂	43.0	+0.443	0	0.32	0.43	12.4	1.72	1.56
oD ₂	43.0	+0.443	0	0.32	0.45	12.4	-	-

Table II

Experimental results for the mixtures studied in this chapter ($T = 300$ K, see table I for the data sources). The values in parentheses are obtained by extrapolation.

gas	z_2	FBR $\alpha'' - \alpha' \perp$ ($10^{-4} \text{ Oe} \cdot \text{cm}^2$) (10^{-16} s)	VME $10^3 \cdot (\frac{\Delta n}{n})_{\text{sat}} (\frac{B}{P})^{\frac{1}{2}}$ (mT/Pa) ($10^{-6} \text{ Pa} \cdot \text{s}$)	DPR $\frac{\Gamma}{n}$ ($\text{m}^2 \cdot \text{mol}^{-1} \cdot \text{s}^{-1}$) ($\text{m}^6 \cdot \text{mol}^{-2} \cdot \text{s}^{-2}$)	$\frac{\Gamma}{n}$ ($\text{m}^2 \cdot \text{mol}^{-1} \cdot \text{s}^{-1}$) ($\text{m}^6 \cdot \text{mol}^{-2} \cdot \text{s}^{-2}$)	VME $10^3 \cdot (\frac{\Delta n}{n})_{\text{sat}} (\frac{B}{P})^{\frac{1}{2}}$ (mT/Pa) ($10^{-6} \text{ Pa} \cdot \text{s}$)	$n(0)$	FBR $\alpha'' - \alpha' \perp$ ($10^{-4} \text{ Oe} \cdot \text{cm}^2$) (10^{-16} s)	VME $10^3 \cdot (\frac{\Delta n}{n})_{\text{sat}} (\frac{B}{P})^{\frac{1}{2}}$ (mT/Pa) ($10^{-6} \text{ Pa} \cdot \text{s}$)	$n(0)$
N ₂ -He	0	0.77	2.6	22.6	20.4	2.9	17.81	0.33	1.6	0.35
	0.20	2.4	2.3			2.1				10.7
	0.30									
	0.36									
	0.45	2.0		15.0	14.0					
	0.50			13.7	11.8	1.8				
	0.60			12.7	11.6					
	0.63	1.5								
	0.68									
	0.70									
N ₂ -Ne	0	0	0	(8.2)	(7.4)	1.5	19.6	0.33	1.6	0.35
	0.20	0.77	2.6	22.6	20.4	1.4	17.81			10.7
	0.25	2.4	2.4	21.6	19.9	(1.2)				
	0.32	2.2		19.2	16.7					
	0.40			16.5	16.3					
	0.50	1.8								
	0.56									
	0.59									
	0.63									
	0.70									
N ₂ -Ar	0	0	0	(14.3)	(14.0)	1.9	31.2	0.33	1.6	0.35
	0.16	0.77	2.6	22.6	20.4	1.8	17.81			10.7
	0.20	2.3	2.3	21.5	20.7					
	0.25			21.4	20.2	2.6				
	0.27	2.0		21.9	20.0					
	0.40									
	0.45	1.6								
	0.50									
	0.55	1.3								
	0.60									
HD-He	0	0	0	(20.0)	(19.8)	2.5	22.3	0	0	(0.53)
	0.20	0.82	0.82							22.3
	0.22	0.41	0.41							
	0.25	0	0							
	0.27									
	0.32									
	0.37									
	0.40									
	0.46									
	0.57									
HD-Ne	0	0	0	(20.0)	(19.8)	2.5	22.3	0	0	(0.53)
	0.20	0.82	0.82							22.3
	0.22	0.41	0.41							
	0.25	0	0							
	0.27									
	0.32									
	0.37									
	0.40									
	0.46									
	0.57									
HD-Ar	0	0	0	(20.0)	(19.8)	2.5	22.3	0	0	(0.53)
	0.20	0.82	0.82							22.3
	0.22	0.41	0.41							
	0.25	0	0							
	0.27									
	0.32									
	0.37									
	0.40									
	0.46									
	0.57									

where \underline{u} is a unit vector along the figure axis and $\alpha^{\parallel}, \alpha^{\perp}$ are the polarizabilities for an electric field parallel and perpendicular to that axis. For linear $^1\Sigma$ molecules the alignment tensor $[\underline{u}]^2$ of a rotating molecule equals minus one half the non-equilibrium average of $[\underline{J}]^2 / (J^2 - \frac{3}{4})$ (14). Thus a macroscopic alignment of the angular momenta of optically anisotropic molecules gives rise to an anisotropy in the dielectric tensor

$$\underline{\underline{\epsilon}} = -\frac{n}{2\epsilon_0} (\alpha^{\parallel} - \alpha^{\perp}) < \frac{[\underline{J}]^2}{J^2 - \frac{3}{4}} > . \quad (14)$$

On the other hand the constitutive relation for flow birefringence can be written in the form

$$\underline{\underline{\epsilon}} = -2 \beta \underline{\underline{\nabla v}} , \quad (15)$$

with β the birefringence coefficient. The non-equilibrium average in eq. (14) can be written as a matrix element of the inverse Waldmann-Snyder collision operator according to chapter I

$$< \frac{[\underline{J}]^2}{J^2 - \frac{3}{4}} > = < \left(\frac{J^2}{J^2 - \frac{3}{4}} \right)^{\frac{1}{2}} \frac{[\underline{J}]^2}{[J^2 (J^2 - \frac{3}{4})]^{\frac{1}{2}}} > \equiv \sqrt{\frac{2}{15}} < d_J \Phi^{02} > =$$

$$\sqrt{\frac{2}{15}} < d_J \Phi^{02} | \Phi > = -\frac{1}{n} \frac{2}{\sqrt{15}} < d_J \Phi^{02} | R^{-1} \Phi^{20} > : \underline{\underline{\nabla v}} . \quad (16)$$

The factor d_J , which is given by

$$d_J = \left[\frac{4J(J+1)}{(2J-1)(2J+3)} \right]^{\frac{1}{2}} , \quad (17)$$

equals unity for molecules which are predominantly in high J -states (in practice $J \geq 2$). Combining eqs. (14), (15) and (16) we then get

$$\beta = -\frac{1}{2\epsilon_0 \sqrt{15}} (\alpha^{\parallel} - \alpha^{\perp}) S^{-1} \begin{pmatrix} 02 \\ 20 \end{pmatrix} . \quad (18)$$

Only for hydrogen isotopes d_J deviates from unity. In this case eq. (18) can be approximated (estimated maximum error 15%) by

$$\beta = -\frac{1}{2\epsilon_0 \sqrt{15}} (\alpha^{\parallel} - \alpha^{\perp}) < d_J > S^{-1} \begin{pmatrix} 02 \\ 20 \end{pmatrix} . \quad (19)$$

Values for $\langle d_J \rangle$ for hydrogen isotopes can be found in table III.

A systematic experimental study of flow birefringence for a large number of linear and symmetric top molecules and for some mixtures has been performed at room temperature by Baas^{15,16}). The results which are used in the analysis in this chapter are listed in tables I and II. Only linear molecules have been considered, since for symmetric top molecules various complications arise, see appendix A. An extension to mixtures can be found in appendix B.

Table III

The average of the weighting function $d_J = \left[\frac{4J(J+1)}{(2J-1)(2J+3)} \right]^{\frac{1}{2}}$ for the hydrogen isotopes at 300 K together with some molecular data. For the other molecules studied in this paper d_J equals unity in good approximation (see text).

molecule	$\frac{\hbar^2}{2kT_{\perp}}$ (K)	$\langle d_J \rangle$
nH ₂	85.3	1.056
pH ₂	85.3	0.517
oH ₂	85.3	1.237
HD	64.3	0.927
nD ₂	43.0	0.905
oD ₂	43.0	0.769
pD ₂	43.0	1.175

4. Comparison of the viscomagnetic effect and flow birefringence

Equation (18) shows that measurement of flow birefringence directly yields a numerical value for a matrix element of the inverse Waldmann-Snyder collision operator. In contrast to the viscomagnetic experiment, in the case of the flow birefringence experiment we do know precisely which polarization we are observing. In order to come to a comparison we expand the tensor observed in the flow birefringence experiment in terms of the functions of set \mathcal{B}

$$\Phi_{\mu}^{02} = \sum_i a_i \Phi_{\mu}^{02i} . \quad (20)$$

The expansion coefficients a_i are given by

$$a_i = \langle \Phi_{\mu}^{02i} | \Phi_{\mu}^{02} \rangle , \quad (21)$$

a scalar product of expansion functions, while

$$\sum_i a_i^2 = 1 , \quad (22)$$

because the functions are normalized. Now we can rewrite the matrix element of the flow birefringence in terms of production matrix elements of set \mathcal{B} . Since $\Phi_{\mu}^{02\pi}$ is the only polarization produced (cf. eq. (8)) we get the simple relation

$$\langle \Phi_{\mu}^{20} | \mathcal{R}^{-1} \Phi_{\mu}^{02} \rangle = a_{\pi} \langle \Phi_{\mu}^{20} | \mathcal{R}^{-1} \Phi_{\mu}^{02\pi} \rangle . \quad (23)$$

Since the matrix element on the left hand side can be determined from the flow birefringence data and the one on the right hand side from the viscosity data, eq. (23) enables us to find an experimental value for a_{π} , which is the "projection" of $\Phi_{\mu}^{02\pi}$ onto Φ_{μ}^{02} . The resulting values, listed in tables IV and V, lead to the following remarks.

- 1) All a_{π} are, within the joint experimental accuracy of 20%, less than or equal to one. This is required by the fact that the expansion functions are normalized. For the mixtures the accuracy is somewhat less due to extrapolations.
- 2) The value of a_{π} is approximately 0.8. The exact form of polarization produced in viscous flow might, however, still be somewhat different for each gas.
- 3) We conclude that the dominant part of the polarization is formed by $[J]_2^2$: $a_{\pi} > 1/2$ for all gases, and therefore $|a_i| < a_{\pi}$ ($i \neq \pi$) (cf. eq. (22)).

5. Depolarized Rayleigh line broadening

Additional information can be obtained by studying the broadening of the depolarized Rayleigh line in polyatomic gases. The frequency distribution of this line is determined by the orientational fluctuations in the gas¹⁷⁾, which,

as we already have seen (cf. eqs. (13) and (14)), are related to the tensor $[\underline{J}]^2$. Thus study of the depolarized Rayleigh line profile will give information on this tensor polarization. The theory for the broadening of the depolarized Rayleigh line in dilute gases of linear molecules was developed by Hess^{14,18)} and Gordon⁴⁾

The depolarized Rayleigh line profile is essentially determined by the correlation function $C(t)$ which describes the decay of orientational fluctuations. Using the relation between $[\underline{u}]^2$ and $[\underline{J}]^2$ we can write down for this correlation function

$$C(t) = \frac{\langle \frac{[\underline{J}]^2}{J^2 - \frac{3}{4}}(0) : \frac{[\underline{J}]^2}{J^2 - \frac{3}{4}}(t) \rangle}{\langle \frac{[\underline{J}]^2}{J^2 - \frac{3}{4}}(0) : \frac{[\underline{J}]^2}{J^2 - \frac{3}{4}}(0) \rangle} \quad (24)$$

The evolution in time is given by

$$\frac{[\underline{J}]^2}{J^2 - \frac{3}{4}}(t) = e^{-n\mathcal{R}t} \frac{[\underline{J}]^2}{J^2 - \frac{3}{4}}(0) \quad , \quad (25)$$

where \mathcal{R} is again the linearized Waldmann-Snider collision operator and n is the density of the gas. By substituting this in eq. (24) and by using normalized tensors (cf. eq. (1)) we get

$$C(t) = \frac{1}{5} \sum_{\mu} \langle \Phi_{\mu}^{02} | e^{-n\mathcal{R}t} \Phi_{\mu}^{02} \rangle \quad , \quad (26)$$

where again the factors d_J have been taken equal to unity. Expansion of the exponential yields

$$\begin{aligned} C(t) = & \sum_{\mu} \frac{1}{5} \langle \Phi_{\mu}^{02} | \Phi_{\mu}^{02} \rangle + \\ & - n \sum_{\mu} \frac{1}{5} \langle \Phi_{\mu}^{02} | \mathcal{R} \Phi_{\mu}^{02} \rangle t + \\ & + \frac{1}{2} n^2 \sum_{\mu} \frac{1}{5} \langle \Phi_{\mu}^{02} | \mathcal{R} \mathcal{R} \Phi_{\mu}^{02} \rangle t^2 + \dots, \end{aligned} \quad (27)$$

Table IV

Results of the data analysis ($T = 300$ K). The cross sections $\mathcal{S}(20)$, $\mathcal{S}(02\pi)$ and $\mathcal{S}(02\pi)^{(20)}$ follow from data on the viscomagnetic effect, $\mathcal{S}(02)$, $\mathcal{S}(020)^{(02)}$ and $\mathcal{S}(020)$ from the depolarized Rayleigh line shape and α_π from the comparison of the viscomagnetic effect and flow birefringence. Finally values for $\mathcal{S}(02\pi)_c$ are given, which have been calculated from the cross sections of the depolarized Rayleigh line and α_π (see also fig. 1). The estimated uncertainties are given in percents. In some cases only a lower limit for $\mathcal{S}(020)$ could be determined.

gas	VME			DPR			FBR+VME+DPR	
	$\mathcal{S}(20)$	$\mathcal{S}(02\pi)$	$\mathcal{S}(02\pi)^{(20)}$	$\mathcal{S}(02)$	$\mathcal{S}(020)^{(02)}$	$\mathcal{S}(020)$	α_π	$\mathcal{S}(02\pi)_c$
	(10^{-20} m^2)			(10^{-20} m^2)			(10^{-20} m^2)	
N ₂	34.4	24	1.5	36	-10	30 ± 10	0.83	24 ± 8
CO	34.9	32	2.0	43	-11	60 ± 30	0.90	34 ± 9
N ₂ O	52.6	64	3.5	-	-	-	0.79	-
CO ₂	52.4	69	3.9	90	-23	80 ± 30	0.84	65 ± 21
OCS	73.4	80	4.8	110	-23	> 64	0.77	> 58
nH ₂	18.7	0.51	0.014	0.51	-0.090	> 0.2	0.67	> 0.24
pH ₂	18.7	0.49	0.020	0.55	-0.12	> 0.4	1.17	> 0.52
HD	18.7	2.2	0.27	3.2	-0.91	4 ± 2	0.97	2.5 ± 0.5
nD ₂	18.7	0.88	0.27	1.0	-0.31	1 ± 0.5	0.98	0.8 ± 0.2
oD ₂	18.7	0.93	0.26	-	-	-	1.2	-
HD (80 K)	24.7	2.9	0.52	2.9	0.000	-	-	-
	1%	5%	3%	3%	5%		20%	

Table V

Results of the data analysis for mixtures ($T = 300$ K). Only the values for the polyatomic gas-noble gas interaction are given, for other values see table IV. For $\mathcal{G}(020)_{12}$ only a lower limit could be determined. For the N_2 -noble gas mixtures a value for α_π calculated from extrapolated flow birefringence data has been used for the determination of $\mathcal{G}(02\pi)_{12c}$. These last results, however, should be considered as just a rough indication. Note that the values for the cross sections for HD-noble gas mixtures are not the same as the previously reported¹⁰⁾ values. The quantity α_π , which follows from a comparison of the viscomagnetic effect and flow birefringence, is concentration dependent and is therefore separately listed below.

gas	VME		DPR			FBR+VME+DPR	
	$\mathcal{G}(02\pi)_{12}$	$\mathcal{G}(02\pi)_{12}^{(20)}$	$\mathcal{G}(02)_{12}$	$\mathcal{G}(020)_{12}^{(20)}$	$\mathcal{G}(020)_{12}$	α_π	$\mathcal{G}(02\pi)_{12c}$
	(10^{-20} m^2)		(10^{-20} m^2)			(10^{-20} m^2)	
N_2 -He	5.6	0.06	6.4	-2.4	> 5.4	(0.7)	> 3
N_2 -Ne	15	0.50	21	-6.2	> 20	(0.8)	> 14
N_2 -Ar	24	0.98	35	-8.8	> 26	(1.0)	> 22
HD-He	2.1	0.16	-	-	-	-	-
HD-Ne	3.3	0.64	-	-	-	-	-
HD-Ar	4.9	1.7	-	-	-	-	-

N_2 -He		N_2 -Ne		N_2 -Ar		HD-He		HD-Ne		HD-Ar	
x_2	α_π	x_2	α_π	x_2	α_π	x_2	α_π	x_2	α_π	x_2	α_π
0.20	0.87	0.19	0.83	0.16	0.86	0.22	1.0	0.22	1.1	0.21	1.0
0.29	0.87	0.32	0.84	0.27	0.89	0.36	1.1	0.37	1.2	0.39	1.0
0.45	0.87	0.56	0.86	0.45	0.90	0.46	1.1	0.46	1.2	0.46	1.1
0.68	0.88	0.70	0.84	0.55	0.90	0.58	1.1	0.57	1.3	0.51	1.0
		0.72	0.89	0.73	1.1	0.74	1.3	0.72	1.1		
		0.87	0.97								

or

$$C(t) = 1 - n S(02) t + \frac{1}{2} n^2 \sum_i S(\begin{smallmatrix} 02 \\ i \end{smallmatrix})^2 t^2 + \dots, \quad (28)$$

where the summation refers to a complete set of orthonormal expansion tensors $\underline{\Phi}^i$.

Measurement of $C(t)$, which is equal to the Fourier transform of the line profile¹⁹), yields the following information. The first derivative with respect to time is given by

$$- \left[\frac{d}{dt} C(t) \right]_{t=0} = n S(02) . \quad (29)$$

For the second derivative we get

$$\left[\frac{d^2}{dt^2} C(t) \right]_{t=0} = n^2 \sum_i S(\begin{smallmatrix} 02 \\ i \end{smallmatrix})^2 = n^2 S(02)^2 + n^2 \sum_{i \neq 02} S(\begin{smallmatrix} 02 \\ i \end{smallmatrix})^2 . \quad (30)$$

The second term in the right hand side of this equation shows the deviation from a Lorentzian line shape, caused by coupling of two different polarizations (transfer of polarization). Such deviations have indeed been found experimentally^{19,20}). Finally the integral of the correlation function yields

$$\int_0^{\infty} C(t) dt = \frac{1}{n} S^{-1}(02) , \quad (31)$$

a matrix element of the inverse collision operator.

Measurements of the depolarized Rayleigh line broadening of some linear molecules and N₂-noble gas mixtures at room temperature were performed by Keijser^{19,21}). For the hydrogen isotopes measurements have also been performed at low temperature²²). Systematic investigations of the temperature and concentration dependence of the line shape for hydrogen noble gas mixtures are still in progress²³).

For the purpose of this chapter the measurements of Keijser have been reanalysed, since no quantitative results for the second derivative of the correlation function were available. Curve fit procedures are used to determine the first and the second derivative of the correlation function at $t = 0$. A discrete Simpson approximation is used to evaluate the integral in eq. (31). The results are listed in tables I and II.

6. Comparison with the viscomagnetic effect and the flow birefringence

In order to get additional information we decompose $\underline{\Phi}^{02\pi}$ in two orthogonal parts, one being proportional to $\underline{\Phi}^{02}$. The exact form of the other part, $\underline{\Phi}^{02D}$, remains still undetermined. Thus we have

$$\underline{\Phi}^{02\pi} = \alpha_{\pi} \underline{\Phi}^{02} + (1 - \alpha_{\pi}^2)^{\frac{1}{2}} \underline{\Phi}^{02D} . \quad (32)$$

Then one can relate the decay rate of the tensor polarization $\underline{\Phi}^{02\pi}$ to the decay rate of $[\underline{J}]^2$. Substitution of eq. (32) in the equation for the decay of the tensor polarization (4), yields

$$\mathfrak{S}(02\pi) = \alpha_{\pi}^2 \mathfrak{S}(02) + 2\alpha_{\pi} (1 - \alpha_{\pi}^2)^{\frac{1}{2}} \mathfrak{S}(\begin{smallmatrix} 02 \\ 02D \end{smallmatrix}) + (1 - \alpha_{\pi}^2) \mathfrak{S}(02D) . \quad (33)$$

The magnitude of $\mathfrak{S}(02\pi)$ follows from the position on the B/p -axis of the field effect on the viscosity (cf. eq. (11)), while $\mathfrak{S}(02)$, the decay cross section of $[\underline{J}]^2$, follows from the depolarized Rayleigh line broadening experiment, cf. eq. (29). Equation (33) clearly shows that the two decay rates do not have to be equal. Distinct deviations may occur due to transfer of polarization. Such a transfer, which also causes deviations from a Lorentzian line shape of the depolarized Rayleigh line as we already have seen (section 5), has indeed been found to exist^{19,21}). If we assume that the results of the depolarized Rayleigh line broadening can be described with the three cross sections on the right hand side, which means that only $\mathfrak{S}(\begin{smallmatrix} 02 \\ 02D \end{smallmatrix})$ would enter eq. (30), eq. (33) can be tested.

The depolarized Rayleigh line shape namely gives three experimental results, from which we are able to find the three cross sections on the right hand side. The coupling coefficient α_{π} has already been determined and thus we can calculate $\mathfrak{S}(02\pi)$. The resulting values are listed in tables IV and V. Fig. 1 shows how well the results agree with the values obtained from the field effect on the viscosity. This confirms our hypothesis that the $\underline{\Phi}^{02}$ fluctuation involves only a coupling to $\underline{\Phi}^{02D}$. Information on the form of $\underline{\Phi}^{02D}$, unfortunately cannot be obtained from these experiments.

The behaviour of HD allows a further conclusion to be drawn. At 80 K it has been verified experimentally that $\mathfrak{S}(02\pi) = \mathfrak{S}(02)$ (cf. table IV). This suggests that $\underline{\Phi}^{02\pi} = \underline{\Phi}^{02}$, which means that the scalar factor of $\underline{\Phi}^{02\pi}$ does not depend on ω^2 . The dependence on \underline{J}^2 vanishes since only the $J=1$ level plays a role for HD at 80 K. Therefore the difference between $\underline{\Phi}^{02\pi}$ and $\underline{\Phi}^{02}$ found at higher

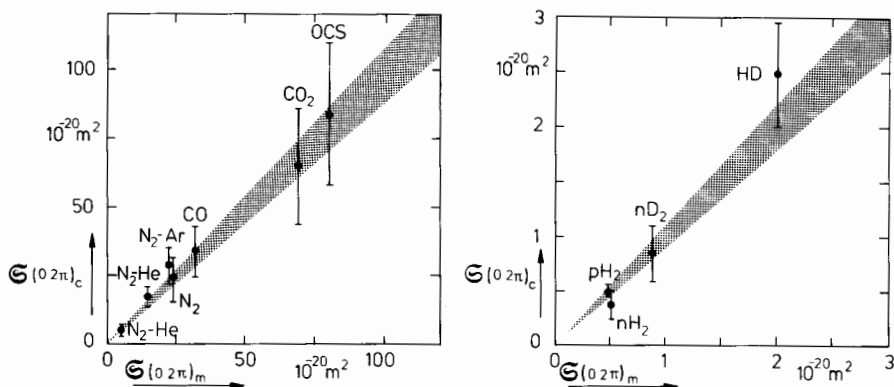


Fig. 1 Calculated versus measured values of $G(0,2\pi)$ for various molecules. In those cases where no upper limit for the error bar exists (see tables V and VI) the value of $G(0,2\pi)$ has been taken as upper limit (cf. eq. (33)). The shaded area reflects the experimental uncertainty in $G(0,2\pi)_m$.

temperature seems to stem only from the presence of more J -levels, giving rise to a scalar factor depending on J^2 . This behaviour agrees with the temperature dependence of $C(t)$ for hydrogen isotopes as found in experiments on depolarized Rayleigh line broadening²²). It is also in agreement with the conclusions of the study of the non-equilibrium distribution function in a heat-conducting gas²⁴).

Taking into consideration all the results, we may conclude that we have found a description which satisfies all experiments mentioned in this chapter. A coherent picture with only two assumptions is available. The first assumption, which states that the tensor polarization produced by a velocity gradient is an eigenvector of the Waldmann-Snider collision operator in the subspace of angular momentum dependent functions (cf. eq. (9)), seems very reasonable since the results obtained for the coupling coefficient a_π are realistic and agree remarkably well with the conclusions of chapter II. The second assumption, concerning the description of the depolarized Rayleigh line shape, also seems to be confirmed by the experiments, although the accuracy is not very high. The remaining unknown scalar factor is very hard to determine. Realistic model calculations, after expansion of this factor into orthogonal polynomials (e.g. Wang-Chang-Uhlenbeck (WCU) polynomials²⁵), may clarify the structure. In the next section some results of recent progress in this field are discussed.

7. Model calculations

The cross sections provided by the experiment can also be compared to the results of model calculations. The theoretical expressions for the cross sections have been evaluated semiclassically²⁶⁾ using a Monte Carlo technique involving the computation of many exact classical trajectories. For the intermolecular potential a short range anisotropic model proposed by MacRury et al.²⁷⁾ is used.

The results for N_2 and CO_2 at room temperature are listed in table VI. The

Table VI

Calculated values of some effective cross sections²⁶⁾ compared to measured values ($T = 300$ K). The values in parentheses are rough estimates. All cross sections in 10^{-20} m².

gas	CALCULATED	MEASURED
CO_2	$\sigma(02) = 91 \pm 1$	$\sigma(02) = 90 \pm 2$
N_2	$\sigma(20) = 35.3 \pm 0.2$	$\sigma(20) = 34.4$
	$\sigma(02) = 29.2 \pm 0.2$	$\sigma(02) = 36 \pm 1$
	$\sigma_{0201}^{02} = -11 \pm 1$	$\sigma_{020}^{02} = -10.3 \pm 0.5$
	$\sigma(0201) = 27 \pm 1$	$\sigma(020) = 30 \pm 10$
	$\sigma_{0202}^{02} = (5)$	
	$\sigma_{0202}^{0201} = (-16)$	
	$\sigma_{02}^{20} = 0.85 \pm 0.10$	
	$\sigma_{0201}^{20} = 1.1 \pm 0.2$	
		$\sigma(02\pi) = 24 \pm 1$
		$\sigma_{02\pi}^{20} = 1.50 \pm 0.04$

calculated values for the gas-kinetic cross section $\mathfrak{G}(20)$, which is mainly determined by the spherical part of the intermolecular potential, and the decay cross section $\mathfrak{G}(02)$ agree well with the experimentally obtained values. The other experimentally determined cross sections cannot be calculated since the exact form of the polarization is not known. Therefore the scalar factor of the polarization is expanded into orthogonal polynomials. The basis functions used are denoted by $\underline{\Phi}^{pqrs}$, where p and q denote the rank in \underline{W} and in \underline{J} respectively, r is the power of the associated Laguerre polynomial in \underline{W}^2 and s the power of the Wang-Chang-Uhlenbeck polynomial in \underline{J}^2 . A similar notation is used for the cross sections. By taking into account the first WCU-polynomial in \underline{J}^2 and by calculating the transfer to and the decay of this polarization we can, however, come to a qualitative comparison. Calculated values for $\mathfrak{G}(0201)$ and \mathfrak{G}_{0201}^{02} for N_2 at 300 K show a remarkable agreement with experimental data (see table VI). Using the experimentally determined value for α_π and the calculated values for the production cross sections, we may now estimate the magnitude of the production of the tensor polarization (for N_2 at 300 K) if we assume that $\underline{\Phi}^{020} \approx \underline{\Phi}^{0201}$. One then obtains

$$\mathfrak{G}_{02\pi}^{20} \approx \alpha_\pi \mathfrak{G}_{02}^{20} + (1 - \alpha_\pi^2)^{\frac{1}{2}} \mathfrak{G}_{0201}^{20} = (1.3 \pm 0.3) * 10^{-20} \text{ m}^2, \quad (34)$$

which is in perfect agreement with the experimental value. We may, however, not identify the unknown part of the tensor polarization with $\underline{\Phi}^{0201}$, since there are strong indications (see table VI) that also transfer to higher polynomials occurs.

References on page 104.

APPENDIX A: Symmetric top molecules

Experimental results for symmetric top molecules have been obtained for the field effect on viscosity^{7,8)} and for flow birefringence¹⁵⁾. For these molecules however, complications arise which make the analysis as given in this chapter impossible. These complications stem from the fact that \underline{J} can have different orientations with respect to the symmetry axis \underline{u} . The relation between $[\underline{u}]^2$ and $[\underline{J}]^2$ has now to be written as²⁸⁾

$$[\underline{u}]^2 = -\frac{1}{2} \left(1 - 3 \frac{(\underline{J} \cdot \underline{u})^2}{\underline{J}^2 - \frac{3}{4}} \right) \frac{[\underline{J}]^2}{\underline{J}^2 - \frac{3}{4}}, \quad (\text{A.1})$$

where $\underline{J} \cdot \underline{u}$ has eigenvalues K with $-J \leq K \leq J$. For linear molecules eq. (A.1) reduces to the corresponding equation for linear molecules, cf. eqs. (13) - (14).

For symmetrical top molecules, on the other hand, the non-equilibrium average of $[\underline{u}]^2$ can no longer directly be related to the matrix element $\mathfrak{G}(02\pi)$. The field parameter ξ now also depends on the value of K ^{7,12)}

$$\xi_{02\pi} = \frac{g_{\perp} \mu_N kT}{\hbar < \nu > \mathfrak{G}(02\pi)} \frac{B}{p} \left(1 + \frac{g_{\parallel} - g_{\perp}}{g_{\perp}} \frac{K^2}{J(J+1)} \right) \equiv \xi_{02\pi}^* \left(1 + \frac{g_{\parallel} - g_{\perp}}{g_{\perp}} \frac{K^2}{J(J+1)} \right). \quad (\text{A.2})$$

For linear molecules the term containing K vanishes and the effect reaches half saturation for $\xi = 1$. This yields a simple relation between the half saturation value of B/p and the matrix element $\mathfrak{G}(02\pi)$, cf. eq. (11). For symmetric top molecules the orientation of the angular momentum with respect to the figure axis is not fixed and the relation now also depends on the value of K , which will result in a spread of $\xi_{02\pi}$. Consequently one has to average over all internal rotational states of the molecules to calculate the value of $\xi_{02\pi}^*$ for which the effect reaches half its saturation value. The average, however, depends on the precise form of the polarization⁸⁾, which unfortunately is not known. For this reason and because of the factor appearing in eq. (A.1) symmetric top molecules are not suitable for the purpose of this chapter.

APPENDIX B: Mixtures

In this appendix we will consider the expressions for a binary mixture consisting of a polyatomic gas (component 1) and a noble gas (component 2). The

matrix elements S then become concentration dependent, since they contain three different types of interactions. According to chapter I we have to replace the S in the expressions for simple gases, as given in the previous sections, by a sum of contributions. For the viscosity e.g., (cf. eq. (12)),

$$S^{-1}(02) = \sum_{k,l} S^{-1}\left(\begin{smallmatrix} 20 \\ 20 \end{smallmatrix} \middle| \begin{smallmatrix} k \\ l \end{smallmatrix}\right). \quad (\text{B.1})$$

These quantities are related to concentration independent cross sections¹¹⁾ and in the theoretical expressions for the viscosity now ten different cross sections will occur, viz.

$$\begin{aligned} & \mathfrak{S}\left(\begin{smallmatrix} 20 \\ 20 \end{smallmatrix} \middle| \begin{smallmatrix} 1 \\ 1 \end{smallmatrix}\right)_{11} \quad \mathfrak{S}\left(\begin{smallmatrix} 02\pi \\ 02\pi \end{smallmatrix} \middle| \begin{smallmatrix} 1 \\ 1 \end{smallmatrix}\right)_{11} \quad \mathfrak{S}\left(\begin{smallmatrix} 20 \\ 02\pi \end{smallmatrix} \middle| \begin{smallmatrix} 1 \\ 1 \end{smallmatrix}\right)_{11}, & \text{which follow from the viscosity data} \\ & \mathfrak{S}\left(\begin{smallmatrix} 20 \\ 20 \end{smallmatrix} \middle| \begin{smallmatrix} 2 \\ 2 \end{smallmatrix}\right)_{22}, & \text{of species 1,} \\ & \mathfrak{S}\left(\begin{smallmatrix} 20 \\ 20 \end{smallmatrix} \middle| \begin{smallmatrix} 1 \\ 2 \end{smallmatrix}\right)_{12} \quad \mathfrak{S}\left(\begin{smallmatrix} 20 \\ 20 \end{smallmatrix} \middle| \begin{smallmatrix} 2 \\ 2 \end{smallmatrix}\right)_{12} \quad \mathfrak{S}\left(\begin{smallmatrix} 20 \\ 20 \end{smallmatrix} \middle| \begin{smallmatrix} 2 \\ 1 \end{smallmatrix}\right)_{12}, & \text{which follows from the field free} \\ & \mathfrak{S}\left(\begin{smallmatrix} 02\pi \\ 02\pi \end{smallmatrix} \middle| \begin{smallmatrix} 1 \\ 2 \end{smallmatrix}\right)_{12}, & \text{viscosity data of species 2,} \\ & \mathfrak{S}\left(\begin{smallmatrix} 20 \\ 02\pi \end{smallmatrix} \middle| \begin{smallmatrix} 1 \\ 1 \end{smallmatrix}\right)_{12} \quad \text{and} \quad \mathfrak{S}\left(\begin{smallmatrix} 20 \\ 02\pi \end{smallmatrix} \middle| \begin{smallmatrix} 2 \\ 2 \end{smallmatrix}\right)_{12}, & \text{which can be calculated from } \Omega\text{-integrals}^{29,10}), \\ & & \text{which follows from } \lim_{x_1 \rightarrow 0} \left(\frac{B}{p}\right)^{\frac{1}{2}} \text{ of the} \\ & & \text{mixture,} \\ & & \text{which will be determined from the} \\ & & \text{concentration dependence of the vis-} \\ & & \text{comagnetic effect.} \end{aligned}$$

The last two cross sections are not independent as can readily be seen by taking the average over centre-of-mass velocities. This results in the relation^{10,30)}

$$\mathfrak{S}\left(\begin{smallmatrix} 20 \\ 02\pi \end{smallmatrix} \middle| \begin{smallmatrix} 1 \\ 1 \end{smallmatrix}\right)_{12} = \frac{m_2}{m_1} \mathfrak{S}\left(\begin{smallmatrix} 20 \\ 02\pi \end{smallmatrix} \middle| \begin{smallmatrix} 2 \\ 2 \end{smallmatrix}\right)_{12}, \quad (\text{B.2})$$

where m_1 and m_2 are the masses of the molecules. The remaining cross section can be determined by studying the concentration dependence of the viscomagnetic effect. The results of the measurements of the viscomagnetic effect have been reanalysed. First, from the viscosity data values for $S\left(\begin{smallmatrix} 20 \\ 02\pi \end{smallmatrix} \middle| \begin{smallmatrix} 1 \\ 1 \end{smallmatrix}\right)$ as a function of concentration are obtained. As expected (cf. chapter I) the quantity $S\left(\begin{smallmatrix} 20 \\ 02\pi \end{smallmatrix} \middle| \begin{smallmatrix} 1 \\ 1 \end{smallmatrix}\right)/(-x_2)$ depends linearly on the concentration, see fig. 2. Extrapolation to $x_2 = 0$ is made in order to determine $\mathfrak{S}\left(\begin{smallmatrix} 20 \\ 02\pi \end{smallmatrix} \middle| \begin{smallmatrix} 1 \\ 1 \end{smallmatrix}\right)_{12}$. The results are listed in table IV. For N_2 they agree with the values given by Burgmans¹⁰⁾, but for the HD-noble gas mixtures the results differ completely from the previously reported values. Apparently the values of the matrix elements have been

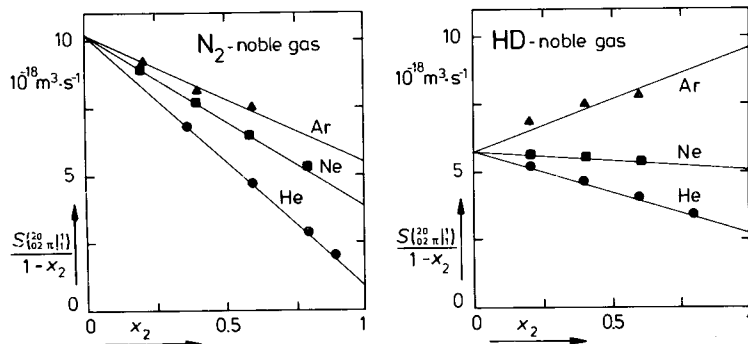


Fig. 2 $S(20 \ 02 \ \pi \ | \ 1) / (1 - x_2)$ versus the noble gas concentration for N_2 -noble gas and HD-noble gas mixtures. The data points have been calculated from data on the viscomagnetic effect.

—: least square line to the data points.

Extrapolations of the lines to $x_2 = 0$ and $x_2 = 1$ yield in the system

N_2 -noble gas the values 10.2 and 5.50, 3.99, $1.06 \cdot 10^{-18} \text{ m}^3 \cdot \text{s}^{-1}$, respectively, and for HD-noble gas the values 5.78 and 9.48, 5.06, $2.83 \cdot 10^{-18} \text{ m}^3 \cdot \text{s}^{-1}$.

divided by an erroneous relative velocity in the previous paper in the case of HD-noble gas.

Also in the expression for the flow birefringence, eq. (19), we have to replace the matrix element as in eq. (B.1). For N_2 -noble gas mixtures data on the depolarized Rayleigh line broadening are also available²¹). Again we have to replace the S in eqs. (28) through (31) by a sum over the various contributions. The first derivative of the correlation function $C(t)$, which has already been analysed by Keijser, depends linearly on the concentration. It can readily be checked that the integral of $C(t)$ is to a good approximation inversely proportional to x_2 , while the second derivative is proportional to the square of x_2 . The results are listed in table II.

References on page 104.

CONCLUDING REMARKS

At this stage it seems appropriate to summarize the conclusions concerning the central theme of this thesis, the scalar structure of non-equilibrium polarizations occurring in gases of rotating molecules.

For the $[\underline{J}]^2$ -type of polarization produced in viscous flow we have reached the following conclusions.

- The measurements of field effects on viscosity (Ch. II) show that the scalar structure of the polarization for symmetric top molecules is not simply given by either $[\underline{J}]^2$ or $[\underline{J}]^2$.
- From a comparison of field effects on the viscosity and optical effects (Ch. IV) we see that the same conclusion holds for linear molecules. The larger part of the polarization, however, is formed by the normalized tensor $[\underline{J}]^2$.
- From the same study we conclude that the scalar factor of the polarization depends upon \underline{J}^2 and not upon ω^2 , which is in agreement with the conclusions from direct measurements of the non-equilibrium distribution function in a heat-conducting gas.
- These results are also in agreement with the results of realistic model calculations (Ch. IV, section 7).

For the polarizations occurring in heat-conducting and diffusing gas mixtures, which are of a more complicated tensorial type, it was found that

- although the polarizations produced by temperature and concentration gradients are of the same tensorial type, they must have a different scalar structure.

REFERENCES

CHAPTER I :

The references quoted in this chapter can not be considered to form a complete list of papers in this field.

- 1) H. Senftleben, Phys. Z. 31 (1930) 822; 31 (1930) 961.
- 2) C.J. Gorter, Naturwissenschaften 26 (1938) 140.
- 3) C.J. Gorter, Ned. Tijdschr. Natuurk. 7 (1940) 89.
- 4) F. Zernike and C. van Lier, Physica 6 (1939) 961.
- 5) Yu.M. Kagan and A.M. Afanas'ev, Sov. Phys. JETP 14 (1962) 1096.
- 6) Yu.M. Kagan and L.A. Maksimov, Sov. Phys. JETP 14 (1962) 604.
- 7) J.J.M. Beenakker, G. Scoles, H.F.P. Knaap and R.M. Jonkman, Phys. Lett. 2 (1962) 5.
- 8) L. Waldmann, Z. Naturforsch. 12a (1957) 660; 13a (1958) 609.
- 9) R.F. Snider, J. Chem. Phys. 32 (1960) 1051.
- 10) F.R. McCourt and R.F. Snider, J. Chem. Phys. 41 (1964) 3185.
- 11) F.R. McCourt and R.F. Snider, J. Chem. Phys. 43 (1965) 2276.
- 12) R.F. Snider, J. Chem. Phys. 41 (1964) 591.
- 13) R.F. Snider, J. Math. Phys. 5 (1964) 1580.
- 14) Yu.M. Kagan and L.A. Maksimov, Sov. Phys. JETP 24 (1967) 1272.
- 15) A. Tip, A.C. Levi and F.R. McCourt, Physica 40 (1968) 435.
- 16) J.A.R. Coope and R.F. Snider, J. Chem. Phys. 57 (1972) 4266.
- 17) L. Waldmann, Z. Naturforsch. 18a (1963) 1033.
- 18) S. Hess and L. Waldmann, Z. Naturforsch. 21a (1966) 1529.
- 19) J.A.R. Coope and R.F. Snider, J. Chem. Phys. 56 (1972) 2056.
- 20) S. Chapman and T.G. Cowling, *The Mathematical Theory of Non-Uniform Gases* (Cambridge University Press, 1970).
- 21) S.R. de Groot and P. Mazur, *Non-Equilibrium Thermodynamics* (North-Holland publishing Co., Amsterdam, 1962).
- 22) G.E.J. Eggermont, H. Vestner and H.F.P. Knaap, Physica 82A (1976) 23.
- 23) H. Moraal, Phys. Rep. 17C (1975) 225.
- 24) A.C. Levi, F.R. McCourt and A. Tip, Physica 39 (1968) 165.
- 25) J.A.R. Coope, R.F. Snider and F.R. McCourt, J. Chem. Phys. 43 (1965) 2269.
- 26) J.A.R. Coope and R.F. Snider, J. Math. Phys. 11 (1970) 1003.
- 27) S. Hess and W.E. Köhler, *Formeln zur Tensor-Rechnung* (Palm & Enke, Erlangen, 1980) ISBN 3-7896-0046-6.
- 28) A.R. Edmonds, *Angular Momentum in Quantum Mechanics* (Princeton University Press, Princeton, N.J., 1957).
- 29) F.M. Chen, H. Moraal and R.F. Snider, J. Chem. Phys. 57 (1972) 542.
- 30) F. Tommasini, A.C. Levi, G. Scoles, J.J. de Groot, J.W. van den Broeke, C.J.N. van den Meijdenberg and J.J.M. Beenakker, Physica 49 (1970) 299.
- 31) W.E. Köhler, H.F.P. Knaap, G.E.J. Eggermont and G.W.'t Hooft, Z. Naturforsch. 33a (1978) 761.
- 32) W.E. Köhler, Z. Naturforsch. 29a (1974) 1705.

- 33) B.J. Thijsse, W.A.P. Denissen, L.J.F. Hermans, H.F.P. Knaap and J.J.M. Beenakker,
Physica 97A (1979) 467.
- 34) P.G. van Ditzhuyzen, B.J. Thijsse, L.K. van der Meij, L.J.F. Hermans and H.F.P. Knaap,
Physica 88A (1977) 53.
- 35) W.E. Köhler and G.W. 't Hooft, Z. Naturforsch. 34a (1979) 1255.
- 36) A.L.J. Burgmans, P.G. van Ditzhuyzen and H.F.P. Knaap, Z. Naturforsch. 28a (1973) 849.

CHAPTER II :

- 1) J.J.M. Beenakker and F.R. McCourt, Ann. Rev. Phys. Chem. 21 (1970) 47.
- 2) J.J.M. Beenakker, *Lecture Notes in Physics* 31 (Springer Verlag, Berlin, 1974) 413.
- 3) H.F.P. Knaap, G.W. 't Hooft, E. Mazur and L.J.F. Hermans,
Proc. 11th Symposium on Rarefied Gas Dynamics (Cannes, 1978) p. 777.
- 4) P.G. van Ditzhuyzen, B.J. Thijsse, L.K. van der Meij, L.J.F. Hermans and H.F.P. Knaap,
Physica 88A (1977) 53.
- 5) A.C. Levi, G. Scoles and F. Tommasini, Z. Naturforsch. 25a (1970) 1213.
- 6) F. Tommasini, A.C. Levi, G. Scoles, J.J. de Groot, J.W. van den Broeke,
C.J.N. van den Meijdenberg and J.J.M. Beenakker, Physica 49 (1970) 299.
- 7) F. Tommasini, A.C. Levi and G. Scoles, Z. Naturforsch. 26a (1971) 1098.
- 8) F.R. McCourt and R.F. Snider, J. Chem. Phys. 47 (1967) 4117.
- 9) Yu.M. Kagan and L.A. Maksimov, Sov. Phys. JETP 24 (1967) 1272.
- 10) H. Hulsman, E.J. van Waasdijk, A.L.J. Burgmans, H.F.P. Knaap and J.J.M. Beenakker,
Physica 50 (1970) 53.
- 11) A.L.J. Burgmans, P.G. van Ditzhuyzen, H.F.P. Knaap and J.J.M. Beenakker,
Z. Naturforsch. 28a (1973) 835.
- 12) A.L.J. Burgmans, P.G. van Ditzhuyzen and H.F.P. Knaap, Z. Naturforsch. 28a (1973) 849.
- 13) H. Hulsman, F.G. van Kuik, K.W. Walstra, H.F.P. Knaap and J.J.M. Beenakker,
Physica 57 (1972) 501.
- 14) B.J. Thijsse, *Thesis*, University of Leiden, 1978.
- 15) L.J.F. Hermans, J.M. Koks, A.F. Hengeveld and H.F.P. Knaap, Physica 50 (1970) 410.
- 16) A.C. Levi, F.R. McCourt and J. Hajdu, Physica 42 (1969) 347.
- 17) A.C. Levi, F.R. McCourt and J.J.M. Beenakker, Physica 42 (1969) 363.
- 18) H. Hulsman, G.F. Bulsing, G.E.J. Eggermont, L.J.F. Hermans and J.J.M. Beenakker,
Physica 72 (1974) 287.
- 19) G.E.J. Eggermont, L.J.F. Hermans, J.J.M. Beenakker and H. Vestner, Physica 91A (1978) 365.
- 20) R.F. Snider, J.A.R. Coope and B.C. Sanctuary, Physica 103A (1980) 379.
- 21) B.J. Thijsse, W.A.P. Denissen, L.J.F. Hermans, H.F.P. Knaap and J.J.M. Beenakker,
Physica 97A (1979) 467.

CHAPTER III :

- 1) J.J.M. Beenakker and F.R. McCourt, *Ann. Rev. Phys. Chem.* 21 (1970) 47.
- 2) J.A.R. Coope and R.F. Snider, *J. Chem. Phys.* 57 (1972) 4266.
- 3) J.J.M. Beenakker, H.F.P. Knaap and B.C. Sanctuary, *AIP Conf. Proc.* 11 (1973) 21.
- 4) J.J.M. Beenakker, *Lecture Notes in Physics* 31 (Springer Verlag, Berlin, 1974) 413.
- 5) R.F. Snider, *Lecture Notes in Physics* 31 (Springer Verlag, Berlin, 1974) 469.
- 6) H. Moraal, *Phys. Rep.* 17C (1975) 225.
- 7) H.F.P. Knaap, G.W. 't Hooft, E. Mazur and L.J.F. Hermans,
Proc. 11th Symposium on Rarefied Gas Dynamics (Cannes, 1978) p. 777.
- 8) J. Korving, H. Hulsman, G. Scoles, H.F.P. Knaap and J.J.M. Beenakker, *Physica* 36 (1967) 177.
- 9) H. Hulsman, F.G. van Kuik, K.W. Walstra, H.F.P. Knaap and J.J.M. Beenakker,
Physica 57 (1972) 501.
- 10) A.L.J. Burgmans, P.G. van Ditzhuyzen, H.F.P. Knaap and J.J.M. Beenakker,
Z. Naturforsch. 28a (1973) 835.
- 11) A.L.J. Burgmans, P.G. van Ditzhuyzen and H.F.P. Knaap, *Z. Naturforsch.* 28a (1973) 849.
- 12) P.G. van Ditzhuyzen, B.J. Thijsse, L.K. van der Meij, L.J.F. Hermans and H.F.P. Knaap,
Physica 88A (1977) 53.
- 13) Chapter II of this thesis.
- 14) L.J.F. Hermans, P.H. Fortuin, H.F.P. Knaap and J.J.M. Beenakker, *Phys. Lett.* 25A (1967) 81.
- 15) L.J.F. Hermans, A. Schutte, H.F.P. Knaap and J.J.M. Beenakker, *Physica* 46 (1970) 491.
- 16) L.J.F. Hermans, J.M. Koks, A.F. Hengeveld and H.F.P. Knaap, *Physica* 50 (1970) 410.
- 17) J.P.J. Heemskerk, F.G. van Kuik, H.F.P. Knaap and J.J.M. Beenakker, *Physica* 71 (1974) 484.
- 18) J.P.J. Heemskerk, G.F. Bulting and H.F.P. Knaap, *Physica* 71 (1974) 515.
- 19) B.J. Thijsse, W.A.P. Denissen, L.J.F. Hermans, H.F.P. Knaap and J.J.M. Beenakker,
Physica 97A (1979) 467.
- 20) A.C. Levi, G. Scoles and F. Tommasini, *Z. Naturforsch.* 25a (1970) 1213.
- 21) F. Tommasini, A.C. Levi, G. Scoles, J.J. de Groot, J.W. van den Broeke,
C.J.N. van den Meijdenberg and J.J.M. Beenakker, *Physica* 49 (1970) 299.
- 22) F. Tommasini, A.C. Levi and G. Scoles, *Z. Naturforsch.* 26a (1971) 1098.
- 23) V.D. Borman, L.L. Gorelik, B.I. Nikolaev, V.V. Sinitsyn and V.I. Troyan,
Sov. Phys. JETP 29 (1969) 959.
- 24) J.J. de Groot, J.W. van den Broeke, H.J. Martinius, C.J.N. van den Meijdenberg and
J.J.M. Beenakker, *Physica* 56 (1971) 388.
- 25) V.D. Borman, B.I. Nikolaev and V.I. Troyan, *Inzh. Fiz. Zh. (J. Eng. Phys.)* 27 (1974) 640.
- 26) G.W. 't Hooft, E. Mazur, J.M. Bienfait, L.J.F. Hermans, H.F.P. Knaap and J.J.M. Beenakker,
Physica 98A (1979) 41.
- 27) E. Mazur, G.W. 't Hooft and L.J.F. Hermans, *Phys. Lett.* 64a (1977) 35.
- 28) E. Mazur, G.W. 't Hooft, L.J.F. Hermans and H.F.P. Knaap, *Physica* 98A (1979) 87.
- 29) H.F. Vugts, A. Tip and J. Los, *Physica* 38 (1968) 579.
- 30) G.E.J. Eggermont, H. Vestner and H.F.P. Knaap, *Physica* 82A (1976) 23.
- 31) W.E. Köhler, *Z. Naturforsch.*, 29a (1974) 1705.
- 32) I. Isenberg, B.R. Russell and R.F. Greene, *Rev. sci. Instr.* 19 (1948) 685, see also:
V. Frank, *Appl. sci. Res. B III* (1953) 129.
- 33) E.A. Mason and T.R. Marrero, *Adv. At. Mol. Phys.* 6 (1970) 155.

CHAPTER IV :

- 1) F.R. McCourt and R.F. Snider, J. Chem. Phys. 47 (1967) 4117.
- 2) Yu.M. Kagan and L.A. Maksimov, Sov. Phys. JETP 24 (1967) 1272.
- 3) S. Hess, Springer Tracts Mod. Phys. 54 (1970) 136.
- 4) R.G. Gordon, J. Chem. Phys. 45 (1966) 1649.
- 5) R.F. Snider, J. Chem. Phys. 41 (1964) 591.
- 6) H. Hulsman, F.G. van Kuik, K.W. Walstra, H.F.P. Knaap and J.J.M. Beenakker, Physica 57 (1972) 501.
- 7) P.G. van Ditzhuyzen, B.J. Thijsse, L.K. van der Meij, L.J.F. Hermans and H.F.P. Knaap, Physica 88A (1977) 53.
- 8) Chapter II of this thesis.
- 9) A.L.J. Burgmans, P.G. van Ditzhuyzen, H.F.P. Knaap and J.J.M. Beenakker, Z. Naturforsch. 28a (1973) 835.
- 10) A.L.J. Burgmans, P.G. van Ditzhuyzen and H.F.P. Knaap, Z. Naturforsch. 28a (1973) 849.
- 11) G.E.J. Eggermont, H. Vestner and H.F.P. Knaap, Physica 82A (1976) 23.
- 12) Chapter I of this thesis.
- 13) B.J. Thijsse, W.A.P. Denissen, L.J.F. Hermans, H.F.P. Knaap and J.J.M. Beenakker, Physica 97A (1979) 467.
- 14) S. Hess, Z. Naturforsch. 24a (1969) 1675.
- 15) F. Baas, J.N. Breunese, H.F.P. Knaap and J.J.M. Beenakker, Physica 88A (1977) 1.
- 16) F. Baas, J.N. Breunese and H.F.P. Knaap, Physica 88A (1977) 34.
- 17) R.G. Gordon, J. Chem. Phys. 44 (1966) 3083.
- 18) S. Hess, Z. Naturforsch. 25a (1970) 350.
- 19) R.A.J. Keijser, K.D. van den Hout, M. de Groot and H.F.P. Knaap, Physica 75 (1974) 515.
- 20) R.A.J. Keijser, M.A. Jansen, V.G. Cooper and H.F.P. Knaap, Phys. Lett., 42A (1972) 109.
- 21) R.A.J. Keijser, K.D. van den Hout and H.F.P. Knaap, Physica 76 (1974) 577.
- 22) K.D. van den Hout, P.W. Hermans and H.F.P. Knaap, Physica 104A (1980) 548.
- 23) P.W. Hermans et al., to be published.
- 24) B.S. Douma, H.F.P. Knaap and J.J.M. Beenakker, Chem. Phys. Lett. 74 (1980) 421.
- 25) C.S. Wang Chang and G.E. Uhlenbeck, Univ. of Michigan Rept. CM-681 (1951).
- 26) A.F. Turfa and H.F.P. Knaap, Chem. Phys. (1981) in press.
- 27) T.B. MacRury, W.A. Steele and B.J. Berne, J. Chem. Phys. 64 (1976) 1288.
- 28) S. Hess, Z. Naturforsch. 29a (1974) 1121.
- 29) S. Chapman and T.G. Cowling, *The Mathematical Theory of Non-Uniform Gases* (Cambridge University Press, 1970).
- 30) W.E. Köhler and G.W. 't Hooft, Z. Naturforsch. 34a (1979) 1255.

NOMENCLATURE

Summary of the symbols, with their units and their meaning, used in this thesis. Throughout SI-units are used. As far as electromagnetic quantities are concerned the *rationalized system with four base quantities* is employed, see the recommendations of the S.U.N.-report in Physica 93A (1978) p. 1. Ch. = chapter, T. = table and eq. = equation.

symbol	numerical values	SI unit	meaning	Ch. eq.
\underline{a}		$\text{m}\cdot\text{s}^{-2}$	particle acceleration	I (1)
α_i	Ch.IV T.IV,V Ch.III T.IV	1	expansion coefficient	IV (21)
\mathcal{A}		-	complete orthonormal set of $\underline{\Phi}$'s	IV (20)
\underline{B}		T	induction of the magnetic field	I (35)
c		1	numerical constant	III (11)
\underline{c}		$\text{m}\cdot\text{s}^{-1}$	molecular velocity	I (1)
C^{α}		-	constant	I (53)
$C(t)$		1	correlation function	IV (24)
c_{rot}		$\text{J}\cdot\text{K}^{-1}$	rotational heat capacity per molecule	I
\underline{d}_J	Ch.IV T.III	1	numerical factor	III (17)
\underline{D}		$\text{m}^2\cdot\text{s}^{-1}$	Dufour tensor	I (116)
\underline{D}_T		$\text{m}^2\cdot\text{s}^{-1}$	thermal diffusion tensor	I (117)
\underline{D}	Ch.III T.IV	$\text{m}^2\cdot\text{s}^{-1}$	diffusion tensor	I (117)
e		1	base of natural logarithms	IV (25)
\underline{E}		$\text{V}\cdot\text{m}^{-1}$	electric field strength	I (36)
E		J	energy	I (25)
f		$\text{s}^3\cdot\text{m}^{-6}$	one particle distribution operator	I (1)
f		1	even in field function	I (87)
F		-	external field: $F = B$ or E .	II (15)
\underline{g}	Ch.II T.II Ch.IV T.I	1	rotational Landé tensor	I (33)
g		1	odd in field function	I (87)
H		J	Hamiltonian	I (1)
\mathcal{H}		-	Hilbert space	I
\hbar	$1.05459\cdot 10^{-34}$	$\text{J}\cdot\text{s}$	Planck constant	I (1)
i	$\sqrt{-1}$	1	imaginary unit	I (1)
I	Ch.II T.II Ch.IV T.I	$\text{kg}\cdot\text{m}^2$	moment of inertia	I (5)
\underline{I}		1	unit tensor	III (20)
\underline{j}_k		$\text{m}^{-2}\cdot\text{s}^{-1}$	particle flux density of species k	III (1)
\underline{J}		1	angular momentum operator	I (5)
J		1	rotational quantum number	I (35)
$[\underline{J}]_v^q$		1	spherical component v of normalized irreducible tensor of rank q in \underline{J}	I (39)

\underline{J}^α		-	generalized thermodynamical flux	I (13)
k	$1.3807 \cdot 10^{-23}$	$J \cdot K^{-1}$	Boltzmann constant	I (2)
K		1	quantum number for J	I (35)
K^α		-	constant	III(A.3)
K_p, K_λ, \dots	Ch.II T.1 Ch.III T.1	Pa	Knudsen correction parameters for $B/p, \lambda, \dots$	II (11)
l		m	dimension (length) of apparatus	III
ℓ		m	dimension (length) of apparatus	II
$L^\alpha \beta$		-	generalized phenomenological coefficient	I (13)
\mathcal{L}		$m^3 \cdot s^{-1}$	Liouville operator	I (34)
m		kg	particle mass	I (2)
n		m^{-3}	particle density	I (2)
P		1	(normalized) scalar factor of $\frac{\Phi}{\Phi}$	I (39)
p		Pa	gas pressure	II (8)
Q_α		-	transported quantity	I (14)
\underline{q}		$W \cdot m^{-2}$	heat flux density	I (23)
\underline{r}		m	particle position vector	I (1)
R		1	angular momentum reversal operator	I (60)
\mathcal{R}		$m^3 \cdot s^{-1}$	Waldmann-Snyder collision operator	I (11)
r		1	constant	I
$S_L(\dots)$		$m^3 \cdot s^{-1}$	reduced matrix element	I (44)
t		s	time	I (1)
τ		m	dimension (thickness) of apparatus	II
T		K	temperature	I (2)
\underline{u}	1	m	unit vector along figure axis	IV (13)
\underline{v}		$m \cdot s^{-1}$	flow velocity	I (3)
\underline{v}_k		$m \cdot s^{-1}$	average velocity of component k	I (89)
$\langle \underline{v} \rangle$		$m \cdot s^{-1}$	average thermal speed (simple gas)	I (47)
\underline{v}_{kT}		$m \cdot s^{-1}$	average thermal speed (mixture)	I (110)
w		m	dimension (width) of apparatus	II
\underline{w}		1	reduced molecular velocity	I (3)
$[\underline{w}]_\mu^p$		1	spherical component μ of irreducible tensor of rank p in \underline{w}	I (39)
\underline{X}^α		-	generalized thermodynamical force	I (13)
x_k		1	molar fraction of component k	I (88)
Z_{rot}		1	rotational partition function	I (2)

GREEK SYMBOLS:

α	Ch.II T.II Ch.IV T.I,II	$F \cdot m^2$	molecular polarizability (the induced electric dipole moment is defined as $p \equiv \alpha E$)	IV (13)
β	Ch.IV T.I,II	s	flow birefringence coefficient	IV (15)
Γ	Ch.IV T.I,II	s^{-1}	first derivative of $C(t)$ at $t = 0$	IV
Γ_2	Ch.IV T.I,II	s^{-2}	second derivative of $C(t)$ at $t = 0$ minus r^2	IV
$\tilde{\Gamma}$	Ch.IV T.I,II	s^{-1}	reciprocal value of surface under $C(t)$	IV
δ_{ij}		1	Kronecker delta	I (41)
ϵ_1, ϵ_2		1	correction parameters	II (11)
ϵ		1	dimensionless rotational energy per molecule	I (25)
ϵ		1	dielectric tensor	IV (13)
η	Ch.II T.I	Pa·s	viscosity tensor	I (115)
\equiv	Ch.IV T.I			I (23)
λ	Ch.III T.IV	$W \cdot K^{-1} \cdot m^{-1}$	thermal conductivity tensor	I (110)
μ		kg	reduced mass	I (32)
μ_e	Ch.II T.II	C·m	electric dipole moment	I (31)
μ_N	$5.0508 \cdot 10^{-27}$	$A \cdot m^2$	nuclear magneton	I (86)
ξ		1	field parameter	I (115)
Π		Pa	pressure tensor	I (2)
π	3.1415927	1	circumference/diameter ratio of a circle	I (46)
$\odot (::)$	Ch.IV T.IV,V,VI Ch.III T.II	m^2	effective cross section	I (86)
τ		s	relaxation time	I (6)
ϕ		1	deviation of f from equilibrium	I (39)
Φ		1	normalized expansion function	I (59)
χ^α		-	function proportional to the polarization produced by the microscopic flux ψ^α	I (11)
ψ		$s^2 \cdot m^{-6}$	inhomogeneous term of linearized WS-equation	I (85)
$\psi^L_{pq\theta}$	Ch.III T.I,III,IV	1	contribution of the pqs -polarization to the field effect on L	I (15)
ψ^α		-	microscopic flux	I (34)
ω		s^{-1}	Larmor frequency	I (45)
$\Omega(...)$		1	numerical factor	

NOTATION:

$\underline{A}, \underline{B}$	vector, tensor in coordinate space
$\underline{A} \cdot \underline{B}$	contraction over 1 index in coordinate space
$\underline{A} \bullet \underline{B}$	contraction over all indices in coordinate space
$\overline{\underline{A}}$	average of quantity A
$\langle A \rangle$	scalar product (in Hilbert space) of the operators A and B
$[A, B]$	commutator of the operators A and B
$\begin{pmatrix} j_1 j_2 j_3 \\ l_1 l_2 l_3 \end{pmatrix}$	3j-symbol (coupling coefficient)
Tr	trace (sum over J, K quantum numbers)
$[\underline{A}]_\mu^p$	spherical component μ of irreducible tensor of rank p in \underline{A}
$\overline{\underline{A}}$	symmetric traceless part of tensor \underline{A}
α^*	complex conjugate of complex quantity α
A^\dagger	Hermitian conjugate of operator A
A^\ddagger	adjoint of (super)operator A
$A \in \mathcal{K}$	A is an element of space or set \mathcal{K}

SAMENVATTING

De laatste twintig jaar is intensief onderzoek verricht naar het niet-sferische gedeelte van de interactie tussen moleculen. Een van de experimentele methodes om informatie hierover te verkrijgen is het meten van de invloed van uitwendige magnetische en elektrische velden op transporteigenschappen van verdunde meeratomige gassen. Deze veldeffecten, bekend onder de naam Senftleben-Beenakker effecten, treden op doordat een macroscopische gradiënt in een gas van niet-bolronde roterende moleculen anisotropieën in de verdeling van impulsmomenten veroorzaakt. Dit houdt in dat er een oriëntatie-voorkeur van moleculaire draaiingsassen optreedt. Zulke anisotropieën worden polarisaties genoemd. Ze kunnen een gecompliceerde structuur hebben doordat ze zowel van de snelheid als van het impulsmoment van de deeltjes kunnen afhangen. Uitwendige velden verstoren deze polarisaties, waardoor op hun beurt de transporteigenschappen van het gas worden beïnvloed.

Het tensoriële karakter van de polarisaties heeft men eënduidig kunnen bepalen uit metingen van veldeffecten bij verschillende veldoriëntaties. Op welke manier deze polarisaties nu van de grootte van de snelheid en van de grootte van het impulsmoment van het molecuul afhangen is echter tot nu toe een onbeantwoorde vraag gebleven.

In dit proefschrift zijn twee experimenten beschreven waaruit duidelijk blijkt dat deze scalaire afhankelijkheid veel ingewikkelder is dan aanvankelijk werd gedacht. Het eerste experiment, beschreven in hoofdstuk II, betreft de meting van de invloed van magnetische en van elektrische velden op de viscositeit voor symmetrische tol moleculen. Uit een vergelijking van de resultaten van deze twee soorten metingen kan men informatie verkrijgen over de manier waarop de polarisatie die optreedt in een visceuze stroming van het impulsmoment afhangt. Het tweede experiment, een onderzoek naar de invloed van een magnetisch veld op de diffusie in mengsels van stikstof en edelgassen, is beschreven in hoofdstuk III. Dit laatste onderzoek schept de mogelijkheid om de theoretische beschrijving te toetsen, door de resultaten te vergelijken met die

van soortgelijke metingen aan de warmtegeleiding en aan de thermodiffusie. Naast de nieuwe numerieke resultaten, die uit de in dit proefschrift beschreven experimenten zijn verkregen, wordt ook duidelijk aangetoond dat de gebruikelijke theoretische beschrijving in bepaalde aspecten, en met name wat betreft de scalaire structuur van polarisaties, tekort schiet.

In hoofdstuk IV wordt beschreven op welke wijze aanvullende informatie omtrent het scalaire deel verkregen kan worden uit een vergelijking van veld-effecten met optische verschijnselen. In de eerste plaats treedt dubbele breking op in gassen waar een oriëntatie-voorkeur voor de moleculen bestaat, zoals bijvoorbeeld in visceuze stroming. Dit is een gevolg van het feit dat de polariseerbaarheid van meeratomige moleculen anisotroop is. Derhalve kan uit metingen van niet-evenwichts dubbele breking informatie worden verkregen over niet-evenwichts polarisaties. Verder geven ook metingen van de gedepolariseerde Rayleigh lijn aanvullende gegevens, doordat de vorm van deze lijn door de levensduur van de (evenwichts) fluctuaties in de impulsmoment-oriëntaties wordt bepaald. Vergelijking van de bovengenoemde (en voor dit doel opnieuw geanalyseerde) optische metingen met de resultaten van metingen aan veldeffecten verduidelijken de structuur van de polarisatie die optreedt in visceuze stroming, en onderstrepen de conclusies uit de hoofdstukken II en III.

Teneinde de resultaten op een uniforme en eënduidige manier te kunnen presenteren is de kinetische theorie van transportverschijnselen in gassen van roterende moleculen enigszins aangepast en uitgebreid. Deze theoretische beschrijving staat aan het begin van dit proefschrift, in hoofdstuk I, beschreven. Enige nieuwe aspecten zijn de afleiding van een ongelijkheid tussen de grootten van de veldeffecten op warmtegeleiding, thermodiffusie en diffusie, en een gewijzigd formalisme voor gasmengsels.

CURRICULUM VITAE

van Eric Mazur, geboren op 14 november 1954 te Amsterdam

Op verzoek van de faculteit der Wiskunde en Natuurwetenschappen volgt hier een overzicht van mijn studie.

Na mijn eindexamen gymnasium β aan het Maerlant-Lyceum te 's-Gravenhage begon ik in 1972 mijn studie aan de Rijksuniversiteit te Leiden. In 1975 legde ik het kandidaatsexamen Natuurkunde en Wiskunde met bijvak Sterrenkunde af. Het experimentele werk voor het doctoraal examen verrichtte ik in de werkgroep Molecuulfysica onder leiding van prof. dr. J.J.M. Beenakker en wijlen prof. dr. H.F.P. Knaap. Eerst werkte ik op het Kamerlingh Onnes Laboratorium bij dr. K.D. van den Hout aan een onderzoek aan de botsingsverbreding van Ramanlijnen van waterstofisotopen bij lage temperaturen. Door een beurs van de Italiaanse regering was het mij mogelijk in 1976 drie maanden aan het "Istituto di Scienze Fisiche" van de Universiteit te Genua te werken. Na vervolgens op het Huygens Laboratorium dr. G.W. 't Hooft geassisteerd te hebben bij het onderzoek naar de invloed van magnetische velden op thermodiffusie in meeratomige gassen, verrichtte ik als afsluiting van mijn studie onderzoek naar de veldinvloed op het Dufoureffect. In 1977 legde ik het doctoraal examen Natuurkunde met bijvak Wiskunde af. Vervolgens maakte ik in 1978, als wetenschappelijk medewerker in dienst bij de Stichting voor Fundamenteel Onderzoek der Materie (FOM), een aanvang met de in dit proefschrift beschreven onderzoekingen.

Tevens assisteerde ik vanaf 1975 bij het geven van werkcolleges.

Aan het diffusieonderzoek werkten mee drs. H.J.M. Hijnen, drs. I. Versluijs en drs. J.B.M.A.M. Völkers. Bij het viscositeitsonderzoek werd ik terzijde gestaan door E. Viswat, terwijl in verschillende stadia ook drs. G.J.H. Burgers en R. Schothorst hun medewerking verleenden. De constructie van de apparaten werd gerealiseerd door P. Zwanenburg en F.A. Robbers. De nodige technische hulp werd verleend door de technische staf, de mechanische en de electronische werkplaatsen van het Huygens Laboratorium en de glastechnische werkplaats van het Kamerlingh Onnes Laboratorium, in het bijzonder door L. van As, J.F. Benning, P. van Biemen, Ing. A. Heijnen, Ing. H.T. Klein Wolterink en S.P.L. Verdegaal. Voor de aanvoer van cryogene vloeistoffen werd zorg gedragen door W. Flanderhijn. Bij de experimenten met PF_3 werd assistentie verleend door de EHBO en de BZB ploeg van het Huygens Laboratorium.

De Stichting FOM stelde mij in staat in 1981 gedurende enige weken aan het "Oddelek za Fiziko" van de Universiteit van Ljubljana theoretisch werk in het kader van het in dit proefschrift beschreven onderzoek te bespreken met prof. I. Kuščer.

De tekeningen zijn vervaardigd door J.J. Ober, de fotografische werkzaamheden werden door L. Zuyderduin verricht.

STELLINGEN

1. De vorm van de paardistributiefunctie van metallische glazen, vaak aangevoerd als argument voor de geldigheid van het DRPHS-structuurmodel, is bij nadere beschouwing juist een aanduiding van de ongeldigheid ervan.

S. Takeuchi en S. Kobayashi, *Phys. Stat. Sol. (a)* 65 (1981) 315.

2. De door Köhler e.a. voorgestelde "alternatieve" splitsing van de botsingsoperator en de hierbij behorende expansie geven bij de berekening van transportcoëfficiënten aanleiding tot niet snel convergerende reeksen.

W.E. Köhler, H.F.P. Knaap, G.E.J. Eggermont en G.W. 't Hooft, *Z. Naturforsch.* 33a (1978) 761.

3. De identificatie die Wdowiak maakt van de waargenomen emissielijnen in de "Red Rectangle" met zijn laboratorium-simulatiespectrum is aanvechtbaar.

T.J. Wdowiak, *Nature* 293 (1981) 724.

4. Teneinde de onlangs verkregen conclusies omtrent de scalaire structuur van niet-evenwichts polarisaties te verifiëren, is het gewenst stromings-dubbele-breking in HD bij 80 K te meten.

Hoofdstuk IV van dit proefschrift.

5. Het verdient aanbeveling om de spin-reoriëntatie processen in de zogenaamde "mixed-phase" van zwak-ferromagnetische metamagneten te bestuderen door *gelijktijdige* meting van de wisselstroom-susceptibiliteit in de antiferromagnetische ordeningsrichting en de magnetisatie in de richting van het zwakke ferromagnetische moment.

6. De door Lielmezs e.a. gemeten verandering van de viscositeit van water ten gevolge van een magnetisch veld is ten minste een factor 100 te groot.

J. Lielmezs en H. Aleman, *Thermochim. Acta* 21 (1977) 225.

7. Bij literatuurwaarden van inversie-invariante grootheden voor optische isomeren geeft het verschil in waarde tussen linksdraaiend en rechtsdraaiend molecuul een indruk van de meetnauwkeurigheid.
8. De uitdrukking "Larmor precessiefrequentie" geeft aanleiding tot misverstanden.
9. Naast de bestaande voorschriften voor eenhedenstelsels zouden ook richtlijnen voor uniforme definities van sommige electromagnetische grootheden, zoals de polariseerbaarheid, moeten worden gegeven.
10. Twee schilderijen van Gerrit Claesz. Bleker staan bekend als voorstellende de bekering van Saul (Handel. IX:18). Terwijl deze interpretatie overtuigend is voor het schilderij dat zich in het museum Boymans van Beuningen bevindt, is zij voor het andere werk niet juist. Veeleer is hier sprake van een uitbeelding van Jozua 10:11 : vanuit de Hemel laat God een regen van stenen neerdalen op de vluchtende Amorieten.